Developmental Patterning in the Inner Ear

Benjamin Robert Thiede
Madison, WI

Bachelor of Science, University of Wisconsin-Madison, 2006

A Dissertation presented to the Graduate Faculty
Of the University of Virginia in Candidacy for the Degree of Doctor of Philosophy

Department of Neuroscience

University of Virginia
March 2014

ABSTRACT

Verbal communication depends on the discrimination of sounds across a wide range of frequencies. The cochlea provides that capacity through mechanical tuning due to the basilar membrane's resonance properties and through responses of specialized sensory receptor cells called hair cells (HCs). Gradients of HC phenotypes parallel the longitudinal, or tonotopic, axis. Projecting from the apical surfaces of HCs are F-actin rich structures, called stereocilia, which are arranged in close-packed rows of increasing length. In the chicken cochlea, proximal-end HCs contain 250 or more stereocilia that reach a maximum length of 1.5 μm, while distal-end HCs contain 50 or fewer stereocilia that reach a maximum length of 5.5 μm. At locations between those ends, the number and length of stereocilia grade from HC to HC. As a result of the graded HC phenotypes and the mechanical properties of the basilar membrane that differ along the longitudinal axis, the cochlea's proximal (or basal) end is tuned for high frequencies of sound and its distal (or apical) end is tuned for low frequencies.

The hundreds of individual cellular phenotypes that are characterized by each HC's integer number of stereocilia provide a uniquely quantifiable and accessible readout of the topographic cellular patterning in the nervous system. A similar spatial gradient occurs in mammalian cochleae. The structural phenotypic differences between HCs also have functional importance in their frequency tuning – shorter bundles respond optimally to high frequency sounds and longer bundles respond better to low frequency sounds.

The graded differences in the number and maximum length of stereocilia produced along the longitudinal axis of the cochlea led me to hypothesize that diffusible, extracellular signaling molecules form morphogenetic gradients along this axis that pattern the HCs during development. In the first series of experiments I found that early in cochlea morphogenesis there are opposing gradients of expression for enzymes that synthesize and degrade retinoic acid (RA), a signaling molecule, across the tonotopic axis of the chicken cochlea. The expression gradients of these enzymes reverse as cochlear development proceeds and HCs begin to differentiate and acquire location-specific phenotypes. This presumptively leads to the formation of a morphogenetic gradient of RA across the distal-to-proximal axis. Through a series of *in vitro* experiments, I found that RA is necessary and sufficient to induce a distal-like HC phenotype throughout the chicken BP. In other experiments, I found that promoting RA signaling enhanced expression of *Espin* and *Fscn2,* actin crosslinking genes involved in stereocilia elongation.

In another series of experiments I found that fluorophore-conjugated phalloidin permeates living HCs and that this permeation requires metabotropic P2Y receptor signaling. These findings provide a novel method for vitally labeling sensory cells in developmental studies, which overcomes some of the limitations of visualizing live HCs with fluorescent styryl dyes, which have broad, fixed absorption spectra.

TABLE OF CONTENTS

LIST OF FIGURES AND TABLES

LIST OF ABBREVIATIONS

± SEM	Plus or minus the standard error of the mean
ADP	Adenosine-5’-diphosphate
ATP	Adenosine-5’-triphosphate
ATRA	All-*trans* Retinoic Acid
BIM II	Bisindolylmaleimide II
Bmp	Bone Morphogenetic Protein
BP	Basilar Papilla
BzATP	2'(3')-*O*-(4-Benzoylbenzoyl)adenosine-5'-triphosphate
E# (e.g. E6.5)	Embryonic day (e.g. Embryonic day 6.5)
DMEM	Dulbecco’s Modified Eagle Medium
DMSO	Dimethyl Sulfoxide
FBS	Fetal Bovine Serum
GFP	Green Fluorescent Protein
GPCR	G Protein-coupled Receptor
HCs	Hair Cells
OATP	Organic Anion Transporting Polypeptide
P# (e.g. P14)	Postnatal day (e.g. Postnatal day 14)
PPADs	Pyridoxalphosphate-6-azophenyl-2’,4’-disulphonic acid
PBS	Phosphate Buffered Saline
RA	Retinoic acid
RT	Room Temperature
SE	Sensory Epithelium
SCs	Supporting Cells
SEM	Scanning Electron Microscopy
UDP	Uridine-5’-diphosphate
UTP	Uridine-5’-triphosphate
qRT-PCR (or qPCR)	Quantitative Real-time Polymerase Chain Reaction

ACKNOWLEDGEMENTS

It has become apparent to me that it is the advisor who trains and educates the student more so than any particular graduate training program. The long list of successful and talented students who have trained under Dr. Jeffrey Corwin's tutelage is a strong testament to this belief. Jeff has had an enormously positive impact on my professional development, and of all the things he has taught me, I specifically want to thank him for teaching me how to be rigorous, thorough, and detail-oriented in my research; for instilling in me a desire to strive for perfection; for teaching me how fun and exciting science can be; and for teaching me the proper usage of the words "of" and "whether."

I also owe tremendous amount of appreciation to my graduate committee consisting of Drs. David Hill, Robert Grainger, Xiaowei Lu, Jung-bum Shin, and Scott Zeitlin. Thank you for all of your input and guidance, which have been instrumental in my thesis research (except for the occasional Chicago Bears comments).

I wish to thank all of my collaborators, specifically Michael Lovett, Matthew Kelley, and Zoe Mann. The research in this dissertation didn't even jump off the ground until I obtained RNA-seq data from Mike, who since then has always been a supportive influence in my research. I also wish to thank Matt and Zoe, who have been like second mentors to me. My experiences with these talented scientists have taught me the importance of seeking expert opinions and guidance in the pursuit of my goals.

I wish to thank the NGP and all of its students and faculty. I am especially grateful for Tracy Mourton, Nadia Cempre, Jane Beckert, Janine Vallee, and Sharon Heyka, who all work tirelessly and thanklessly behind the scenes. I also must thank Stacey Guillot, Barbee Hermann, and Jan Redick of the Advanced Microscopy Core who all have provided enormous assistance.

I also wish to thank all the people I've had the privilege of working with in the Corwin lab, especially Joseph Burns, Sol Collado, Wendy Baker, Derek Robinson, Mark Schneyer, and Eric Oliver. Thank you Joe for being a great person to bounce ideas off of, for being one of my groomsmen, and for persistently searching for ways to regenerate the hair cells I inevitably will lose as I age. Thank you Sol too for all of your guidance and wisdom over the years.

I wish to thank my family, especially my parents and my grandparents, who always have believed in me more than anybody else. I owe everything to you, thank you so much for supporting me my whole life, teaching me the importance of a hard work ethic, and for inspiring me to reach for my dreams. To Becky and Megan: thank you for being the best sisters I could ask for. I also need to thank all of my incredibly supportive and generous aunts, uncles and cousins. Thank you too to my grandparents-in-law, Granny and Jim. You have already done so many wonderful things for me and taught me many essential lessons, such as the importance of having "scanning ability."

I also must give thanks and praise to God, through whom all things are possible, even a cure for deafness (Mark 7:31-37). All of my accomplishments and any perceived successes are because of Him. It truly has been a privilege to study His divine creation on a scientific level.

Finally, I wish to thank my wonderful wife, Christa, who daily offers me enormous love and support! She also perhaps best understands how ironic it is that I have studied a protein called ESPN. Christa truly is my inspiration; even beyond her "Lorax" recycling ways, the world is a much better place because of her love, kindness, and compassion. I don't believe there is anything I could ever accomplish in my research that would ever have a larger impact on society than she does with her personality alone.

“Sometimes the questions are complicated

and the answers are simple.”

-Dr. Seuss

“The simplest explanation for some phenomenon is more

likely to be accurate

than more complicated explanations.”

-Occam’s Razor

“Everything should be made as simple as possible,

but no simpler.”

-Albert Einstein

CHAPTER 1

Introduction

General Background

The inner ear is responsible for hearing and maintaining balance. Anatomically, it is comprises a membranous labyrinth encased within the outer wall of a bony labyrinth. The membranous labyrinth consists of fluid-filled sacs that contain the inner ear sensory organs, which are partitioned into auditory and vestibular systems. The auditory system includes the sound-detecting cochlea and the vestibular system includes the otolith organs that detect linear acceleration and the semicircular canals that sense angular rotations.

The complex structures of the inner ear develop from a simple beginning when the cranial ectoderm thickens to form a placode. The placode then invaginates to form the otic vesicle, or otocyst, which is further patterned to produce the cochleo-vestibular ganglion and all of the sensory organs. The mechanosensitive receptor cell type in all of these sensory organs is the hair cell, an epithelial cell with specialized filamentous actin-rich protrusions called stereocilia. Stereocilia are directionally polarized and organized into rows of increasing height to form a hair bundle, which transduce an electrical signal when deflected (Figure 1-1). The details of these developmental events that give rise to the components of the inner ear are further described and expanded upon in the sections that follow.

In the auditory system, complex sounds, such as speech and bird song, are separated into their component frequencies by the basilar membrane's longitudinal gradient of mechanical vibration responses and by the differing phenotypic characteristics of the HCs at different positions along the cochlear sensory epithelium. Those HCs and their afferent neurons give rise to tonotopically-mapped representations of the component frequencies extending from the brainstem to cortical levels. Despite its importance and prevalence, our understanding of how this organization originates is rudimentary. In the following sections I outline more specific details on how the tonotopic organization of HCs develops, the importance of studying and understanding how this organization is established, and introduce the retinoic acid signaling pathway, which I discovered to be critically important in the developmental patterning of HCs in the chicken cochlea.

Inner Ear Development

Pre-placodal region

At the end of gastrulation, the anterior ectoderm is subdivided into four domains: the neural plate, neural crest, future epidermis, and pre-placodal regions. The pre-placodal region is a specialized horseshoe-shaped region that develops lateral to the neural plate and neural crest boundaries and is the location where individual placodes develop bilaterally to produce all of the craniofacial sensory organs. These placodes are, in order from anterior to posterior: the olfactory (forms the nasal epithelium), adenohypophyseal (anterior

pituitary gland), lens, ophthalmic and maxillomandibular placodes of the trigeminal (somatosensory neurons), otic (inner ear epithelium and cochlear vestibular ganglion), and epibranchial (Baker and Bronner-Fraser, 2001; Schlosser, 2006; Streit, 2004). Transplantation, fate-mapping, and *in vitro* experiments have shown that the ectodermal tissue throughout the entire pre-placodal region is competent to give rise to all of the placodal-types (Bailey et al., 2006; Jacobson, 1963; Kozlowski et al., 1997; Streit, 2002).

Pre-placodal region formation is induced from a combination of signals that emanate from the head mesoderm and neural plate regions. These include signals that activate the Fgf signaling pathway and other signals that inhibit the Bmp and Wnt signaling pathways (Litsiou et al., 2005). This narrow region in anterior ectoderm then becomes molecularly defined by the conserved expression of *Six1, Eya1,* and *Eya2* (Brugmann et al., 2004; Mishima and Tomarev, 1998; Schlosser and Ahrens, 2004).

Otic induction

The complex inner ear architecture develops from the otic placode, a focal thickening of the non-neural cranial ectoderm that forms at the border of the cranial neural plate and epidermis at the level of the 5th and 6th rhombomeres of the hindbrain (Baker and Bronner-Fraser, 2001; Bancroft and Bellairs, 1977). The placode becomes morphologically apparent as a surface depression in chickens at stage 9 [HH9, or 7 somite stage (Hamburger and Hamilton, 1951)] and at E8.5 in mice (Alvarez and Navascues, 1990; Kiernan et al., 2002). Within the pre-

placodal region, the otic placode is induced by Fgf signals emanating from the underlying mesoderm, the adjacent hindbrain, and the endoderm (Kil et al., 2005; Ladher et al., 2005; Wright and Mansour, 2003). After this, the size of the otic placode territory is specified and refined by the Wnt and Notch signaling pathways, which cooperatively guide cells to differentiate as placodal epithelium rather than cranial epidermis (Jayasena et al., 2008; Ohyama et al., 2006). *Pax8* and *Pax2* transcription factors are the earliest genes expressed in the otic placode, although their use as markers for inner ear induction is limited since they are additionally expressed in the epibranchial placode and since *Pax2* expressing cells additionally give rise to cranial epidermis (Heller and Brandli, 1999; Ohyama and Groves, 2004; Streit, 2002).

Otocyst Formation and Patterning

By E9.5 in mice and E3 in chickens, the otic placode invaginates to form a closed vesicle entirely surrounded by mesenchymal tissue, termed the otocyst or otic vesicle (Bissonnette and Fekete, 1996; Kiernan et al., 2002). Bony fish uniquely don't form vesicles, but rather a thickened ball that hollows out through cavitation (Haddon and Lewis, 1996). Regional patterning and morphogenesis of the otocyst along the antero-posterior (A-P), dorso-ventral (D-V), and medio-lateral (M-L) axes completely produces the complex membranous labyrinth of the inner ear, including the auditory system, vestibular system, endolymphatic duct and sac, and the cochlear vestibular ganglion.

Graded Shh signaling emanating from the notochord and ventral neural tube and Wnt signaling from the dorsal neural tube specify the D-V axis of the otocyst, thereby partitioning the developing inner ear into a dorsal component that produces the vestibular organs and a ventral component that forms the auditory organ (Bok et al., 2007b; Riccomagno et al., 2005). During similar developmental stages, a rostro-caudal wave of retinoic acid (RA) activity patterns the A-P axis of the otocyst, establishing an anterior component that gives rise to the sensory organs and a posterior component that largely forms the nonsensory components of the inner ear (Bok et al., 2011). The identity and nature of the tissues and signals that specify the M-L axis are currently unknown (Bok et al., 2007a).

Cochlea Morphogenesis and Patterning

The auditory organ in birds, mammals, and reptiles is the cochlea. Sound entering through the outer ear is converted by the middle ear into a traveling wave, which the cochlea detects and transmits as an electrical signal to higher processing centers in the brain (Hudspeth, 1989). In mice, the cochlear duct, which contains the sensory epithelium called the organ of Corti, the cochlear nerve, and other non-sensory components, begins growing out from the posterior-lateral region of the otocyst by E12 (Bok et al., 2007a). The cochlea increases in length from the proximal end and coils, forming 1.75 turns in mice and 2.5 in humans (Cantos et al., 2000). In contrast with that, the cochlea in birds is flat and sickle-shaped, where the proximal end is narrow and tapered,

while the distal end is more broad and rounded. The avian cochlear duct also houses an auditory sensory epithelium, termed the basilar papilla (BP), comprising HCs along with neighboring supporting cells (SCs). Within the avian cochlear duct there also are sensory nerves, non-sensory components, as well as an additional otolithic organ, the lagena macula, which forms at the distal tip of the developing cochlear duct, which is thought to be used for magnetoreception (Wu and Dickman, 2012). The cochlea in chickens begins forming from the ventral otocyst around E5 (Wu and Oh, 1996). It reaches 1.1 mm long at E9 and continues to elongate throughout development, such that it has doubled in length by E15 and eventually becomes 2.6 mm long by hatching (21 days of incubation) (Tilney et al., 1986).

The sensory cell in the inner ear is the hair cell (HC), which is an epithelia cell with F-actin rich structures called stereocilia that project from the apical surfaces in close-packed rows of increasing length, collectively called the hair bundle. Sound-induced traveling waves causes hair bundles to deflect, which modulates ion flow through mechanotransduction channels located at the tips of stereocilia and generates a receptor potential. In contrast to cochleae in therian mammals (marsupials and placental mammals), which display a precise alignment of HCs into four highly ordered rows that extend from end-to-end along the longitudinal axis (Figure 1-2), the sensory epithelium of avian cochlea produces hair cells throughout the whole width, from the superior (or neural) to the inferior axis (or abneural). Interestingly, the organ of Corti in extant prototheria mammals, which includes the Monotremata order comprising

platypus and echidna, have regions of HCs that are rigidly organized into ordered rows similar to mice and humans and other regions where the HCs are loosely-ordered into a number of irregular rows that more closely resemble the avian cochlea. These monotremes, which represent an early divergence of the mammalian evolutionary tree that occurred 163-191 Myr, additionally have an uncoiled cochlea that contains an apically-located lagena macula, similar to avians (Ladhams and Pickles, 1996; Vater and Kossl, 2011). Sequencing the platypus genome has also revealed features common between mammals, birds, and reptiles (Warren et al., 2008). Since monotreme cochleae have shared traits between birds and humans, studies on its cochlear development have the potential to provide extraordinary insights into how the therian cochlea became specialized evolutionary, although this is not a focus of this thesis.

A common feature of cochleae, from birds where the sensory epithelium is as small as only a couple millimeters long, to mammals, where it can reach lengths up to 71 mm in blue whales (Ketten, 2000; Vater and Kossl, 2011), is that it is tonotopically tuned along its longitudinal axis. This tonotopic representation means that the cochlea is topographically organized to sense different tone frequencies at different regions, with similar frequencies sensed adjacently. High frequencies of sound are sensed near the base, or proximal end of the cochlea while lower frequencies of sound are sensed more apically (or distally). This frequency tuning occurs based upon passive properties of the basilar membrane that underlie the sensory epithelium (Von Bekesy, 1960) and by active properties of the HCs, which have morphological and mechanoelectrical properties that

differ along the tonotopic axis of the cochlea (Figure 1-3) (Mann and Kelley, 2011).

A gradient of HC phenotypes parallels the tonotopic, or longitudinal, axis of the BP. In chickens, proximal-end HCs contain 250 or more stereocilia that reach a maximum length of 1.5 μm, while distal-end HCs contain 50 or fewer stereocilia that reach a maximum length of 5.5 μm. At locations between those ends, the number and length of stereocilia grade from HC to HC (Tanaka and Smith, 1978; Tilney and Saunders, 1983). A similar spatial gradient occurs in cochleae of mammals (Lim, 1980; Lim, 1986). The structural phenotypic differences between HCs have functional importance in their tuning to different sound frequencies – shorter bundles respond optimally to high frequency sounds and longer bundles respond better to low frequency sounds (Frishkopf and DeRosier, 1983; Holton and Hudspeth, 1983). Differential expression of ion channel splice variants occurs along the longitudinal axis of the cochlea and also contributes to the frequency selectivity of these HCs (Miranda-Rottmann et al., 2010; Ramanathan et al., 1999). One of the major aims of this dissertation is to gain an understanding how the gradient of HC phenotypes is patterned during development.

Hair cell development in the basilar papilla

As the cochlea develops in chickens, the first HCs are produced when a narrow, longitudinal band of cells along the length of the longitudinal axis first exit the cell cycle at E6. New HCs are then added appositionally at the edges of this

band until nearly all HCs have become postmitotic by E9 (Katayama and Corwin, 1989). HC differentiation then occurs along a spatio-temporal gradient that begins on E6 apically and progresses to the basal tip of the chicken cochlea by E9 (Cotanche and Kaiser, 2010; Cotanche and Sulik, 1984; Tilney et al., 1986). By E10 to E11, the cochlea contains ~10,500 HCs, equivalent to the number found in adult birds (Tilney et al., 1986). The full length of the mature cochlea is then achieved as these cells increase in size and surface area.

Hair cells assemble their complex hair bundles over the course of development in a number of sequential steps. Stereocilia formation first becomes evident at E8, and by E9 the entire HC apical surface is filled with stereocilia. By E10.5, one of the first longitudinal HC phenotypic gradients becomes apparent as the HCs at different positions along the cochlea show differences in stereocilia number. HCs near the proximal end have formed up to ~200 stereocilia and HCs near the distal end have formed ~50 stereocilia, with intermediate numbers grading from HC to HC between these ends. In E10.5 BPs, the total number of stereocilia formed is approximately the same that are found in the HCs at identical relative positions within mature cochlea (Tilney et al, 1992).

Stereocilia located nearest the kinocilium begin elongating at E10.5. These stereocilia will eventually form the tallest row in the hair bundle. At E10.5, HCs throughout the BP have hair bundles with circular outlines, but as stereocilia begin to elongate, the bundle rearranges into semicircular, or rectangular shapes by E12. Stereocilia in proximal HCs reach their mature length of 1.5 to 2 μm by

E12 and will cease elongating, while stereocilia in the distal region continue to elongate during development. Although elongation in these distal HCs is not yet completed even at the time of hatching, the longitudinal gradient in maximal hair bundle lengths is apparent by E13 (Tilney et al., 1992; Tilney and Saunders, 1983; Tilney et al., 1988; Tilney et al., 1986).

Impact of studying the development of tonotopy

Despite an extensive, detailed characterization of the development of these HC phenotypes in the developing chicken cochlea by Lewis Tilney and colleagues and even though this patterning is critically required for proper frequency discrimination, we have a very limited knowledge of how this organization develops. The primary goal of this dissertation is to gain a comprehension of the identity and nature of the signals that set up the pattern of different HC phenotypes across the pitch axis of the chicken cochlea.

This understanding should have numerous applications on studies and cases that involve sensory cell loss. While cochlear HCs are indispensible for sensing sound, they are few in number, totaling around only 16,000 in a typical human cochlea. They also are limited in their regenerative potential in mammals, with nearly all hair cells produced during embryogenesis—creating a lifelong challenge to retain these cells and maintain functioning levels of hearing (Burns and Corwin, 2013; Meyers and Corwin, 2008). Humans and other mammals incur permanent hearing loss when auditory HCs are lost, so there is a need for therapies aimed at both replacing lost sensory cells and for protecting HCs.

Therapies that replace lost sensory cells must ensure that the new hair cells establish the anatomical patterning essential for generating the tonotopic gradient needed for frequency discrimination.

According to the NIDCD, almost half the population aged 75 years or older suffers from presbycusis, which is the gradual loss of hearing that occurs as we age. This loss is commonly associated with an inability to hear high-pitched sounds, which collectively is the most common type of hearing impairment. High frequency hearing loss is largely caused by the selective loss of HCs from the basal end of the cochlea. These HCs, which are responsible for transducing the highest frequency of sounds, appear to be more vulnerable than apical HCs to die and become permanently lost due to causes such as age, extended exposure to loud sounds, and infections (Turner, 2006). People with selective high frequency hearing impairments retain an ability to hear vowels adequately, but unfortunately experience deficits in understanding certain consonants such as T, K, F, S, Th, Sh, and Z. So while these people can hear low frequency sounds such as a ringing telephone, they have difficulties communicating since the speech comprehension is mostly dependent upon the higher frequencies of the acoustic spectrum.

Current treatments involve the use of hearing aids to amplify high frequency sounds, but their effectiveness are limited if the extent of cell loss is severe enough (Seldran et al., 2011). Cochlear implants additionally have been used in profound cases of sensorineural hearing loss. A more thorough understanding of how HCs are patterned during development may have

enormous implications and applications for studies focused on preserving and restoring these cells.

Retinoic acid signaling

In chapter two, I outline the role a putative gradient of RA activity plays in patterning the gradient of HC phenotypes across the longitudinal axis of the BP. RA is a metabolite of vitamin A, or retinol, which circulates throughout the bloodstream and can enter cells via the membrane receptor Stra6. Within the cytoplasm, retinol is synthesized to RA through two sequential oxidation reactions, where either the alcohol dehydrogenase (Adh) or retinol dehydrogenase (Rdh) enzymes oxidize retinol to retinaldehyde, and then one of three retinaldehyde dehydrogenases (Raldh1, Raldh2, or Raldh3) catalyze the synthesis of RA from retinaldehyde (Maden, 2007). Since the retinaldehyde dehydrogenases generate the tissue and region-specific patterns of RA synthesis, their spatio-temporal expression is carefully regulated during development (Duester, 2008). These enzymes also have non-overlapping, required roles in generating RA during embryogenesis, as individual genetic knockout of these enzymes results in unique, tissue-specific phenotypic deficits (Duester, 2008). Some cells express cellular retinoic acid binding proteins, Crabp1 and Crabp2. Although the function of these proteins in the RA signaling pathway is not completely resolved, it is considered that Crabp1 binds RA and sequesters it in the cytoplasm while Crapb2 binds RA and transports it to the nucleus (Napoli, 2012). Within the nucleus, RA binds a pair of nuclear receptors

from the RAR and RXR families, which collectively binds as a transcription factor complex to DNA sequences called retinoic acid response elements (RARE), which then recruits other transcriptional co-activators or co-repressors to modulate target gene expression.

RA signaling is turned off by the cytoplasmic actions of the cytochrome p450 family 26 class of enzymes, of which there are three members: Cyp26a1, Cyp26b1, and Cyp26c1. These enzymes are uniquely required to catalyze the degradation of RA into inactivate metabolites, and similar to the Raldh enzymes, have distinct expression domains during embryonic development to regulate RA activity (Maden, 2007).

Retinoid gradients are involved in patterning numerous tissues during vertebrate development, including the spinal cord, heart, somites, and eyes (Duester, 2008). Morphogenetic gradients are established between localized sources (regions of synthesis) and sinks (regions of degradation) (Rogers and Schier, 2011). In conformation to this classical model, robust RA morphogenetic gradients are similarly achieved through juxtaposed expression patterns of RA synthesizing (Raldh) and degrading (Cyp26) enzymes (Reijntjes et al., 2004; Schilling et al., 2012).

As an illustrative example, the A-P axis of the developing hindbrain is patterned by a spatial RA gradient, which is established between a region of posterior mesoderm that expresses Raldh2 and a region of anterior mesoderm that expresses Cyp26c1 (Glover et al., 2006; Niederreither and Dolle, 2008; Reijntjes et al., 2004). The hindbrain develops from the caudal neural ectoderm,

which becomes transiently segmented into seven rhombomeres, numbered r1 through r7 from anterior to posterior. During hindbrain specification, the boundaries of expression for these RA regulatory enzymes shift caudally during embryogenesis, such that the RA gradient temporally becomes superimposed upon more posterior regions of the neural ectoderm. Posterior hindbrain and rhombomere identity then becomes specified by higher levels of RA than anterior regions as a result of this shifting wave of RA activity (Reijntjes et al., 2004; Sirbu et al., 2005). These shifting boundaries of RA activity also pattern the developing otocyst, which develops adjacent to the 5^{th} and 6^{th} rhombomeres (Bok et al., 2011). Interestingly, although RA synthesizing and degrading enzymes are expressed in cochlear and vestibular tissues, there is limited knowledge on the role of RA signaling in patterning later stages of inner ear development (Romand et al., 2006).

In vitro investigations into tonotopic patterning

In chapter two I describe the role of RA signaling in patterning the HCs along the longitudinal axis of the cochlea during development using an *in vitro* organ culture model (Figure 1-4). This model was chosen to avoid significant potential limitations inherent to an *in vivo* exploration.

The major issue that may arise with an *in vivo* analysis is that even local modulations of RA signaling have the potential to produce indirect effects on cochlear development. RA signaling is involved in the development of the otocyst at stages that precede cochlear formation by several days (Frenz et al.,

2010; Bok et al., 2011). Additionally, studies that modulate RA *in vivo* have resulted in embryonic lethality prior to the stages when the cochlea forms, or have resulted with embryos that develop substantially malformed or absent cochlea (Choo et al., 1998; Niederreither et al., 1999; Kil et al., 2005; Bok et al., 2011). As mentioned in the section above, RA signaling also patterns the posterior hindbrain, which neighbors and influences the development of the inner ear (Lufkin et al., 1991; Represa et al., 1991; White et al., 2000; Glover et al., 2006). Modulating RA levels *in vivo* have the potential to disrupt hindbrain patterning, which also could indirectly affect inner ear development and cochlear patterning.

All these issues can impede a clear analysis of the role RA signaling may play in patterning the tonotopic gradient of cochlear HCs. This organ culture system minimizes the potential impact of such confounding complications. Since cochleae that develop from this model under control conditions form HCs that express the full range of phenotypes and the normal tonotopic pattern of those *in vivo*, this model can be utilized to more directly assess the role of candidate signals in patterning the tonotopic axis of the cochlea.

Summary

The ability to communicate and discern or distinguish sounds from the surrounding environment results primarily from specialization of the cochlea. The cochlea is organized along its tonotopic axis such that HCs are tuned to a particular sound frequency based upon their relative location along the length of

the cochlea. As a result of this tuning, the high sound frequencies are sensed in the proximal end and lower frequencies are sensed progressively more distally. This tonotopic specialization is mediated by the passive properties of the underlying basilar membrane and by the HC phenotypes that systematically vary from point-to-point along this axis of the cochlea. Using the chicken cochlea as a model, this dissertation seeks to significantly advance the field by:

- Identifying factors that may be involved in establishing the location-specific phenotypes of HCs.

- Determining whether candidate signaling pathways influence the development of the location-specific phenotypes.

- Investigating potential mechanisms of how these signals pattern the HCs along the longitudinal axis during development.

References

Alvarez, I.S., and J. Navascues. 1990. Shaping, invagination, and closure of the chick embryo otic vesicle: scanning electron microscopic and quantitative study. *Anat Rec*. 228:315-326.

Bailey, A.P., S. Bhattacharyya, M. Bronner-Fraser, and A. Streit. 2006. Lens specification is the ground state of all sensory placodes, from which FGF promotes olfactory identity. *Dev Cell*. 11:505-517.

Baker, C.V., and M. Bronner-Fraser. 2001. Vertebrate cranial placodes I. Embryonic induction. *Dev Biol*. 232:1-61.

Bancroft, M., and R. Bellairs. 1977. Placodes of the chick embryo studied by SEM. *Anat Embryol (Berl)*. 151:97-108.

Bissonnette, J.P., and D.M. Fekete. 1996. Standard atlas of the gross anatomy of the developing inner ear of the chicken. *J Comp Neurol*. 368:620-630.

Bok, J., W. Chang, and D.K. Wu. 2007a. Patterning and morphogenesis of the vertebrate inner ear. *Int J Dev Biol*. 51:521-533.

Bok, J., D.K. Dolson, P. Hill, U. Ruther, D.J. Epstein, and D.K. Wu. 2007b. Opposing gradients of Gli repressor and activators mediate Shh signaling along the dorsoventral axis of the inner ear. *Development*. 134:1713-1722.

Bok, J., S. Raft, K.A. Kong, S.K. Koo, U.C. Drager, and D.K. Wu. 2011. Transient retinoic acid signaling confers anterior-posterior polarity to the inner ear. *Proc Natl Acad Sci U S A*. 108:161-166.

Brugmann, S.A., P.D. Pandur, K.L. Kenyon, F. Pignoni, and S.A. Moody. 2004. Six1 promotes a placodal fate within the lateral neurogenic ectoderm by functioning as both a transcriptional activator and repressor. *Development*. 131:5871-5881.

Burns, J.C., and J.T. Corwin. 2013. A historical to present-day account of efforts to answer the question: "what puts the brakes on mammalian hair cell regeneration?". *Hear Res*. 297:52-67.

Cantos, R., L.K. Cole, D. Acampora, A. Simeone, and D.K. Wu. 2000. Patterning of the mammalian cochlea. *Proc Natl Acad Sci U S A*. 97:11707-11713.

Choo, D., J.L. Sanne, and D.K. Wu. 1998. The differential sensitivities of inner ear structures to retinoic acid during development. *Developmental Biology*. 204:136-150.

Cotanche, D.A., and C.L. Kaiser. 2010. Hair cell fate decisions in cochlear development and regeneration. *Hear Res*. 266:18-25.

Cotanche, D.A., and K.K. Sulik. 1984. The development of stereociliary bundles in the cochlear duct of chick embryos. *Brain Res*. 318:181-193.

Duester, G. 2008. Retinoic acid synthesis and signaling during early organogenesis. *Cell*. 134:921-931.

Frenz, D.A., W. Liu, A. Cvekl, Q. Xie, L. Wassef, L. Quadro, K. Niederreither, M. Maconochie, and A. Shanske. 2010. Retinoid signaling in inner ear development: A "Goldilocks" phenomenon. *Am J Med Genet A*. 152A:2947-2961.

Frishkopf, L.S., and D.J. DeRosier. 1983. Mechanical tuning of free-standing stereociliary bundles and frequency analysis in the alligator lizard cochlea. *Hear Res*. 12:393-404.

Glover, J.C., J.S. Renaud, and F.M. Rijli. 2006. Retinoic acid and hindbrain patterning. *Journal of neurobiology*. 66:705-725.

Haddon, C., and J. Lewis. 1996. Early ear development in the embryo of the zebrafish, Danio rerio. *J Comp Neurol*. 365:113-128.

Hamburger, V., and H. Hamilton. 1951. A series of normal stages in the development of the chick embryo. *J Morphol*. 88:49-92.

Heller, N., and A.W. Brandli. 1999. Xenopus Pax-2/5/8 orthologues: novel insights into Pax gene evolution and identification of Pax-8 as the earliest marker for otic and pronephric cell lineages. *Dev Genet*. 24:208-219.

Holton, T., and A.J. Hudspeth. 1983. A micromechanical contribution to cochlear tuning and tonotopic organization. *Science*. 222:508-510.

Hudspeth, A.J. 1989. How the ear's works work. *Nature*. 341:397-404.

Jacobson, A.G. 1963. The Determination and Positioning of the Nose, Lens and Ear. I. Interactions within the Ectoderm, and between the Ectoderm and Underlying Tissues. *J Exp Zool*. 154:273-283.

Jayasena, C.S., T. Ohyama, N. Segil, and A.K. Groves. 2008. Notch signaling augments the canonical Wnt pathway to specify the size of the otic placode. *Development*. 135:2251-2261.

Katayama, A., and J.T. Corwin. 1989. Cell production in the chicken cochlea. *J Comp Neurol*. 281:129-135.

Ketten, D.R. 2000. Cetacean ears. *In* Hearing by Whales and Dolphins. W.W.L.A. (Ed.), editor. Springer-Verlag, New York. 43-109.

Kiernan, A.E., K.P. Steel, and D.M. Fekete. 2002. Development of the mouse inner ear. *In* Mouse Development: Patterning Morphogenesis and Organogenesis. J. Rossant and P. Tam, editors. Academic Press, San Diego, CA. 539-566.

Kil, S.H., A. Streit, S.T. Brown, N. Agrawal, A. Collazo, M.H. Zile, and A.K. Groves. 2005. Distinct roles for hindbrain and paraxial mesoderm in the

induction and patterning of the inner ear revealed by a study of vitamin-A-deficient quail. *Dev Biol*. 285:252-271.

Kozlowski, D.J., T. Murakami, R.K. Ho, and E.S. Weinberg. 1997. Regional cell movement and tissue patterning in the zebrafish embryo revealed by fate mapping with caged fluorescein. *Biochem Cell Biol*. 75:551-562.

Lufkin, T., A. Dierich, M. LeMeur, M. Mark, and P. Chambon. 1991. Disruption of the Hox-1.6 homeobox gene results in defects in a region corresponding to its rostral domain of expression. *Cell*. 66:1105-1119.

Ladhams, A., and J.O. Pickles. 1996. Morphology of the monotreme organ of Corti and macula lagena. *J Comp Neurol*. 366:335-347.

Ladher, R.K., T.J. Wright, A.M. Moon, S.L. Mansour, and G.C. Schoenwolf. 2005. FGF8 initiates inner ear induction in chick and mouse. *Genes Dev*. 19:603-613.

Lim, D.J. 1980. Cochlear anatomy related to cochlear micromechanics. A review. *J Acoust Soc Am*. 67:1686-1695.

Lim, D.J. 1986. Functional structure of the organ of Corti: a review. *Hear Res*. 22:117-146.

Litsiou, A., S. Hanson, and A. Streit. 2005. A balance of FGF, BMP and WNT signalling positions the future placode territory in the head. *Development*. 132:4051-4062.

Maden, M. 2007. Retinoic acid in the development, regeneration and maintenance of the nervous system. *Nat Rev Neurosci*. 8:755-765.

Mann, Z.F., and M.W. Kelley. 2011. Development of tonotopy in the auditory periphery. *Hearing research*. 276:2-15.

Meyers, J.R., and J.T. Corwin. 2008. Morphological Correlates of Regeneration and Repair in the Inner Ear. *In* Hair Cell Regeneration, Repair, and Protection. Vol. 33. R.J. Salvi, A.N. Popper, and R.R. Fay, editors. Springer Handbook of Auditory Research. 39-75.

Miranda-Rottmann, S., A.S. Kozlov, and A.J. Hudspeth. 2010. Highly specific alternative splicing of transcripts encoding BK channels in the chicken's cochlea is a minor determinant of the tonotopic gradient. *Mol Cell Biol*. 30:3646-3660.

Mishima, N., and S. Tomarev. 1998. Chicken Eyes absent 2 gene: isolation and expression pattern during development. *Int J Dev Biol*. 42:1109-1115.

Napoli, J.L. 2012. Physiological insights into all-trans-retinoic acid biosynthesis. *Biochim Biophys Acta*. 1821:152-167.

Niederreither, K., and P. Dolle. 2008. Retinoic acid in development: towards an integrated view. *Nature reviews. Genetics*. 9:541-553.

Niederreither, K., V. Subbarayan, P. Dollé, and P. Chambon. 1999. Embryonic retinoic acid synthesis is essential for early mouse post-implantation development. *Nat Genet*. 21:444-448.

Ohyama, T., and A.K. Groves. 2004. Generation of Pax2-Cre mice by modification of a Pax2 bacterial artificial chromosome. *Genesis*. 38:195-199.

Ohyama, T., O.A. Mohamed, M.M. Taketo, D. Dufort, and A.K. Groves. 2006. Wnt signals mediate a fate decision between otic placode and epidermis. *Development*. 133:865-875.

Ramanathan, K., T.H. Michael, G.J. Jiang, H. Hiel, and P.A. Fuchs. 1999. A molecular mechanism for electrical tuning of cochlear hair cells. *Science*. 283:215-217.

Reijntjes, S., E. Gale, and M. Maden. 2004. Generating gradients of retinoic acid in the chick embryo: Cyp26C1 expression and a comparative analysis of the Cyp26 enzymes. *Dev Dyn*. 230:509-517.

Represa, J., Y. Leon, C. Miner, and F. Giraldez. 1991. The int-2 proto-oncogene is responsible for induction of the inner ear. *Nature*. 353:561-563.

Riccomagno, M.M., S. Takada, and D.J. Epstein. 2005. Wnt-dependent regulation of inner ear morphogenesis is balanced by the opposing and supporting roles of Shh. *Genes Dev*. 19:1612-1623.

Rogers, K.W., and A.F. Schier. 2011. Morphogen gradients: from generation to interpretation. *Annual review of cell and developmental biology*. 27:377-407.

Schilling, T.F., Q. Nie, and A.D. Lander. 2012. Dynamics and precision in retinoic acid morphogen gradients. *Curr Opin Genet Dev*. 22:562-569.

Schlosser, G. 2006. Induction and specification of cranial placodes. *Dev Biol*. 294:303-351.

Schlosser, G., and K. Ahrens. 2004. Molecular anatomy of placode development in Xenopus laevis. *Dev Biol*. 271:439-466.

Seldran, F., S. Gallego, C. Micheyl, E. Veuillet, E. Truy, and H. Thai-Van. 2011. Relationship between age of hearing-loss onset, hearing-loss duration, and speech recognition in individuals with severe-to-profound high-frequency hearing loss. *J Assoc Res Otolaryngol*. 12:519-534.

Sirbu, I.O., L. Gresh, J. Barra, and G. Duester. 2005. Shifting boundaries of retinoic acid activity control hindbrain segmental gene expression. *Development*. 132:2611-2622.

Streit, A. 2002. Extensive cell movements accompany formation of the otic placode. *Dev Biol*. 249:237-254.

Streit, A. 2004. Early development of the cranial sensory nervous system: from a common field to individual placodes. *Dev Biol*. 276:1-15.

Tanaka, K., and C.A. Smith. 1978. Structure of the chicken's inner ear: SEM and TEM study. *Am J Anat*. 153:251-271.

Tilney, L.G., D.A. Cotanche, and M.S. Tilney. 1992. Actin filaments, stereocilia and hair cells of the bird cochlea. VI. How the number and arrangement of stereocilia are determined. *Development*. 116:213-226.

Tilney, L.G., and J.C. Saunders. 1983. Actin filaments, stereocilia, and hair cells of the bird cochlea. I. Length, number, width, and distribution of stereocilia of each hair cell are related to the position of the hair cell on the cochlea. *J Cell Biol*. 96:807-821.

Tilney, L.G., M.S. Tilney, and D.A. Cotanche. 1988. Actin filaments, stereocilia, and hair cells of the bird cochlea. V. How the staircase pattern of stereociliary lengths is generated. *J Cell Biol*. 106:355-365.

Tilney, L.G., M.S. Tilney, J.S. Saunders, and D.J. DeRosier. 1986. Actin filaments, stereocilia, and hair cells of the bird cochlea. III. The development and differentiation of hair cells and stereocilia. *Dev Biol*. 116:100-118.

Turner, C.W. 2006. Hearing loss and the limits of amplification. *Audiol Neurootol*. 11 Suppl 1:2-5.

Vater, M., and M. Kossl. 2011. Comparative aspects of cochlear functional organization in mammals. *Hear Res*. 273:89-99.

Von Bekesy, G. 1960. Experiments in Hearing. McGraw Hill, New York.

Warren, W.C., L.W. Hillier, J.A. Marshall Graves, E. Birney, C.P. Ponting, F. Grutzner, K. Belov, W. Miller, L. Clarke, A.T. Chinwalla, S.P. Yang, A. Heger, D.P. Locke, P. Miethke, P.D. Waters, F. Veyrunes, L. Fulton, B. Fulton, T. Graves, J. Wallis, X.S. Puente, C. Lopez-Otin, G.R. Ordonez, E.E. Eichler, L. Chen, Z. Cheng, J.E. Deakin, A. Alsop, K. Thompson, P. Kirby, A.T. Papenfuss, M.J. Wakefield, T. Olender, D. Lancet, G.A. Huttley, A.F. Smit, A. Pask, P. Temple-Smith, M.A. Batzer, J.A. Walker, M.K. Konkel, R.S. Harris, C.M. Whittington, E.S. Wong, N.J. Gemmell, E. Buschiazzo, I.M. Vargas Jentzsch, A. Merkel, J. Schmitz, A. Zemann, G. Churakov, J.O. Kriegs, J. Brosius, E.P. Murchison, R. Sachidanandam, C. Smith, G.J. Hannon, E. Tsend-Ayush, D. McMillan, R. Attenborough, W. Rens, M. Ferguson-Smith, C.M. Lefevre, J.A. Sharp, K.R. Nicholas, D.A. Ray, M. Kube, R. Reinhardt, T.H. Pringle, J. Taylor, R.C. Jones, B. Nixon, J.L. Dacheux, H. Niwa, Y. Sekita, X. Huang, A. Stark, P. Kheradpour, M.

Kellis, P. Flicek, Y. Chen, C. Webber, R. Hardison, J. Nelson, K. Hallsworth-Pepin, K. Delehaunty, C. Markovic, P. Minx, Y. Feng, C. Kremitzki, M. Mitreva, J. Glasscock, T. Wylie, P. Wohldmann, P. Thiru, M.N. Nhan, C.S. Pohl, S.M. Smith, S. Hou, M. Nefedov, et al. 2008. Genome analysis of the platypus reveals unique signatures of evolution. *Nature*. 453:175-183.

White, J.C., M. Highland, M. Kaiser, and M. Clagett-Dame. 2000. Vitamin A deficiency results in the dose-dependent acquisition of anterior character and shortening of the caudal hindbrain of the rat embryo. *Dev Biol*. 220:263-284.

Wright, T.J., and S.L. Mansour. 2003. Fgf3 and Fgf10 are required for mouse otic placode induction. *Development*. 130:3379-3390.

Wu, D.K., and S.H. Oh. 1996. Sensory organ generation in the chick inner ear. *J Neurosci*. 16:6454-6462.

Wu, L.Q., and J.D. Dickman. 2012. Neural correlates of a magnetic sense. *Science*. 336:1054-1057.

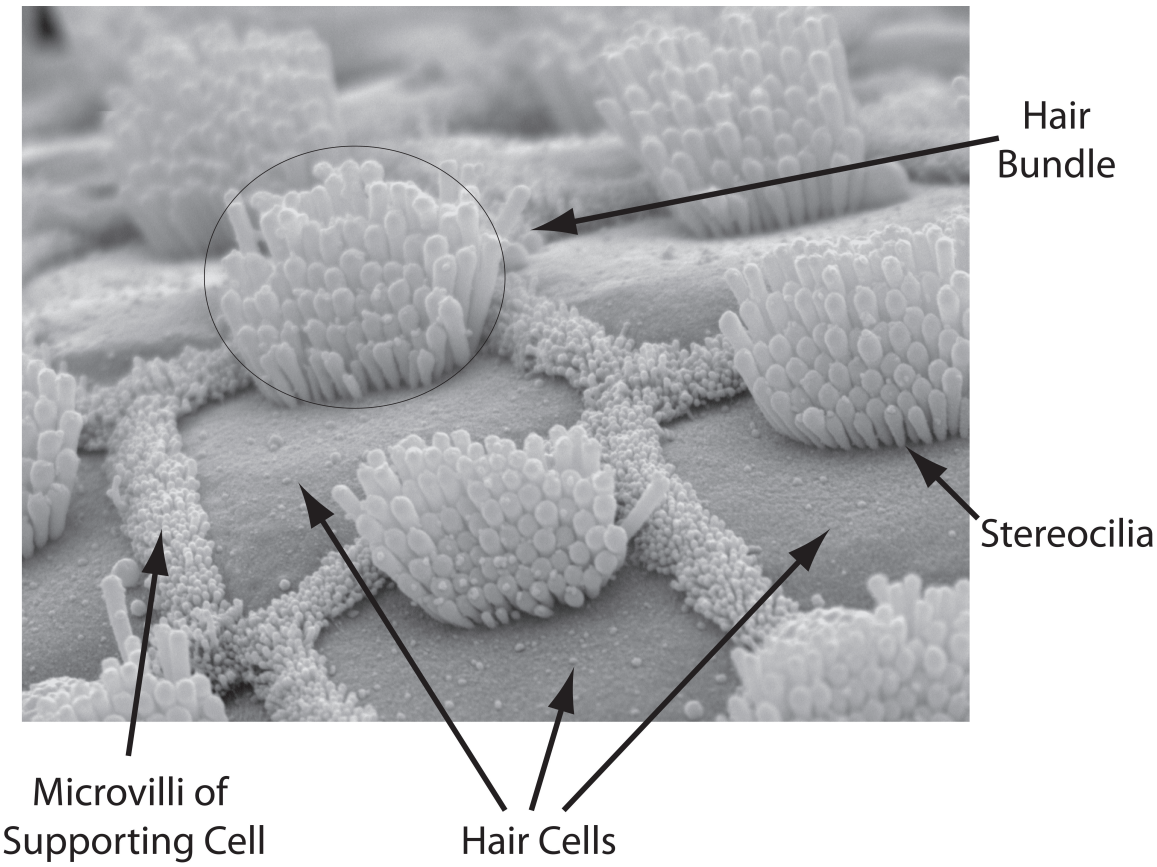

Figure 1-1. High magnification scanning electron micrograph (SEM) taken from the apical surface of a chicken cochlea showing the hair bundles of auditory hair cells. These bundles are composed of filamentous actin-rich stereocilia organized in a staircase array. The hair cells are surrounded by a honeycomb-like pattern of microvilli on the surfaces of supporting cells.

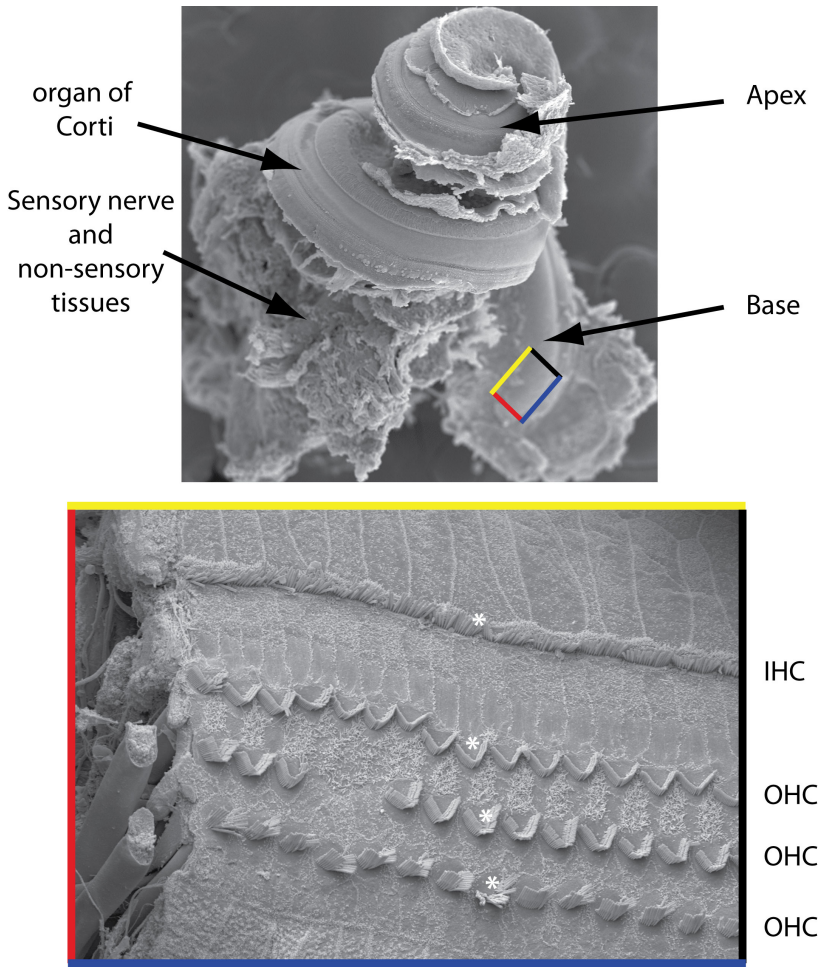

Figure 1-2. The mammalian cochlea contains a coiled organ of Corti with four ordered rows of sensory hair cells. Top: Scanning electron micrograph (SEM) of a P4 mouse cochlea where non-sensory regions have been removed to afford a view of the sensory epithelium. The overlaid rectangle depicts the representative orientation and relative region where the higher magnification image on the bottom was taken from. Bottom: SEM image of a P7 guinea pig cochlea showing the four ordered rows of hair cells that are arranged along the longitudinal axis in mammals (marked with *). The top row is the inner hair cells (IHC) and the bottom three rows are the outer hair cells (OHC). IHCs and OHCs in mammals have different functions and roles in auditory perception.

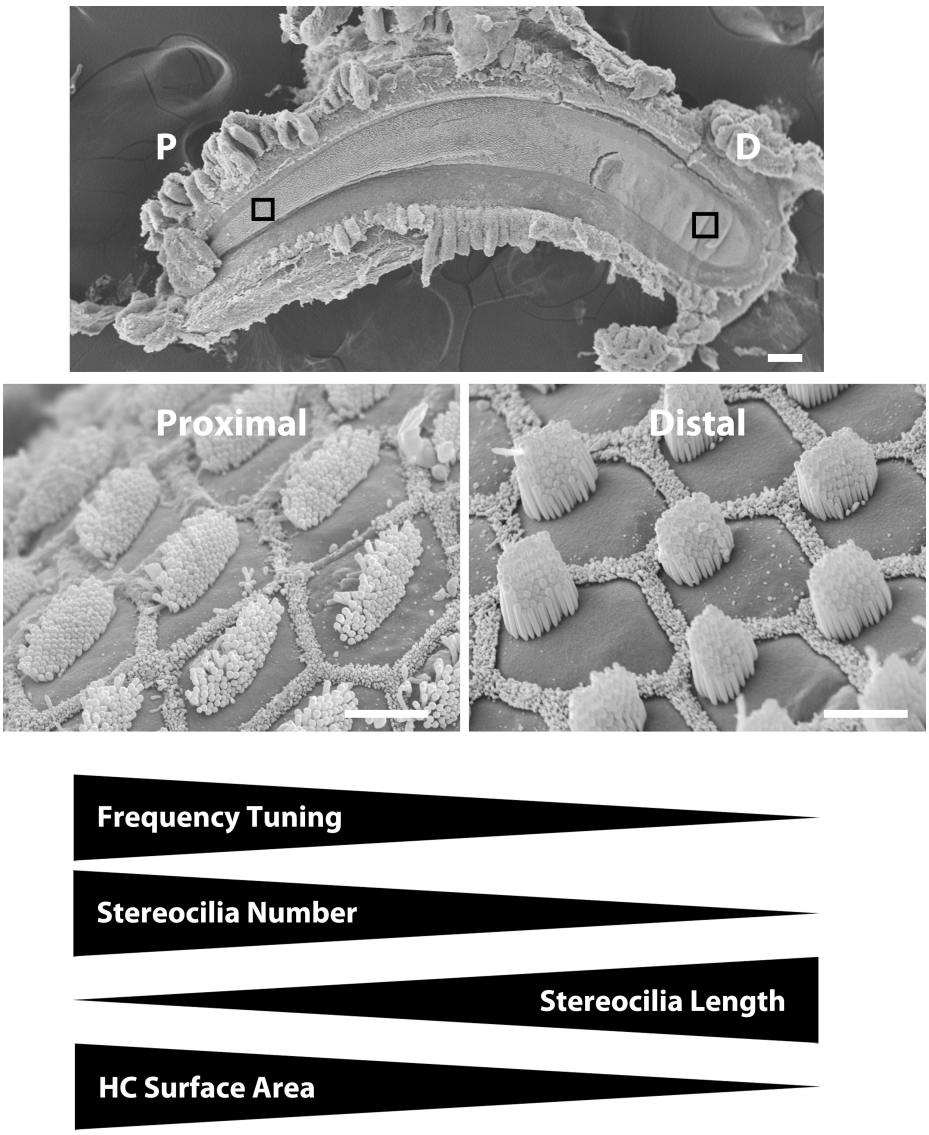

Figure 1-3. Hair cells in the chicken cochlea develop a gradient of >100 individually distinct phenotypes extending from the proximal high-frequency-sensitive end to the distal low-frequency-sensitive end of the BP sensory epithelium. Top: Scanning electron micrograph (SEM) image showing the BP sensory epithelium, which is narrow and tapered at the proximal end (P) and broadens at more distal regions (D). Black rectangles depict the relative regions where the higher magnification images shown in the middle were taken from. Scale bar 100 μm. Middle: SEM images showing the short and numerous

mechanosensory stereocilia that project from the apical surfaces of proximal HCs and the taller stereocilia in distal HCs. Scale bars 5 μm. Bottom: There are several gradients of HC phenotypes that systematically vary along the tonotopic axis of the chicken cochlea.

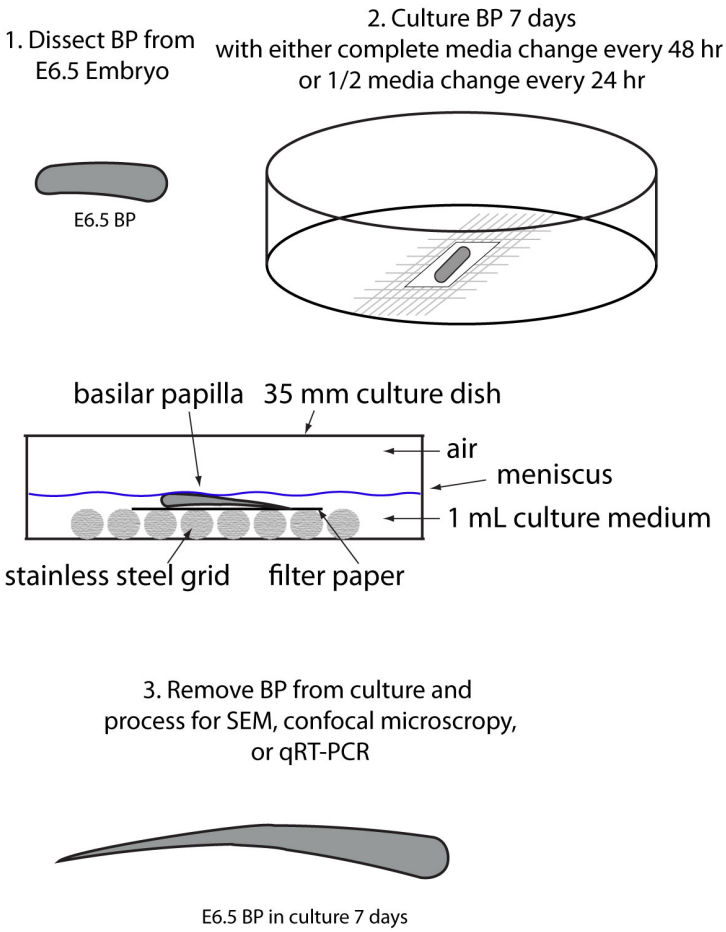

Figure 1-4. Organ culture model. Step 1: Basilar papillae (BP) were dissected from E6.5 chicken embryos (Hamburger Hamilton Stage 29). At this stage, hair cells are beginning to exit the cell cycle and are starting to differentiate. Stereocilia formation has not yet begun. Step 2: Organs were placed nerve-side-down on top of filter paper situated on stainless steel grids in 35 mm dishes containing 1 mL culture medium. This volume formed a meniscus over the BPs. Organ cultures were then maintained at 37ºC in an incubator for 7 days, where complete medium changes were carried out every 48 hr or half medium changes every 24 hr. Step 3: After 7 days, organs were removed and processed for

phenotypic analyses. BPs cultured in control medium formed expected gradients in HC phenotypes.

CHAPTER 2

Retinoic Acid Signaling Regulates the Development of Tonotopically Patterned Hair Cells in the Chicken Cochlea[1]

SUMMARY

Precise frequency discrimination is a hallmark of auditory function in birds and mammals and is required for distinguishing similar sounding words, like “bat,” “cat,” and “hat.” In the cochlea, tuning and spectral separation result from longitudinal differences in basilar membrane stiffness and numerous individual gradations in sensory hair cell phenotypes, but it is unknown what patterns the phenotypes. I used RNA-seq to compare transcriptomes from proximal, middle, and distal regions of the embryonic chicken cochlea, and found opposing longitudinal gradients of expression for retinoic acid (RA) synthesizing and degrading enzymes. *In vitro* experiments showed that RA is necessary and sufficient to induce the development of distal-like hair cell phenotypes and promotes expression of the actin crosslinking proteins, Espin and Fscn2. These and other findings highlight the role that RA signaling plays in patterning the development of a longitudinal gradient of >100 individually distinct, frequency tuned hair cell phenotypes in the cochlea.

[1] This chapter is submitted for peer-review at the time of writing this dissertation. It has been re-formatted to match the terminology and style within this dissertation.

INTRODUCTION

In the elongated cochleae of birds and mammals, sound stimulation causes peaks of vibration at different longitudinal positions extending from the high-frequency-sensitive proximal end to the low-frequency-sensitive distal end (Mann and Kelley, 2011). Hair cells (HCs) in these cochleae exhibit longitudinal variations in their physiological properties and striking differences in the number and length of actin-filled stereocilia that make up their apical mechanoreceptive hair bundles. In the chicken cochlea's basilar papilla (BP) sensory epithelium, hair bundles at the proximal, high-frequency-sensitive end contain >250 stereocilia that reach a maximum length of 1.5 μm, while those in the distal, low-frequency-sensitive end contain <50 stereocilia with a maximum length of 5.5 μm (Fig. 2-1a,b,c) (Tilney and Saunders, 1983; Tilney et al., 1992). At locations between those ends, the number and length of the tallest stereocilia vary progressively and often from cell to cell. Similar spatial gradients occur in the mammalian cochlea (Lim, 1980, 1986), and differences in bundle phenotypes have physiological consequences. Short, broad hair bundles respond best to high frequencies, while longer bundles respond best to low frequencies (Frishkopf and DeRosier, 1983; Holton and Hudspeth, 1983).

The tonotopic (longitudinally frequency-tuned) gradients in HC phenotypes form even in cochleae derived from otocysts that have been denervated after 3 days of incubation (E3) (Corwin and Cotanche, 1989; Swanson et al., 1990). Yet, the signals that pattern the phenotypes are unknown. Hypothesizing that morphogen levels might differ as the gradient of phenotypes developed, I

sequenced the transcriptomes of the proximal, middle, and distal thirds of the chicken cochlea at E6.5, when postmitotic HCs first form (Katayama and Corwin, 1989). Of >1000 differentially expressed genes, one involved in the synthesis of RA (*Raldh3*) and one involved in its degradation (*Cyp26c1*) displayed opposing longitudinal gradients of expression. In the developing retina and hindbrain, morphogenetic gradients of RA are established and confined between regions of high Raldh and Cyp26 expression (Reijntjes et al., 2004; Schilling et al., 2012), and such gradients play crucial roles in patterning the anterior-posterior axis of the early embryo, the spinal cord, and the early otocyst (E2-E3) (Maden, 2007; Duester, 2008; Bok et al., 2011; Schilling et al., 2012).

To investigate whether RA plays a role in patterning the gradient of HC phenotypes, I developed an *in vitro* model that supports cochlear development, free from potentially confounding influences of most neighboring tissues. Using that model, I found that proximal HCs acquired distal-like phenotypes when they differentiated in the presence of exogenous RA, and distal HCs developed proximal-like phenotypes when they differentiated in the presence of RA antagonists. These, and other findings, show that RA signaling is both necessary and sufficient for the specification of important features of distal-like HC phenotypes.

MATERIALS AND METHODS

Embryonic Basilar Papilla Dissection

White Leghorn chicken embryos (Spafas) were incubated at 38-39^{o} C in a humidified chamber with turning. Embryos were removed from the shell,

transferred to DMEM/F-12 at 4°C under sterile conditions, staged according to Hamburger and Hamilton (Hamburger and Hamilton, 1951), and then decapitated. Throughout the text, the embryonic age at the time of dissection is given (i.e. E6.5, E8, E10, and E13), but experiments with E6.5 embryos were carried out only using embryos at stage 29, E8 at stage 34, E10 at stage 36, and E13.5 at stage 39.

All subsequent dissections and harvesting were performed under aseptic conditions while the tissue was held at 4°C on the dissection microscope. A transverse cut posterior to the midbrain and eyes was made to bisect the head, leaving the inner ears in the posterior portion. The skin, dorsal cranium, and brain were removed to allow visualization of the cochlear ducts that lie in the base of the skull, projecting ventromedially. The mandible was removed and the cochlear ducts were dissected from a ventral approach using fine forceps. Connective tissues were teased away with fine forceps and the proximal attachment to the remainder of the labyrinth was cut off using a sapphire knife. The cochlear and lagena nerve branches were trimmed off using a sapphire knife and fine forceps.

Organ Culture

Explants were cultured nerve-side-down on nucleopore filters atop stainless steel grids (Small Parts Inc., Seattle, WA) in 35 mm dishes with 1 mL DMEM/F-12 containing 1% FBS, 0.25 µg/mL Fungizone (Invitrogen) and 10 µg/mL Ciprofloxacin (Bayer, Berlin, Germany). Either complete medium changes

were made every 2 days or half the medium was changed every 24 h. Explants were cultured with 500 nM all-*trans* retinoic acid (Sigma), 5 μM citral (Sigma), 10 μM BMS 493 (Tocris Bioscience), 400 ng/mL Bmp7 (R&D Systems), 100 ng/mL Noggin (R&D Systems), or with 0.1% DMSO vehicle as a control.

RNA extraction and quantitative PCR

RNA was extracted using the RNAqueous kit (Ambion) according to the manufacturer's protocol and was reverse transcribed using a High Capacity RNA-to-cDNA kit (Applied Biosystems). Quantitative PCR was performed in triplicates using a SensiMix SYBR Green and Fluorescein kit (Quantace) on a MyIQ/iCycler (Biorad). The number of times each experiment was independently replicated is indicated throughout the results. Gene expression was analyzed using the Real-time PCR miner algorithm (Zhao and Fernald, 2005). *Rplp0* was used as an endogenous reference (Forward: GCTTTGTGTTCACCAAGGAG; Reverse: GTCACATCACAGGGAGCAAT). Gene-specific primer sets were used as described for *Kcnbm1* (Bai et al., 2011) (Forward: ACATGAGCGTGGGCCAAAGGA; Reverse: CCCCGGCAACTCCGAGAACG). Other primers used were *Aldh1a2 (Raldh2)* (Forward: AGATCCTGCCGCTCTGATGGC; Reverse: GCGAGCTGCTCTCACTGCCTT), *Aldh1a3 (Raldh3)* (Forward: ACGGCCTCTGAGGGGTTTGGA; Reverse: TGCTGCCTTTGCTGCTTCCAC), *Espin* (Forward: ATCTACGTGCAGGCCAAGAA; Reverse: GTAGTAGTCACCTGTGCTCGG), *Cyp26b1* (Forward: TAAGGACTACGCCGATGCAC; Reverse:

CGAAGATGAGCTCCAGGGTG), *Cyp26c1* (Forward: TTCTGCTGGGACTCCGTCTGGAG; Reverse: ATGCAGCATGTCCCGTGCTTTGA), *Pls1* (Forward: CTCCCTGGTCGGTATTGCTG; Reverse: ACCCTCTCCAAGGTCTGACA), *Pls3* (Forward: AAAAAGTTGCCAGGCACTCG; Reverse: AGATCGCATGGTGACAGCC), *Fscn2* (Forward: AACGGCAGATTCGTCTCCAT; Reverse: GCGCCACTCGATGTCAAACA), *RXRg* (Forward: TCATTAAGTTTCCTGCGGGCT; Reverse: TGGATGATGGGCTCACAGAC), *RARa* (Forward: CAGAAGTGCTTCGAGGTCGG; Reverse: TTCGGCACGTCCTTCTTCTT), *RARb* (Forward: GTGTCAGTGCTTGTGAGGGA; Reverse: TGCAGTACTGGCAGCGATTT) and *Bmp7* (Forward: TGGTCATGAGCTTCGTCAAC; Reverse: CCTCTGGGATTCTGGAGAGA).

Next-Gen Sequencing

RNA Preparation

Three samples were collected from each cochlear duct by cutting the duct into three approximately equal sized pieces to produce proximal, middle, and distal pieces. Each sample contained a portion of the future tegmentum vasculosum and the basilar papilla sensory epithelium. The distal piece also contained region of the future lagena. The pieces were immediately transferred into three 1.5 mL eppendorf tubes containing 0.5 mL Tri Reagent RT (Molecular

Research Center, Inc., Cincinnati, OH) and kept on ice until all pieces were collected. The samples were stored at -20°C until further processing.

Samples from each section of the basillar papilla were processed using Illumina mRNA-seq or TrueSeq preparation kits. Separate biological replicates were also prepared and similarly analyzed. In brief, mRNA was selected by oligo-dT magnetic beads and fragmented. First-strand cDNA was generated using random primers. Second-strand synthesis, end repair, addition of a single A base and adaptor ligation were then performed. Each RNA-seq library was DNA sequenced using either the Illumina Genome Analyzer IIx or HiSeq 2000.

RNA-Seq data analyses

Raw reads in FASTQ format were aligned to the Ensembl *Gallus gallus* reference genome (WUGSC2.1) using Tophat v1.4.0 (Trapnell et al., 2009). The output .bam file was processed by Partek Genomics Suite v6.6 (Partek Inc., St. Louis, MO) to assemble reads into transcripts and estimate their abundances. A gene model data set combining Ensembl and NCBI annotations was used to generate RPKM (Reads Per Kilobase of exon per Million fragments mapped) for known genes and potential novel transcripts. Statistical significance levels were calculated by one-way analysis of variance (ANOVA). Reads mapped to different isoforms of a given gene were combined for analysis. At least one region of the basilla papilla (proximal, middle or distal) was required to be ≥ 0.5 RPKM. A fold-change of ≥2 was imposed for the comparison between distal and proximal regions. An additional filter was imposed where middle samples had to

exhibit RPKM values intermediate between the two ends of the basilla papilla in order to selectively capture transcripts that exhibit a gradient between the two ends. Gene lists from clustering analysis were uploaded to g:Profiler and analyzed by gene group functional profiling (Reimand et al., 2011). Pathways that were predicted from g:Profilers database of literature-supported interaction datasets were visualized by Cytoscape (Smoot et al., 2011).

Ingenuity Pathway Analysis

Ingenuity Pathway Analyses (IPA) was performed as described to discover potential upstream activators (Viljoen and Blackburn, 2013). The dataset containing both the list of genes that are differentially expressed between the E6.5 proximal and distal thirds of the cochlea, and the fold-change difference in those genes that are expressed between the proximal and distal ends, was uploaded to IPA. The IPA Upstream Regulator analytic was then performed, which generated a list of 747 potential upstream transcriptional regulators that may be involved in establishing the differences in gene expression between the proximal and distal ends of the E6.5 BP. Potential regulators were ranked based upon absolute activation Z-scores, and the top ten most significant potential regulators are shown in Table 2-4.

Retinoic Acid Reporter Cell Line

The RARE reporter cell line F9-RARE-LacZ, which has a retinoic acid response element (RARE) driving *LacZ* expression, was obtained from Tuanlian

Luo (Harvard University) (Wagner et al., 1992). Cells were grown to confluence in 0.1% gelatin-coated 24-well plates in DMEM/F-12 containing 10% FBS, 0.5 mg/mL G418, 0.25 µg/ml Fungizone and 10 µg/ml Ciprofloxacin. Immediately prior to co-culturing with cochlea, the medium was changed to DMEM/F-12 containing 1% FBS, 0.25 µg/mL Fungizone and 10 µg/mL Ciprofloxacin. E10 cochleae were dissected, the tegmentum vasculosum was carefully removed with fine forceps, and the nerve was trimmed with a sapphire blade. The lagena maculae were then cut away using a sapphire blade and the non-sensory regions of the cochlea were trimmed close to the sensory epithelium. BPs were then cut in half to produce proximal and distal segments. Retinal tissue from E10 embryos was also isolated and used as a positive control tissue. Proximal and distal cochlea segments and retina epithelium were plated on top of the reporter cells and maintained at 37°C. RARE-LacZ cells in some wells were exposed to media that were supplemented with 5 nM RA or 100 nM RA. After 12 hrs in culture, the samples were fixed in 1% glutaraldehyde in 0.1M PBS for 15 minutes at room temperature (RT), washed three times with 0.1M PBS containing 0.1% deoxycholate, 0.2% NP-40, and 2 mM $MgCl_2$, and then X-Gal stained overnight at 37ºC (1 mg/mL 5-bromo-4-chloro-3-indolyl-B-D-galacto-pyranoside with 5 mM potassium ferricyanide and 5 mM potassium ferrocyanide at pH 7.3 in 0.1 M PBS and with 0.1% deoxycholate, 0.2% NP-40, and 2 mM $MgCl_2$). Brightfield images were acquired using an Olympus SZX12 stereomicroscope.

Immunohistochemistry

The primary antibodies used were: rabbit anti-Raldh3 (Aldh1a3; Abgent), rabbit anti-pan-Espin (generous gift from Dr. James Bartles, Northwestern University), rabbit anti-RXR-gamma (Abgent), and the monoclonal antibody HCS-1. Rabbit anti-RFP (Rockland Immunochemicals) was used as a negative control. The RXR-gamma, HCS-1, and Espin antibodies recognize those antigens in chicken tissue. The Raldh3 antibody was tested via Western blotting of chicken kidney tissue and it labeled a band at 56 kDa, the expected size for Raldh3 protein (Fig. 2-1f).

Explants were fixed in 4% paraformaldehyde in PBS for 25 minutes at room temperature. Then the tegmentum vasculosum and the tectorial membrane was removed. Samples were then blocked at RT for 1 h in PBS/0.02% Triton X-100 (PBST) containing 10% normal goat serum (Vector Laboratories), then incubated overnight in primary antibodies, followed by incubation with Alexa Fluor-conjugated secondary antibodies (Invitrogen). Samples were mounted in SlowFade (Invitrogen) and images were taken with Zeiss LSM 510 or Zeiss LSM 710 confocal microscopes.

Immunoblots

Eight cochleae from E6.5, E10 and E18 embryos were dissected as described above. Proximal and distal tissues were then separately pooled and analyzed through immunoblotting with the rabbit antibody against Raldh3. Kidney from E18 chicken embryos was used as a positive control. Organs were homogenized in reducing SDS-PAGE sample buffer, heated to 70°C for 15 min and

microcentrifuged for 30 sec to remove insoluble debris. Protein was resolved with Bis-Tris SDS PAGE gel (Novex 4-12%, Invitrogen and TGX gels from Bio-Rad), transferred to PVDF membranes and stained with India Ink. Blots were blocked in blocking buffer (ECL primer blocking reagent, GE Healthcare) for 1 h and probed with goat anti-rabbit Aldh1a3 primary antibody (Abgent; 1:000) in blocking buffer overnight at RT. β-actin was used as a loading control. The next day, blots were washed four times for 5 min with PBS/0.3% Tween 20 then incubated with HRP-conjugated secondary antibodies (Cell Signaling Technology) for 1 h at RT. Bands were then visualized with ECL reagent (GE Healthcare). Chemiluminescence was detected using an ImageQuant LAS4000 mini imager (GE Healthcare), and band intensity was measured and normalized against the average intensity of the actin band using ImageJ densitometry software analysis. Raldh3 levels were normalized to actin values from the same lane. Each experiment was independently analyzed three times.

Scanning Electron Microscope

Immediately prior to fixation, the tegmentum vasculosum was carefully opened with fine forceps and the tectorial membrane was pulled away to expose the sensory epithelium. Cultures were fixed in 2.5% glutaraldehyde in 0.10 M cacodylate buffer and 2 mM $CaCl_2$ at pH 7.35 for 2 h at RT. After postfixation in 1% OsO4 in the same buffer for 1 h at RT, the tissue was washed in cacodylate buffer and processed by the Osmium-Thiocarbohydrazide-Osmium method (Davies and Forge, 1987). Cochleae were then dehydrated through a graded ethanol series, critical point dried, mounted on stubs, and sputter coated with

gold palladium. Samples were examined in either a JEOL 6400 or Zeiss Sigma VP HD field emission scanning electron microscope.

Analysis

Stereocilia Number

Scanning electron micrographs were used to quantify numbers of stereocilia. To characterize the HC phenotypes, I took high magnification SEM images (approximately 20 HCs per image) midway between the inferior (abneural) and superior (neural) edges of the BP. To avoid bias, the regions selected for analysis were chosen from a low magnification view of the BP where HC phenotypes were not distinguishable. The extreme proximal and distal edges and the superior or inferior edges of the BP were avoided in image capture. Once regions were selected, high magnification images were captured from three neighboring fields in the proximal region and three neighboring fields in the distal region (6 images per BP). From each micrograph, all of the stereocilia were counted on at least three HCs. HCs that had any stereocilia blocked from view or stereocilia that were not clearly discernable were excluded.

The quantification was performed blindly. One investigator took high magnification scanning electron micrographs and then coded them. A different investigator performed the stereocilia counts without knowledge of the specific treatment or the region the micrographs were from. Stereocilia counts from the three micrographs were used to determine the average number of stereocilia that formed in HCs from proximal and distal regions of each BP. The dataset was

then decoded and statistically analyzed using one-way ANOVA with Newman-Keuls Post-test (GraphPad Prism).

Length measurements from Confocal Microscopy

Using a 63X 1.4 NA oil-immersion objective, I captured stacks of confocal images from the proximal and distal BP regions with 0.37 μm steps and a 2.0X zoom factor. At least three images from neighboring fields were captured midway between the superior and inferior edges in the BP's proximal and distal regions. Hair bundle lengths were measured from the middle of the hair bundle base to the tip of the tallest stereocilia with the 3D Imaris software (Bitplane). Values were typically measured for 8 hair bundles per image. Stereocilia lengths were then averaged from the micrographs to obtain an average length that formed in HCs from proximal and distal regions for each BP. Tests for statistical significance were conducted with GraphPad Prism 8.0.

Luminal Surface Area

HC luminal surface areas were measured from LSM 510 and LSM 710 confocal micrographs using NIH ImageJ. Tests for statistical significance were conducted with GraphPad Prism 8.0.

Hair cell counts

To count the number of hair cells that formed in the cultured explants, BPs that were cultured for 7 days were fixed as above and then labeled with Alexa

Fluor 488-phalloidin and HCS-1. Low magnification micrographs were taken on a Zeiss 710 confocal microscrope. Hair cells were counted using NIH ImageJ.

Stereocilia Length Measurements from SEM Stereoimaging

For an independent method of measuring stereocilia lengths, I used scanning electron microscopy (SEM) stereoimaging (Lelli et al., 2009). E6.5 BPs were cultured in media containing 500 nM RA, or 5 μM citral or 0.1% DMSO alone for 7 days, then fixed for SEM as described above. To make unbiased selections of sites in the BPs for these measurements, low magnification images of the entire BP were taken to determine the relative positions of regions located midway between the neural and abneural edges and a distance approximately equivalent to 18% of the total length of the BP away from the distal tip and 18% of the total length of the BP away from the proximal tip. Stereopair images from four neighboring fields were then taken at these two regions (proximal and distal) at 15,000X magnifications. The stereocilia lengths were then analyzed blindly. One individual investigator took high magnification scanning electron micrographs and then coded them. A different investigator performed the stereocilia measurements with no information on specific treatment or which region the images were from. Stereocilia lengths were then averaged from the four micrographs to obtain an average length of stereocilia that formed in HCs from proximal and distal regions for each BP. The dataset was then unblinded, quantified and statistically analyzed using one-way ANOVA with Newman-Keuls Post-test (GraphPad Prism).

Bead Implantation

80-100 mm diameter anion exchange resin beads AGI-X8 (Bio-Rad) were washed in 100% DMSO then soaked in either DMSO containing 0.5 mg/mL RA or 100% DMSO alone for 20 min at RT. Beads were then briefly washed three times in 100% DMEM/F-12 and then carefully implanted inside the proximal tip of an E6.5 BP. Implanted cochleae were cultured on stainless steel grids for 6 days, fixed with 4% PFA and stained with Alexa Fluor 488-phalloidin as described.

RESULTS

RNA-seq Analysis

We isolated mRNA from proximal, middle, and distal sections of E6.5 BPs for Illumina sequence analysis aimed at identifying gradients of gene expression along the tonotopic axis. The datasets for all three regions and biological replicates comprise >10,000 detectably expressed genes. Raw sequences have been submitted to NCBI GEO (accession number applied for). In addition to the developing BP, the avian cochlear duct also houses the lagena, an otolithic organ, which I were not able to distinguish or separate from the BP at E6.5. Therefore, the sequencing results from the distal E6.5 BP may contain lagena-expressed genes.

To identify transcripts that might reveal gradients of morphogen expression, I applied three filters. First, I selected only genes that exhibited ≥2-

fold change between the proximal and distal regions. I then eliminated genes that failed to pass a ≥0.5 RPKM (Mortazavi et al., 2008) abundance threshold in either region, and I removed genes that exhibited peaks or valleys of expression in the middle of the BP. The resulting data set includes 1,254 genes that exhibit gradients of transcript abundance between the two ends of the BP. The top 30 most differentially expressed genes we measured in the proximal and distal regions are shown in Tables 2-1 and 2-2, respectively. Interestingly, this data set is heavily biased towards genes that show much higher transcript abundance in the proximal BP (1104 genes) than in the distal BP (150 genes). Among these results are genes in seven signaling pathways that play a role in inner ear development: Retinoic acid (RA), Hedgehog, FGF, Wnt, Notch, TGF-β, and IGF signaling.

Our RNA-seq results suggested the presence of a source and sink for RA at opposing ends of the BP at E6.5, as indicated by the high expression of *Raldh3* in the proximal BP and the high expression of *Cyp26c1* in the distal BP (Table 2-3). Retinaldehyde dehydrogenase 3, Raldh3 (also Aldh1a3), is one of three dehydrogenases that catalyze retinaldehyde oxidation to produce RA, and is required for patterning the retina (Suzuki et al., 2000). Cyp26c1 is one of three cytochrome p450 (Cyp26) enzymes that regulate RA signaling by catalyzing RA degradation (Reijntjes et al., 2004). The RNA-seq results also show that *RAR*α and *RXR*γ, which encode two retinoid receptors, and *Crabp1,* which encodes the cellular retinoic acid binding protein 1, are expressed at levels that are respectively 2.2-fold, 3.1-fold, and 5-fold higher proximally than distally. Although

Crabp1 function is not completely resolved, evidence suggests it may have a role in binding and sequestering RA in the cytoplasm (Napoli, 2012).

Additional evidence for the involvement of RA was provided by network analysis, through which I identified 112 transcription-factor-encoding (TF) genes that are expressed in gradients along the BP. The data set containing the differentially expressed genes between the proximal and distal ends of the E6.5 BP was uploaded to g:Profiler and analyzed by gene-group functional profiling (Reimand et al., 2011), which showed literature-supported interactions among 75 genes that are differentially expressed along the BP, including *RAR*α and *RXR*γ and 21 additional TF genes (Supplemental Fig. 2-1). Among these are RA-responsive genes, such as *Hoxd4,* and the nuclear hormone receptor genes for Thyroid Hormone Receptor β (*THRB*) and the Peroxisome Proliferator-Activated Receptor (*PPAR*). Network analysis also identified the Androgen Receptor (*AR*), which is known to have inhibitory interactions with *RXR* family members (Chuang et al., 2005). In the BP, *AR* is expressed in a distally high gradient, opposite to the gradient of *RXRγ* expression. The data set containing the differentially expressed genes was also analyzed with the Ingenuity Pathway Analysis (IPA) Upstream Regulator analytic to search out candidate upstream transcriptional regulators that might be involved in establishing gene expression differences between the proximal and distal parts of the BP. All-*trans* retinoic acid (aka tretinoin) was the most significant candidate detected (by absolute activation z-score, Table 2-4), further implicating RA as a candidate patterning signal.

The gradients of RA pathway genes reverse as the BP develops

To validate the RNA-seq results and determine whether expression levels change between E6.5 and P14, I isolated samples from the proximal and distal ends of BPs over the course of development and performed qRT-PCR (Fig 2-1d,e). The PCR results confirmed the presence of reciprocal *Raldh3* and *Cyp26c1* expression gradients at E6.5, and revealed marked changes in expression at later stages. *Raldh3* expression increased dramatically in the distal BP at E8, and it continued to increase through P14. At the same time, its expression in the proximal BP decreased and *Cyp26c1* expression declined to barely detectable levels (Fig. 2-1d,e). The longitudinal gradient in the number of stereocilia per HC becomes evident by E10.5 and the developing gradient in hair bundle lengths becomes evident by E12 (Cotanche and Sulik, 1984; Tilney and DeRosier, 1986; Tilney et al., 1988; Tilney et al., 1992a). Consistent with the possibility that high distal RA promotes distal-like hair bundle phenotypes, the reversal of the *Raldh3* expression gradient shown in the qRT-PCR data occurs during the stages when the longitudinal gradients of HC phenotypes first become evident.

Our immunoblot experiments showed that Raldh3 protein levels at E6.5 are 4.43-fold greater in the proximal BP than in the distal BP, but levels for E10 proximal and distal samples do not appear to differ (Fig. 2-1f). As in the qRT-PCR data, our immunoblot experiments showed that a reversal of the gradient of Raldh3 protein expression occurred later in development, with distal protein levels from E18 BPs 3.87-fold greater than the levels in proximal samples.

Immunohistochemistry in E8 BPs showed strong Raldh3 expression in the presumptive supporting cells (SCs), which were negative for the HCS-1 antigen, otoferlin (Fig. 2-2). At E10, however, Raldh3 appeared to be expressed in the SCs and also in the HCS-1-positive HCs. By E18, Raldh3 was expressed predominately in HCs in both the proximal and distal ends of the BP. I hypothesize that the reversal of the longitudinal gradient of *Raldh3* mRNA expression that occurs between E6.5 and E10 is linked to the change from expression of Raldh3 protein in SCs to expression that is predominantly in HCs.

To investigate and compare levels of RA itself, I dissected E10 BPs, and then separately cultured their proximal and distal halves on RA-reporter cells (Wagner et al., 1992; Kelley et al., 1993). E10 retina and media that contained either 5 nM or 100 nM RA were used as positive controls. Few reporter cells in the vicinity of the proximal halves were positive for the blue *LacZ* signal, but many were positive in the vicinity of the distal halves, consistent with greater levels of soluble RA distally (Fig. 2-3). Thus, at the stages of development when the location-specific HC phenotypes first become evident, the levels of *Raldh3* mRNA, Raldh3 protein, and soluble RA are higher in the distal BP than in the proximal BP.

The cellular effects of RA are mediated through RAR and RXR nuclear receptor families that form heterodimers (Maden, 2007). Our sequencing results from the E6.5 BP showed significant expression of two RARs, *RARα* and *RARβ*, but only one of the RXR nuclear receptors, *RXR*γ. Like the RNA-seq analysis, qRT-PCR showed that *RXR*γ is expressed in a proximal-high gradient at E6.5,

but the *RXR*γ expression gradient reverses and becomes a distal-high gradient at E8 and E10, contemporaneous with the reversal of the *Raldh3* expression gradient (Fig. 2-4a). Throughout the stages of development that I assessed, the potential *RXR*γ dimerization partners, *RARα* and *RARβ*, were expressed in both ends of the BP (Fig. 2-4c).

HCs in the developing mouse cochlea are known to express RA receptors and are responsive to RA signals (Raz and Kelley, 1999). In the BPs of E18 chickens, immunolabeling with an antibody against RXRγ clearly labeled HCs, while a negative control antibody (to Red Fluorescent Protein) produced no labeling (Fig. 2-4b,d). Since our results show that HCs express the RA synthesizing enzyme, Raldh3, and the nuclear receptor, RXRγ, RA may have autocrine signaling effects in these sensory cells. The release of soluble RA that was detected by reporter cells growing in the vicinity of cultured BP tissues (Fig. 2-3) is also consistent with RA-mediated paracrine signaling. Thus, autocrine or paracrine signaling may both potentially play roles during BP development, perhaps at different stages.

RA signaling induces the formation of distal-like hair cell phenotypes

To determine whether the distally-high RA gradient influences the patterning of HC phenotypes, I cultured E6.5 BPs for 7 days, which allowed the HCs to progress through differentiation of their location-specific phenotypes. Experimental cultures were maintained in medium supplemented with 500 nM all-

trans-retinoic acid (hereafter RA) and control cultures were maintained in medium containing vehicle alone. I then fixed the cultures and assessed the phenotypic characteristics of the mechanoreceptive hair bundles that developed near the proximal and distal ends. The resulting quantified HC phenotypes and number of BPs analyzed for each experimental treatment (control, RA, or citral) are shown in Table 2-5. In the control cultures, proximal HCs developed more stereocilia than distal HCs, paralleling the gradient that forms *in ovo* (Fig. 2-5c). BPs cultured with RA also developed a gradient of stereocilia number, but with fewer stereocilia per cell. HCs in the proximal end of RA-treated BPs developed 68.6% of the number of stereocilia that formed in proximal HCs of control cultures, while distal HCs formed 53.5% of the number in the distal HCs of controls (Fig. 2-5c, $p < 0.05$ for each, $n_{BPs} = 6$; except when indicated, p-values were from one-way ANOVA with Newman-Keuls Post-test).

To determine whether the exposure to exogenous RA affected the height of the hair bundles or the size of the luminal surfaces of the HCs that developed in the cultured BPs, I used confocal micrographs and 3D images produced using Imaris software (Bitplane). In control cultures, proximal HCs formed shorter stereocilia and larger luminal surface areas than distal HCs (Fig. 2-6q,r). In contrast, proximal HCs in BPs that were cultured with added RA developed stereocilia that were 62.6% longer than those of proximal HCs in the controls ($p < 0.05$, $n_{BPs} = 9$), and luminal surfaces that reached just 52.2% of the size formed in controls ($p < 0.05$, $n_{BPs} = 20$, Fig. 2-6q,r). Surprisingly, the direction of the longitudinal gradient of stereocilia lengths reversed in BPs that were cultured with

exogenous RA. Proximal HCs developed significantly longer stereocilia than distal HCs in RA-treated BPs ($p < 0.05$, Student's *t*-test), and both the proximal and distal HCs resembled the distal HC phenotypes that formed in BPs cultured in control medium. Taken together, these results indicate that RA signaling is sufficient to induce distal-like HC phenotypes, even in the proximal BP.

RA signaling is necessary to induce aspects of distal-like hair bundle phenotypes

To determine whether RA signaling is necessary for the formation of distal-like HC phenotypes, I cultured E6.5 BPs for seven days in medium containing 5 μM citral, a competitive inhibitor of Raldhs that has been used to block RA synthesis in multiple systems, including the mouse cochlea and retina (McCaffery et al., 1992; Marsh-Armstrong et al., 1994; McCaffery et al., 1996; Kikonyogo et al., 1999; Raz and Kelley, 1999). HCs that developed in the citral-treated BPs formed 31.9% more stereocilia in the proximal and 17.1% more stereocilia in the distal region than HCs at similar locations in the control cultures ($p < 0.05$ for each, $n_{BPs} = 8$, Fig. 2-5c). Distal HCs that differentiated in the presence of citral developed stereocilia that also reached only 59.4% of the mean stereocilia length measured in controls ($p < 0.05$, $n_{BPs} = 6$) and 23% larger luminal surfaces than their counterparts in controls ($p < 0.05$, $n_{BPs} = 12$, Fig. 2-6q,r).

In an independent, higher-resolution analysis, I sampled the different parts of BPs that were fixed and processed for scanning EM after culturing for 7

days in media containing 500 nM RA, 5 μM citral, or vehicle alone. At each location sampled I captured SEM images in stereo pairs, which were then given a coded identifier. A laboratory member, who was "blind" to the treatment and location associated with each image pair, then measured the stereocilia lengths. Calculations from this unbiased measurement method showed that proximal HCs in the RA-treated BPs grew stereocilia that were more than two times the length (128% longer) than those in control cultures ($p < 0.05$, $n_{BPs} = 4$). Contrasting with this, distal HCs in citral-treated BPs developed stereocilia that averaged just 62.7% of the mean length of stereocilia in the distal half of the control cultures ($p < 0.05$, $n_{BPs} = 4$, Fig. 2-7). The stereoimaging measurements in SEM and the 3D confocal imaging measurements were consistent and supported the same conclusions.

As an additional means of interrupting cellular responses to RA signaling, I cultured E6.5 BPs in medium containing 10 mM BMS 493, which antagonizes RA signaling by strongly enhancing nuclear corepressor binding to RARs (Germain et al., 2009). In BMS 493-treated cultures, distal HCs developed stereocilia that were 71.3% of the mean length of stereocilia that developed in distal HCs of controls ($p < 0.05$, $n_{BPs} = 6$) and luminal surfaces that were 43% larger ($p < 0.05$, $n_{BPs} = 6$, Fig. 2-6q,r).

To rule out the possibility that the exogenous RA might have prevented differentiation of HCs at the proximal end of the cultured BPs or that the citral treatments might have prevented differentiation of HCs at the distal end, I immunostained BPs with the HCS-1 antibody and Alexa Fluor 488-phalloidin,

then used ImageJ (NIH) to count hair bundles and HCS-1+ HC somata that differentiated under those conditions. The counts showed that BPs cultured in control medium developed 8478 ± 196 HCs (mean ± SEM; n_{BPs} = 3), while BPs cultured with 500 nM RA developed 8390 ± 128 HCs (n_{BPs} = 3) and those cultured with citral developed 8511 ± 326 HCs (n_{BPs} = 3). Since the BPs that developed in control medium and media containing RA or citral all formed 80-85% of the ~10,500 HCs that develop *in ovo*(Tilney et al., 1986), it is unlikely that the effects of the RA and citral treatments result from suppression of HC differentiation. Thus, RA signaling appears to be necessary to induce the formation of distal-like HC phenotypes.

RA influences the development of longitudinal variation in the electrical tuning of HCs

Electrical tuning plays a large role in auditory frequency selectivity in reptiles and birds and is dependent on differential gating kinetics of calcium-activated-potassium BK channels. In the BP, BK channel kinetics are slowed by the presence of auxillary β subunits, which are more highly expressed in low frequency-sensitive distal HCs (Ramanathan et al., 1999; Miranda-Rottmann et al., 2010; Bai et al., 2011). To test whether RA signaling could influence the development of the gradient of expression of the β_1 subunit (*Kcnmb1*), I cultured E6.5 BPs with 500 nM RA or control media for three days and then divided each into proximal and distal halves. For each condition, I pooled samples from 6 BPs and measured levels of *Kcnmb1* using qRT-PCR. In the BPs cultured with RA,

Kcnmb1 expression in the proximal halves was 7.9-fold higher than in controls ($p < 0.05$, Student's *t*-test, $n = 6$), and 4.8-fold higher in distal halves ($p < 0.05$, Student's *t*-test, $n = 7$). The results are consistent with the hypothesis that RA is sufficient to induce a distal-like phenotype in the proximal region of the BP.

Local application of RA causes HCs in the proximal end of the BP to develop distal-like phenotypes

To determine whether a local source of exogenous RA would cause proximal HCs to develop distal-like properties, I soaked 80-100 mm ion-exchange beads (AGIX-8, Biorad) in RA or vehicle alone and implanted a single bead in the proximal end of E6.5 BPs before culturing them for 6 days. HCs that differentiated within 100 mm of the RA-soaked beads developed smaller luminal surfaces ($p = 0.0013$, Student's *t*-test, $n = 6$, Supplemental Fig. 2-2d) and longer stereocilia ($p = .0015$, Student's *t*-test, $n = 6$, Supplemental Fig. 2-2e) than HCs that developed in similar locations adjacent to DMSO-soaked beads that were implanted in the controls.

RA upregulates the expression of two actin crosslinking proteins

Espin, Fascin-2 (Fscn2), Fimbrin (Pls1), and T-plastin (Pls3) are crosslinking proteins that regulate the elongation of the actin-filled stereocilia (Flock et al., 1982; Daudet and Lebart, 2002; Loomis et al., 2003; Rzadzinska et al., 2005b; Shin et al., 2010; Avenarius et al., 2013). In the embryonic chicken

BP, Espin is expressed in a spatial pattern that mirrors the growth of stereocilia (Li et al., 2004). To test whether RA regulates actin crosslinker expression, I cultured E6.5 BPs in media containing 500 nM RA or vehicle alone for three days, and used qRT-PCR to assess *Espin, Fscn2, Pls1,* and *Pls3* mRNA levels in proximal and distal halves. The control and the RA-treated BPs showed no differences in *Pls1* or *Pls3* expression (data not shown), but mRNA levels for *Espin* increased 1.9-fold proximally and 2.3-fold distally in the RA-treated BPs over levels in the control halves. Likewise, *Fscn2* expression increased 3.0-fold and 2.8-fold in proximal and distal halves, respectively (Fig. 2-8a,b). Since it is well established that Espin levels regulate stereocilia length (Rzadzinska et al., 2005a; Sekerkova et al., 2011), I cultured BPs in RA or vehicle control media for 24 h to investigate whether brief treatments would influence its expression. This resulted in a pronounced 19.2-fold upregulation of *Espin* proximally and a 4.8-fold upregulation distally, compared to controls ($p < 0.05$ for each, Student's *t*-test, $n = 6$). The greater apparent increase in RA-induced *Espin* expression at the proximal end of the BP likely stems in part from the relatively low *Espin* expression that occurs at that location in controls, and is consistent with longitudinal differences in Espin expression onset *in ovo*, where distal expression precedes proximal expression by 2-3 days (Li et al., 2004).

Ultrastructural observations have shown that differences in the onset times and the durations of phases of stereocilia elongation underlie the length gradations that develop within and among the hair bundles in the chicken BP (Tilney et al., 1988). To test whether increasing the duration of the exposure to

exogenous RA would stimulate precocious elongation in proximal hair bundles, I cultured 4 pairs of BPs from E6.5 chicken embryos for 4 days. The BP from the right ear of each pair was cultured in RA medium and the BP from the left was cultured in control medium. When I fixed and immunolabeled the BPs for Espin, I observed that the proximal hair bundles in the control cultures were circular in outline and exhibited limited Espin expression. After 4 days in culture with exogenous RA, proximal cells in the BPs from the right ears of the same embryos developed taller, semicircular hair bundles and more pronounced Espin immunofluorescence (Fig. 2-8c,d,e). *In ovo* E10.5 BPs have hair bundles that are circular in outline and comprised of uniformly short stereocilia (Tilney et al., 1986), which will begin to elongate and express Espin as they progress from circular to rectangular outlines between E10-E12 (Cotanche and Sulik, 1984; Li et al., 2004). Since the bundles in the proximal halves of the RA-treated BPs exhibit characteristics that normally do not develop *in ovo* until E12 (Tilney et al., 1992b), these findings raise the possibility that the 4-day exposure to exogenous RA stimulated precocious development of the hair bundles.

Interactions between RA and Bmp7 Signaling Pathways

A distal-to-proximal gradient of bone morphogenetic protein 7 (Bmp7) occurs in BPs from E6.5 through post-hatch ages (Mann et al., submitted). In other systems, RA can act as either an inhibitor or an activator of *Bmp7* expression (Paralkar et al., 2002; Guo et al., 2008), so I investigated whether RA signaling would influence the Bmp7 gradient. For this, I cultured groups of six

E6.5 BPs in media that contained 500 nM RA, 5 mM citral, or vehicle alone for 24 h and used qRT-PCR to assess *Bmp7* mRNA levels in the proximal and distal halves. mRNA levels in proximal and distal regions of citral-treated BPs and the levels in the distal regions of RA-treated BPs did not show clear differences from controls. However, levels of *Bmp7* mRNA in the proximal half of RA-treated BPs decreased to 59.9% of the levels measured in controls, suggesting that RA suppressed *Bmp7* expression (n = 10, Supplemental Fig. 2-3a). To determine whether Bmp7 would have a reciprocal inhibitory effect on RA signaling, I cultured groups of six E6.5 BPs in media containing either 400 ng/mL Bmp7, 100 ng/mL noggin, a potent antagonist of Bmp and TGF-β, or vehicle alone and assessed *Raldh3* mRNA. I did not detect differences in *Raldh3* expression levels between the proximal and distal halves of the Bmp7-treated BPs or between the distal halves of noggin-treated BPs and distal halves of controls, but the noggin treatment increased *Raldh3* mRNA 2.26-fold in the proximal end (n = 4, Supplemental Fig. 2-3b), suggesting that Bmp signaling may normally inhibit proximal *Raldh3* expression at E6.5. Taken together with our RA-treatment results, these data are consistent with the possibility that the longitudinal counter gradients of *Bmp7* and *Raldh3* expression are maintained at E6.5 through reciprocal inhibitory feedback.

At E6.5, when *Raldh3* is expressed in a proximal-to-distal gradient, the progenitors of HCs have begun to exit the cell cycle (Katayama and Corwin, 1989), but most of the postmitotic HCs have formed and started to develop location-specific phenotypes at E10 (Tilney et al., 1986). Since the *Raldh3*

expression gradient reverses between E6.5 and E10, and becomes a distal-to-proximal gradient, like the gradient of *Bmp7* expression, I tested for positive interactions of these signaling pathways at E10. For this, I cultured groups of six E10 BPs in media containing 500 nM RA, 5 mM citral, or vehicle alone for 24 h and measured *Bmp7* expression. There were no detectable differences in *Bmp7* expression in either region of the citral-treated BPs or in the distal region of RA-treated BPs, but *Bmp7* expression increased 2.96-fold in the proximal end of RA-treated BPs (n = 5, Supplemental Fig. 2-3c). I then measured *Raldh3* expression in E10 BPs cultured with 400 ng/mL Bmp7, 100 ng/mL noggin, or vehicle alone for 24 h. Similar to the effects of noggin at E6.5, *Raldh3* mRNA increased 2.41-fold in the distal end of noggin-treated BPs. In contrast to the E6.5 BPs where *Raldh3* levels were suppressed by Bmp7, in the E10 BPs *Raldh3* expression increased 2.29-fold and 4.06-fold in the proximal and distal ends with the Bmp7 treatments (n = 7, Supplemental Fig 2-3d). The increase in *Bmp7* expression after RA treatments of E10 BPs and increased *Raldh3* expression after Bmp7 treatments at that age suggest these signaling pathways may positively reinforce their distal-to-proximal gradients at the stage when HC phenotypes differentiate.

Discussion

Despite its importance in speech comprehension and in communication, our understanding of how the phenotypic characteristics of HCs are organized at different positions along the cochlear sensory epithelium is rudimentary. In this study RNA-seq analysis identified signaling pathways that appear to regulate the

developmental acquisition of HC phenotypes in the chicken cochlea. I chose to focus on RA signaling because the RNA-seq data suggested that one end of the cochlea contains a source and the other a sink. Also, RA is known to play roles in patterning other embryonic tissues (Gavalas, 2002; Maden, 2007), such as the early embryonic otocyst that will eventually form the inner ear(Kelley et al., 1993; Raz and Kelley, 1999; Bok et al., 2011). The significance of the proximal-to-distal *Raldh3* expression gradient evident in both the RNA-seq and qPCR data at the earliest time point (E6.5) is unclear. As our results show (Supplemental Fig. 2-3), RA can inhibit Bmp7 signaling, so the proximally high *Raldh3* expression at E6.5 may underlie RA-mediated enforcement of a distal-to-proximal gradient of Bmp7 that is expressed between E6 and E8, which has been explored in the accompanying article (Mann et al, submitted).

It is intriguing that the gradient of *Raldh3* mRNA (Fig. 2-1) reverses after E6.5 and becomes an increasingly strong distal-to-proximal gradient at later stages as HCs differentiate and begin to express different phenotypes. I hypothesize that local differences in the numbers and spatial densities of HCs, which differ progressively along the sickle-shaped sensory epithelium of the chicken cochlea, may underlie that reversal. From its narrow proximal end to its broad and rounded distal end the BP gradually expands in width (Fig. 2-1b). Near its distal end, a transverse row through the BP contains as many as 46 HCs, but transverse rows through the much narrower proximal end contain far fewer HCs (Tanaka and Smith, 1978). Since there is a switch from predominant expression of the RA-synthesizing enzyme Raldh3 from SCs at E6.5 to

predominant expression in HCs as development progresses (Fig. 2-2), the greater number of HCs that form in the distal BP may lead to the formation of the distal-to-proximal gradients of Raldh3 message and protein (Fig. 2-1) and RA signaling itself (Fig. 2-3).

Since culturing with exogenous RA caused HCs in the proximal part of the BP to develop fewer and taller stereocilia, smaller luminal surfaces, and higher levels of expression of the β subunit of the BK channel, than their counterparts in control cultures, I conclude that RA promotes the development of a distal-like HC phenotype. Moreover, the positive effects of RA on the expression of *Espin* and *Fscn2*, which encode proteins that crosslink actin filaments and are known to be expressed in developing stereocilia at levels that correlate with their eventual length (Sekerkova et al., 2006; Shin et al., 2010), suggest a potential mechanism whereby RA signaling could regulate the patterning of bundle morphology. RA treatments induce RAR binding at *Espin's* transcriptional start site, and a consensus retinoic acid response element has been identified within the *Fscn2* promoter *(*Tubb et al., 2000; Moutier et al., 2012). The increased *Espin* and *Fscn2* expression observed after RA treatments (Fig. 2-8) are consistent with the hypothesis that RA binding with its nuclear receptors regulates stereocilia length by promoting transcription of these crosslinkers. The stereocilia on proximal HCs cease elongating by E12 *in ovo*, but those on distal HCs continue to elongate for the first two weeks post-hatching (Tilney et al., 1986; Tilney et al., 1988). The RA synthetic enzyme, *Raldh3,* may have a role in this extended distal stereocilia

elongation since it continues to be highly expressed distally in BPs from 14-day-old chicks (Fig. 2-1d).

It has been proposed that each HC may use the same amount of F-actin when forming a hair bundle, because proximal HC bundles in the BP contain large numbers of short stereocilia, while distal HC bundles contain low numbers of much longer stereocilia, with these two characteristics of the hair bundle phenotypes progressively changing in a near reciprocal relationship along the length of the BP (Tilney and Tilney, 1988). If this proposal is correct, then the >100 hair bundle phenotypes observed at the different longitudinal positions in the BP might result from the utilization of a fixed cellular pool of actin that is controlled by oppositely directed signals that regulate and balance stereocilia elongation and number in each HC. As a result of stimulating HCs to form longer stereocilia, RA signaling, by extension, may subsequently cause HCs to form fewer stereocilia.

The results in this and the accompanying article (Mann et. al., submitted) suggest a model in which Bmp7 and RA each play roles in patterning the development of the longitudinal phenotypic gradient of HCs in the chicken BP. At early stages, the proximal-to-distal gradient of RA opposes and is likely to antagonize the early distal-to-proximal gradient of Bmp7. Subsequently, as HCs begin to differentiate, there is weakening of the Bmp7 gradient throughout the BP while the gradient of the RA synthesis enzyme*, Raldh3,* reverses, becoming a distal-to-proximal gradient that increases and persists. That synthesis gradient appears to lead to a distal-to-proximal gradient of RA that contributes to the

specification of HC phenotypes by promoting bundle elongation and the expression of the b subunit for the BK channel. Future investigations into the interactions between these signaling pathways may elucidate mechanistic insights that support or refute this model.

REFERENCES

Avenarius MR, Saylor KW, Lundeberg MR, Wilmarth PA, Shin JB, Spinelli KJ, Pagana JM, Andrade L, Kachar B, Choi D, David LL, Barr-Gillespie PG (2013) Correlation of Actin Crosslinker and Capper Expression Levels with Stereocilia Growth Phases. Mol Cell Proteomics.

Bai JP, Surguchev A, Navaratnam D (2011) beta4-subunit increases Slo responsiveness to physiological Ca2+ concentrations and together with beta1 reduces surface expression of Slo in hair cells. American journal of physiology Cell physiology 300:C435-446.

Bok J, Raft S, Kong KA, Koo SK, Drager UC, Wu DK (2011) Transient retinoic acid signaling confers anterior-posterior polarity to the inner ear. Proc Natl Acad Sci U S A 108:161-166.

Chuang KH, Lee YF, Lin WJ, Chu CY, Altuwaijri S, Wan YJ, Chang C (2005) 9-cis-retinoic acid inhibits androgen receptor activity through activation of retinoid X receptor. Molecular endocrinology 19:1200-1212.

Corwin JT, Cotanche DA (1989) Development of location-specific hair cell stereocilia in denervated embryonic ears. J Comp Neurol 288:529-537.

Cotanche DA, Sulik KK (1984) The development of stereociliary bundles in the cochlear duct of chick embryos. Brain Res 318:181-193.

Daudet N, Lebart MC (2002) Transient expression of the t-isoform of plastins/fimbrin in the stereocilia of developing auditory hair cells. Cell Motil Cytoskeleton 53:326-336.

Davies S, Forge A (1987) Preparation of the mammalian organ of Corti for scanning electron microscopy. Journal of microscopy 147:89-101.

Duester G (2008) Retinoic acid synthesis and signaling during early organogenesis. Cell 134:921-931.

Flock A, Bretscher A, Weber K (1982) Immunohistochemical localization of several cytoskeletal proteins in inner ear sensory and supporting cells. Hearing research 7:75-89.

Frishkopf LS, DeRosier DJ (1983) Mechanical tuning of free-standing stereociliary bundles and frequency analysis in the alligator lizard cochlea. Hear Res 12:393-404.

Gavalas A (2002) ArRAnging the hindbrain. Trends in neurosciences 25:61-64.

Germain P, Gaudon C, Pogenberg V, Sanglier S, Van Dorsselaer A, Royer CA, Lazar MA, Bourguet W, Gronemeyer H (2009) Differential action on coregulator interaction defines inverse retinoid agonists and neutral antagonists. Chemistry & biology 16:479-489.

Guo L, Zhao YY, Zhang SL, Liu K, Gao XY (2008) Retinoic acid down-regulates bone morphogenetic protein 7 expression in rat with cleft palate. Chin Med Sci J 23:28-31.

Hamburger V, Hamilton H (1951) A series of normal stages in the development of the chick embryo. J Morphol 88:49-92.

Holton T, Hudspeth AJ (1983) A micromechanical contribution to cochlear tuning and tonotopic organization. Science 222:508-510.

Katayama A, Corwin JT (1989) Cell production in the chicken cochlea. J Comp Neurol 281:129-135.

Kelley MW, Xu XM, Wagner MA, Warchol ME, Corwin JT (1993) The developing organ of Corti contains retinoic acid and forms supernumerary hair cells in response to exogenous retinoic acid in culture. Development 119:1041-1053.

Kikonyogo A, Abriola DP, Dryjanski M, Pietruszko R (1999) Mechanism of inhibition of aldehyde dehydrogenase by citral, a retinoid antagonist. European journal of biochemistry / FEBS 262:704-712.

Lelli A, Asai Y, Forge A, Holt JR, Geleoc GS (2009) Tonotopic gradient in the developmental acquisition of sensory transduction in outer hair cells of the mouse cochlea. J Neurophysiol 101:2961-2973.

Li H, Liu H, Balt S, Mann S, Corrales CE, Heller S (2004) Correlation of expression of the actin filament-bundling protein espin with stereociliary bundle formation in the developing inner ear. J Comp Neurol 468:125-134.

Lim DJ (1980) Cochlear anatomy related to cochlear micromechanics. A review. J Acoust Soc Am 67:1686-1695.

Lim DJ (1986) Functional structure of the organ of Corti: a review. Hear Res 22:117-146.

Loomis PA, Zheng L, Sekerkova G, Changyaleket B, Mugnaini E, Bartles JR (2003) Espin cross-links cause the elongation of microvillus-type parallel actin bundles in vivo. The Journal of cell biology 163:1045-1055.

Maden M (2007) Retinoic acid in the development, regeneration and maintenance of the nervous system. Nature reviews Neuroscience 8:755-765.

Mann ZF, Kelley MW (2011) Development of tonotopy in the auditory periphery. Hearing research 276:2-15.

Marsh-Armstrong N, McCaffery P, Gilbert W, Dowling JE, Dräger UC (1994) Retinoic acid is necessary for development of the ventral retina in zebrafish. Proc Natl Acad Sci U S A 91:7286-7290.

McCaffery P, Mey J, Dräger UC (1996) Light-mediated retinoic acid production. Proc Natl Acad Sci U S A 93:12570-12574.

McCaffery P, Lee MO, Wagner MA, Sladek NE, Dräger UC (1992) Asymmetrical retinoic acid synthesis in the dorsoventral axis of the retina. Development 115:371-382.

Miranda-Rottmann S, Kozlov AS, Hudspeth AJ (2010) Highly specific alternative splicing of transcripts encoding BK channels in the chicken's cochlea is a minor determinant of the tonotopic gradient. Mol Cell Biol 30:3646-3660.

Mortazavi A, Williams BA, McCue K, Schaeffer L, Wold B (2008) Mapping and quantifying mammalian transcriptomes by RNA-Seq. Nat Methods 5:621-628.

Moutier E, Ye T, Choukrallah MA, Urban S, Osz J, Chatagnon A, Delacroix L, Langer D, Rochel N, Moras D, Benoit G, Davidson I (2012) Retinoic acid receptors recognize the mouse genome through binding elements with diverse spacing and topology. The Journal of biological chemistry 287:26328-26341.

Napoli JL (2012) Physiological insights into all-trans-retinoic acid biosynthesis. Biochim Biophys Acta 1821:152-167.

Paralkar VM, Grasser WA, Mansolf AL, Baumann AP, Owen TA, Smock SL, Martinovic S, Borovecki F, Vukicevic S, Ke HZ, Thompson DD (2002) Regulation of BMP-7 expression by retinoic acid and prostaglandin E(2). J Cell Physiol 190:207-217.

Ramanathan K, Michael TH, Jiang GJ, Hiel H, Fuchs PA (1999) A molecular mechanism for electrical tuning of cochlear hair cells. Science 283:215-217.

Raz Y, Kelley MW (1999) Retinoic acid signaling is necessary for the development of the organ of Corti. Dev Biol 213:180-193.

Reijntjes S, Gale E, Maden M (2004) Generating gradients of retinoic acid in the chick embryo: Cyp26C1 expression and a comparative analysis of the Cyp26 enzymes. Dev Dyn 230:509-517.

Reimand J, Arak T, Vilo J (2011) g:Profiler--a web server for functional interpretation of gene lists (2011 update). Nucleic Acids Res 39:W307-315.

Rzadzinska A, Schneider M, Noben-Trauth K, Bartles JR, Kachar B (2005a) Balanced levels of Espin are critical for stereociliary growth and length maintenance. Cell Motil Cytoskeleton 62:157-165.

Rzadzinska A, Schneider M, Noben-Trauth K, Bartles JR, Kachar B (2005b) Balanced levels of Espin are critical for stereociliary growth and length maintenance. Cell Motil Cytoskeleton 62:157-165.

Schilling TF, Nie Q, Lander AD (2012) Dynamics and precision in retinoic acid morphogen gradients. Current opinion in genetics & development 22:562-569.

Sekerkova G, Richter CP, Bartles JR (2011) Roles of the espin actin-bundling proteins in the morphogenesis and stabilization of hair cell stereocilia revealed in CBA/CaJ congenic jerker mice. PLoS genetics 7:e1002032.

Sekerkova G, Zheng L, Mugnaini E, Bartles JR (2006) Differential expression of espin isoforms during epithelial morphogenesis, stereociliogenesis and postnatal maturation in the developing inner ear. Developmental biology 291:83-95.

Shin JB, Longo-Guess CM, Gagnon LH, Saylor KW, Dumont RA, Spinelli KJ, Pagana JM, Wilmarth PA, David LL, Gillespie PG, Johnson KR (2010) The R109H variant of fascin-2, a developmentally regulated actin crosslinker in hair-cell stereocilia, underlies early-onset hearing loss of DBA/2J mice. The Journal of neuroscience : the official journal of the Society for Neuroscience 30:9683-9694.

Smoot ME, Ono K, Ruscheinski J, Wang PL, Ideker T (2011) Cytoscape 2.8: new features for data integration and network visualization. Bioinformatics 27:431-432.

Suzuki R, Shintani T, Sakuta H, Kato A, Ohkawara T, Osumi N, Noda M (2000) Identification of RALDH-3, a novel retinaldehyde dehydrogenase, expressed in the ventral region of the retina. Mech Dev 98:37-50.

Swanson GJ, Howard M, Lewis J (1990) Epithelial autonomy in the development of the inner ear of a bird embryo. Dev Biol 137:243-257.

Tanaka K, Smith CA (1978) Structure of the chicken's inner ear: SEM and TEM study. Am J Anat 153:251-271.

Tilney LG, Saunders JC (1983) Actin filaments, stereocilia, and hair cells of the bird cochlea. I. Length, number, width, and distribution of stereocilia of each hair cell are related to the position of the hair cell on the cochlea. J Cell Biol 96:807-821.

Tilney LG, DeRosier DJ (1986) Actin filaments, stereocilia, and hair cells of the bird cochlea. IV. How the actin filaments become organized in developing stereocilia and in the cuticular plate. Dev Biol 116:119-129.

Tilney LG, Tilney MS (1988) The actin filament content of hair cells of the bird cochlea is nearly constant even though the length, width, and number of stereocilia vary depending on the hair cell location. The Journal of cell biology 107:2563-2574.

Tilney LG, Tilney MS, Cotanche DA (1988) Actin filaments, stereocilia, and hair cells of the bird cochlea. V. How the staircase pattern of stereociliary lengths is generated. J Cell Biol 106:355-365.

Tilney LG, Cotanche DA, Tilney MS (1992a) Actin filaments, stereocilia and hair cells of the bird cochlea. VI. How the number and arrangement of stereocilia are determined. Development 116:213-226.

Tilney LG, Tilney MS, DeRosier DJ (1992b) Actin filaments, stereocilia, and hair cells: how cells count and measure. Annu Rev Cell Biol 8:257-274.

Tilney LG, Tilney MS, Saunders JS, DeRosier DJ (1986) Actin filaments, stereocilia, and hair cells of the bird cochlea. III. The development and differentiation of hair cells and stereocilia. Dev Biol 116:100-118.

Trapnell C, Pachter L, Salzberg SL (2009) TopHat: discovering splice junctions with RNA-Seq. Bioinformatics 25:1105-1111.

Tubb BE, Bardien-Kruger S, Kashork CD, Shaffer LG, Ramagli LS, Xu J, Siciliano MJ, Bryan J (2000) Characterization of human retinal fascin gene (FSCN2) at 17q25: close physical linkage of fascin and cytoplasmic actin genes. Genomics 65:146-156.

Viljoen KS, Blackburn JM (2013) Quality assessment and data handling methods for Affymetrix Gene 1.0 ST arrays with variable RNA integrity. BMC Genomics 14:14.

Wagner M, Han B, Jessell TM (1992) Regional differences in retinoid release from embryonic neural tissue detected by an in vitro reporter assay. Development 116:55-66.

Zhao S, Fernald RD (2005) Comprehensive algorithm for quantitative real-time polymerase chain reaction. J Comput Biol 12:1047-1064.

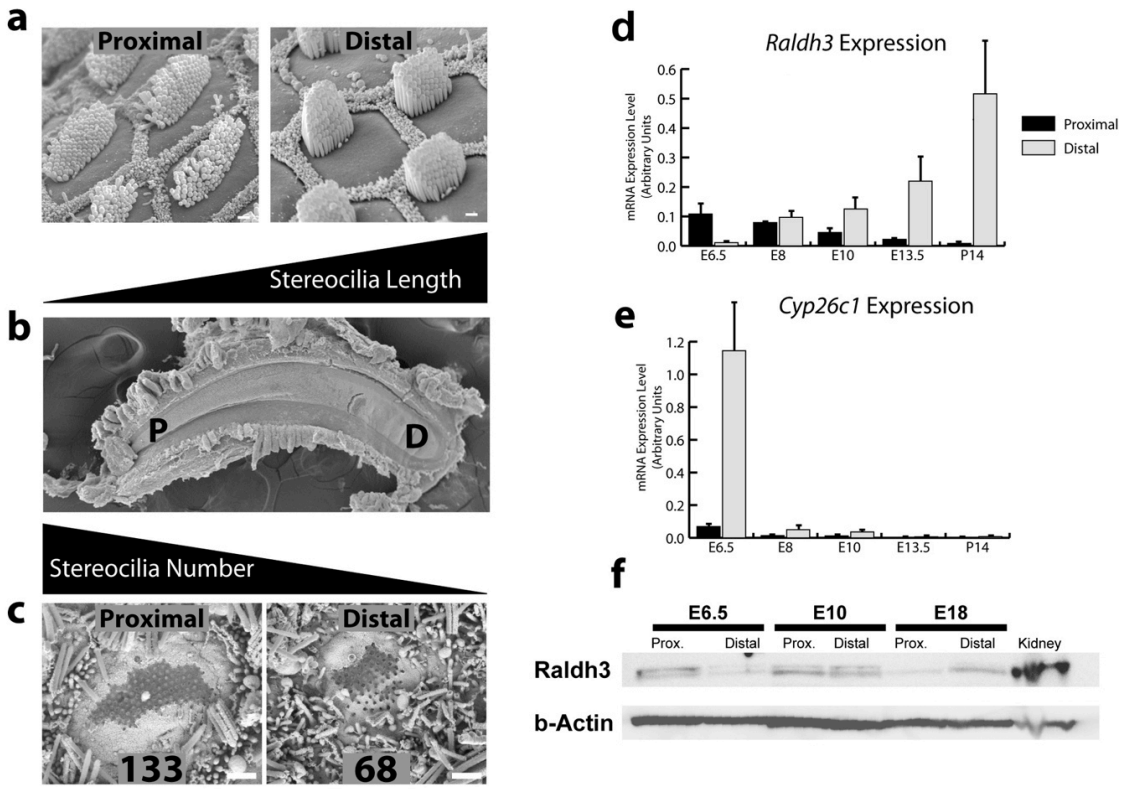

Figure 2-1. The chicken cochlea develops a gradient of >100 individually distinct auditory receptor cell phenotypes extending from its proximal high-frequency-sensitive end to its distal low-frequency-sensitive end.

(a) Scanning electron micrographs (SEM) showing short sensory hair bundles that project from the apical surfaces of hair cells (HCs) at the proximal end of the BP sensory epithelium and tall bundles of HCs at the distal end. The HCs are surrounded by honeycomb-like patterns comprised of the microvilli covered surfaces of supporting cells. (b) Low magnification SEM image showing the sickle-shaped BP, which is narrow proximally (P) and broad distally (D). (c) SEM images of HCs that formed *in vitro* in E6.5 BPs cultured in control medium for 7

days. The hair bundles in these micrographs were broken off so that the bases of the individual stereocilia could be counted, which showed that the HCs at the proximal end of cultured BPs contained more stereocilia than HCs at the distal end as do HCs that develop *in ovo*. (d) Histogram showing developmental changes in mRNA levels for the RA synthetic enzyme, *Raldh3,* in the proximal (dark bars) and distal (light bars) halves of BP as measured in qRT-PCR. At E6.5, *Raldh3* is expressed in a proximal-to-distal gradient, which reverses and becomes a strengthening distal-to-proximal gradient at later stages of cochlear development. (e) Histogram of mRNA levels for the RA catabolizing enzyme, *Cyp26c1,* measured from qRT-PCR. At E6.5, *Cyp26c1* is expressed in a distal-to-proximal gradient, but mRNA expression declines to barely detectable levels at later developmental stages. (d) Representative Western blot for of Raldh3 and β-actin protein in the proximal and distal halves of E6.5, E10, and E18 cochlea (*n* = 3). E18 kidney was used as a positive control tissue and β-actin was used as a loading control. At E6.5, Raldh3 was enriched 4.43-fold in the proximal BP compared to the distal BP, but the relative protein levels reverse as development progressed, with 3.87-fold more Raldh3 protein in the distal BP than in proximal BP at E18. Levels were approximately equivalent in the proximal and distal E10 BPs. Scale bars are 1 *μ*m.

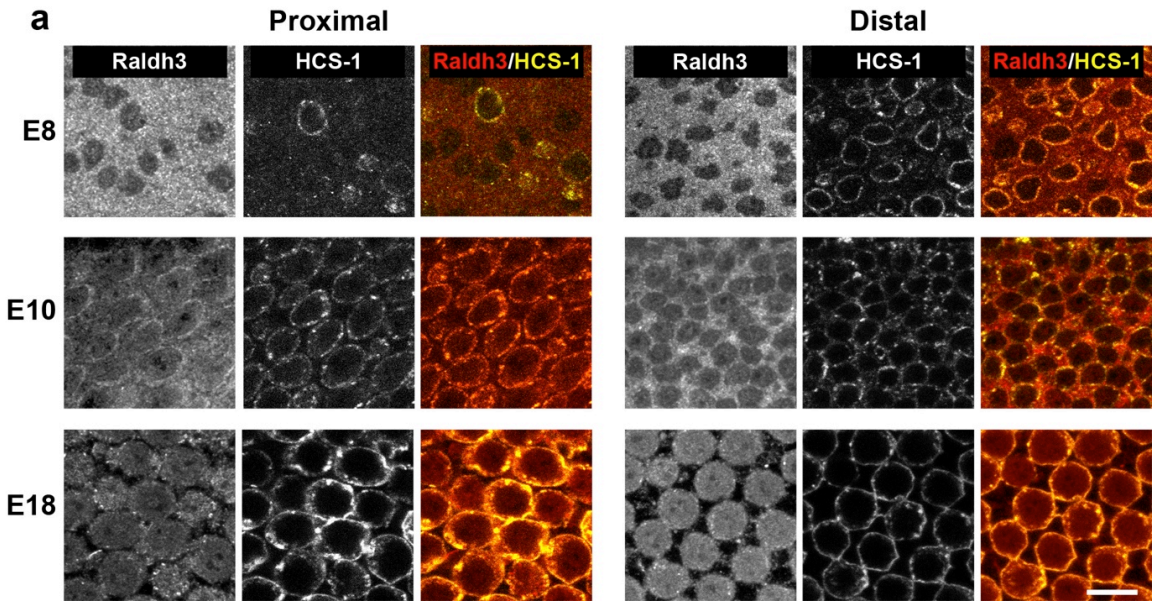

Figure 2-2. Raldh3 is predominately expressed in supporting cells early in development, but HCs become the predominant expressers at later stages.

(a) Immunolabeling using antibodies to Raldh3 and HCS-1 (otoferlin) in the proximal (left) and distal (right) regions of the BPs from embryos at E8, E10, and E18. The gray scale images in the far left on each side show Raldh3 immunofluorescence. Middle panel images show HCS-1 immunofluorescence, and images in the far right panels on each side show the merged immunofluorescence from Raldh3 (red) and HCS-1 (yellow). At E8, the antibody to Raldh3 most strongly labeled the supporting cells, which are negative for HCS-1, but labeling in HCs increased at E10, and at E18, Raldh3 was predominantly expressed by HCs. Scale bar is 10 μm.

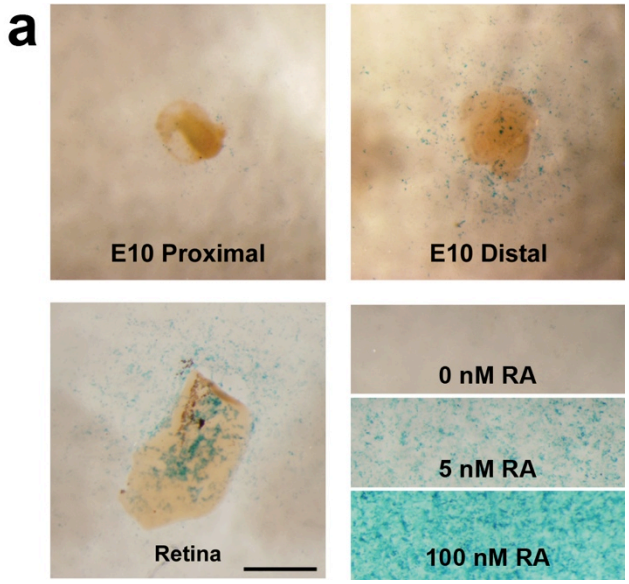

Figure 1-3. Soluble RA levels are higher in the distal half of the BPs at E10.

(a) Brightfield images of *LacZ* expression in RA reporter cells (F9 RARE-LacZ) that were co-cultured with proximal and distal halves from the same E10 BP. Many cells in the vicinity of the distal samples were positive for the blue *LacZ* signal while few in the vicinity of the proximal sample were. E10 retinal tissue was used as a tissue-control. As pharmacological-controls, reporter cells in separate wells were exposed to 0 nM, 5 nM and 100 nM RA. Scale bar is 1 mm.

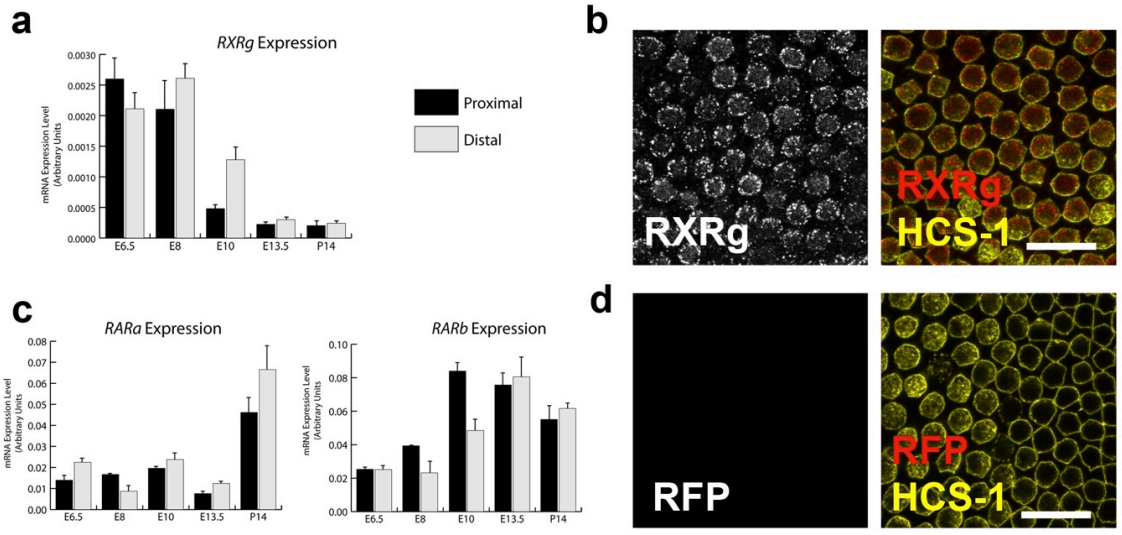

Figure 2-4. RA nuclear receptor expression in the developing cochlea

(a) Histogram showing *RXRg* mRNA expression levels measured from qRT-PCR of the proximal (dark bars) and distal (light bars) regions of E6.5, E8, E10, E13.5, and P14 BPs. RXRg becomes expressed in a distal-to-proximal gradient at E8 and E10. (b) Confocal micrograph showing RXRg (red) and HCS-1 (yellow) immunofluorescence in E18 BPs. Left panel shows gray scale from RXRg alone and the right panel shows the merged immunofluorescence from RXRg (red) and HCS-1 (yellow). RXRg immunofluorescence is observable within the HCS-1 positive HCs. (c) Histograms showing mRNA expression levels for *RAR*α and *RAR*β in proximal (dark bars) and distal (light bars) regions of E6.5, E8, E10, E13.5, and P14 BPs. Throughout the stages of development assessed, these nuclear receptors were expressed in both ends of the BP. (d) Negative control immunofluorescence with red fluorescence protein (RFP) antibody. Left panel

shows gray scale from RFP alone and right panel shows immunofluorescence from RFP (red) and HCS-1 (yellow). Scale bars are 20 μm.

.

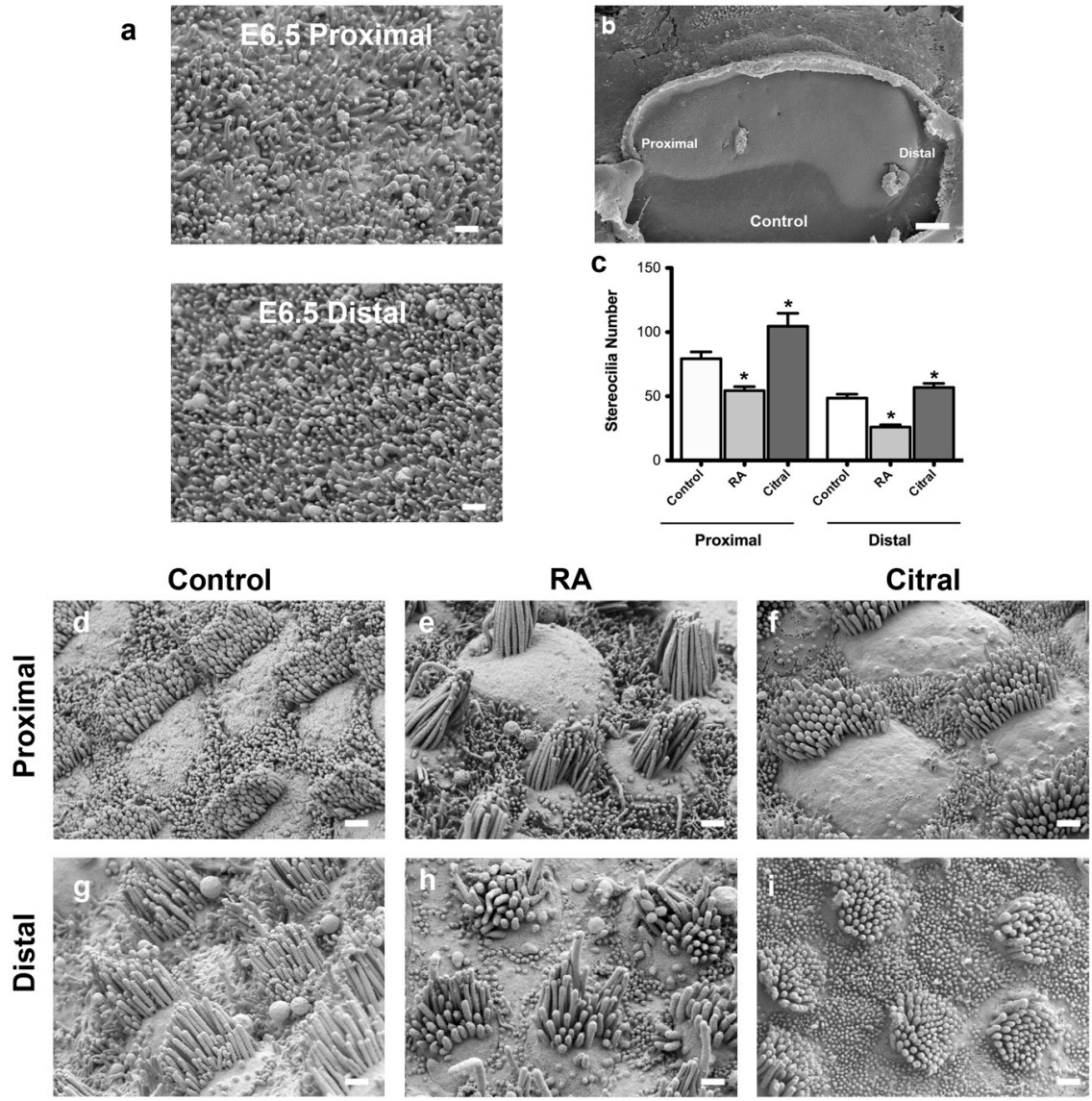

Figure 2-5. Modulating retinoic acid signaling disrupts tonotopic gradient of stereocilia number.

(a) Representative scanning electron micrograph of proximal and distal regions of E6.5 BPs. There is no apparent stereocilia formation at this stage in either region. (b) Micrograph of E6.5 BP explant cultured 7 days in control medium. Proximal and distal regions are indicated. (c) Quantification of the number of

stereocilia that formed in the proximal and distal regions of treated BPs. HCs form fewer stereocilia in both proximal and distal regions in RA-treated BPs. HCs form more stereocilia in proximal and distal regions of citral-treated BPs. *$p < 0.05$; One-way ANOVA with Newman-Keuls Post-test. (d-i) Representative micrographs of hair cells that form in the proximal and distal regions of E6.5 BPs cultured 7 days in control media (d,g), with RA (e,h), or with citral (f,i). Total number of BPs analyzed are $n = 8$ for control; $n = 6$ for RA; $n = 8$ for citral. Graph shows mean ± S.E.M. Scale bars in b: 100 μm; a, c-h, 1 μm

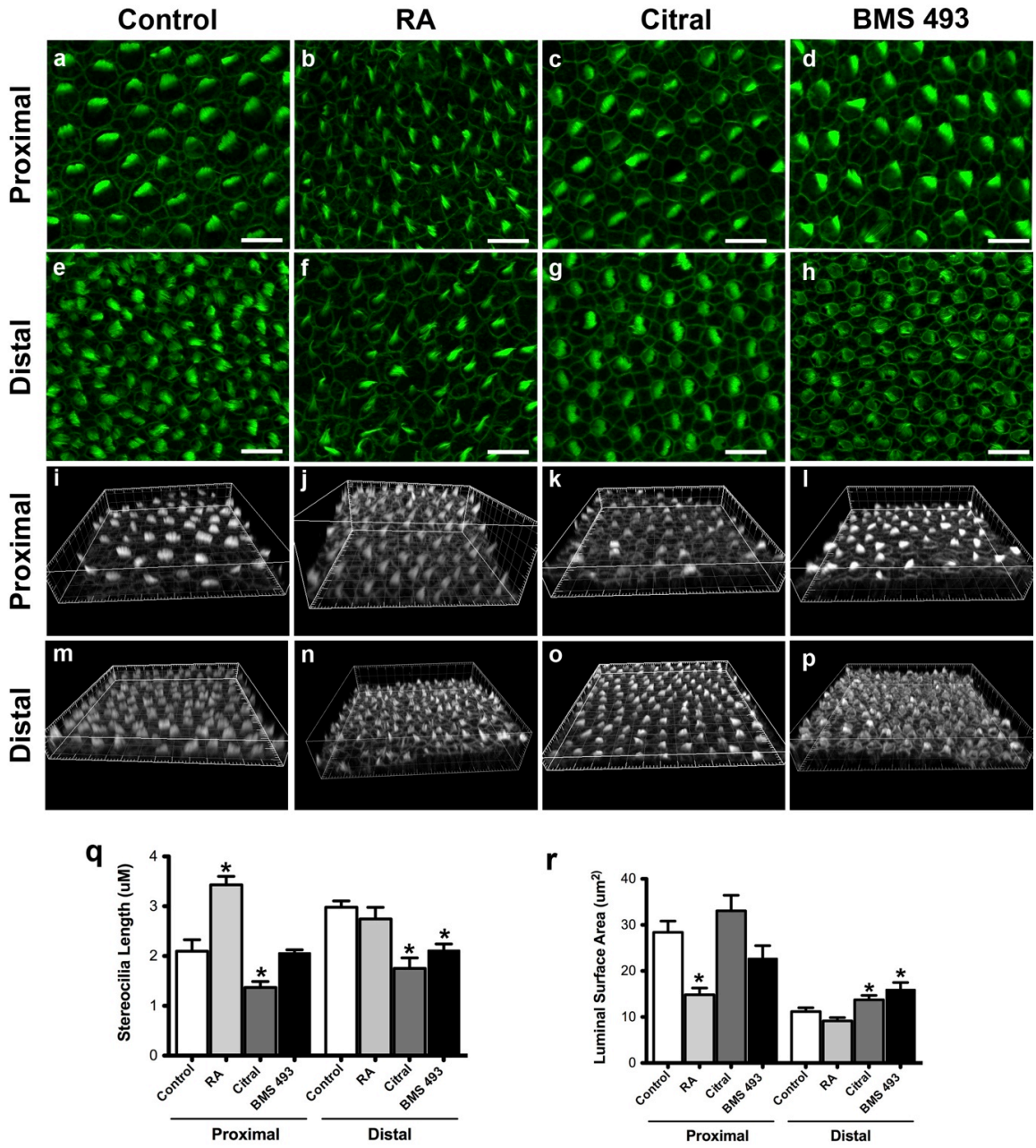

Figure 2-6. Modulating retinoic acid signaling disrupts tonotopic gradients of stereocilia length and hair cell luminal surface area.

Example micrographs of HCs that form in the proximal and distal regions of E6.5 BPs cultured 7 days with control media (a,e), RA (b,f), citral (c,g), or BMS 493 (d,h). Stereocilia lengths were analyzed from confocal micrographs using Imaris 3D software (Bitplane). Shown are example 3D-rendered images of HCs that form in the proximal and distal regions of E6.5 BPs cultured 7 days with control media (i,m), RA (j,n), citral (k,o) or with BMS 493 (l,p). (q) Quantification of the maximal stereocilia lengths that formed in the proximal and distal regions of treated BPs. Proximal HCs formed longer hair bundles in RA-treated BPs compared to control proximal HCs. In addition, citral treatments lead to significantly shorter hair bundles in both proximal and distal regions compared to controls. BPs treated with BMS 493 developed shorter hair bundles in the distal region (n_{BPs} = 6). *p < 0.05; One-way ANOVA with Newman-Keuls Post-test. Total number of BPs analyzed are n = 8 for control; n = 9 for RA; n = 8 for citral; n = 6 for BMS 493 treatments. (r) Quantification of HC luminal surface areas that formed in the proximal and distal regions of treated BPs measured using ImageJ from confocal maximum projections. HCs that formed in the proximal region of BPs treated with RA developed smaller luminal surfaces than HCs that formed in the proximal region of control BPs. Further, HCs that formed in the distal region of BMS 493 and citral-treated cochlea developed larger luminal surfaces than HCs that formed in the distal regions of control BPs. *p < 0.05; One-way ANOVA with Newman-Keuls Post-test. Total number of BPs analyzed are n = 15 for control; n = 20 for RA; n = 12 for citral; n = 6 for BMS 493 treatments. Graph shows mean ± S.E.M. Scale bars are 10 μm.

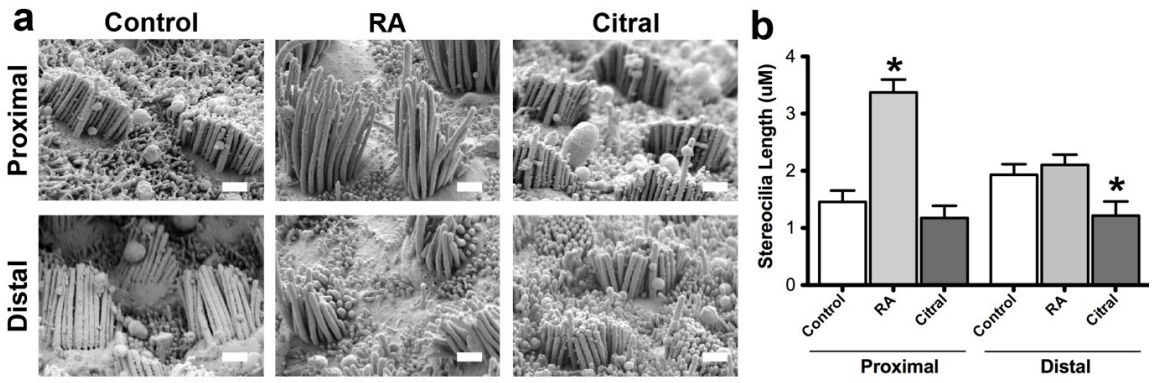

Figure 2-7. SEM stereoimaging validation of stereocilia length measurements

(a) Representative micrographs of E6.5 BPs that were cultured 7 days in control medium or media supplemented with RA or citral. HCs were viewed from behind the longest stereocilia and stereopair images were taken from four neighboring fields at a distance approximately 18% of the total length of the BP away from the proximal and distal ends (n_{BPs} = 4 for each treatment). Micrographs were blinded and stereocilia lengths were then measured from stereopair images. b) Quantifications of the stereocilia lengths that were measured from stereopair SEM images taken at 15,000X. Proximal HCs were taller in the RA-treated BPs compared to control BPs: 3.37 ± 0.22 μm versus 1.46 ± 0.20 μm, respectively. Further, distal HCs were shorter in the BPs treated with citral compared to controls: 1.21 ± 0.25 μm versus 1.93 ± 0.19 μm, respectively. *p < 0.05; One-way ANOVA with Newman-Keuls Post-test. Graph shows the mean stereocilia length measured in the proximal and distal regions ± S.E.M. Scale bars are 1 μm.

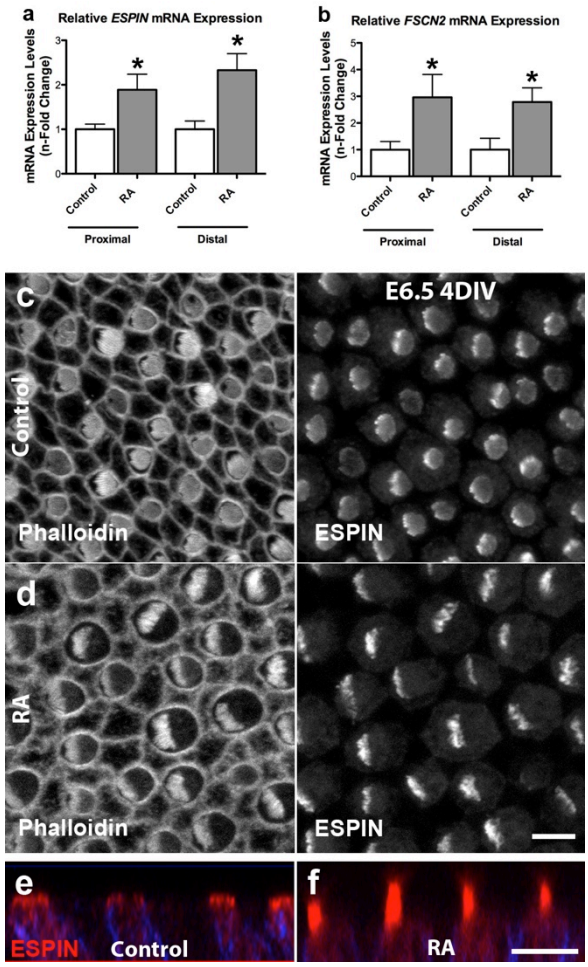

Figure 2-8. RA treatments upregulate expression for actin crosslinking proteins expressed within stereocilia.

(a) Relative mRNA expression levels for *Espin* in proximal and distal regions of E6.5 BPs cultured 3 days in control media or media supplemented with RA. Expression levels were normalized relative to the average mRNA expression in vehicle controls. *Espin* expression was 1.9-fold greater in the proximal region with RA treatments ($p = 0.0147$; Student's *t*-test; $n = 5$) and 2.3-fold greater in the distal region ($p = 0.0079$, Student's *t*-test; $n = 7$). (b) Relative mRNA

expression levels for *Fscn2* in proximal and distal regions of E6.5 BPs cultured 3 days in control media or media supplemented with RA. Expression levels were normalized relative to the average mRNA expression in vehicle controls. *Fscn2* expression was 3.0-fold greater in the proximal region with RA treatments (p = 0.0295, Student's t-test; n = 3) and 2.8-fold greater in the distal region (p = 0.0305; Student's t-test; n = 4). (c) Proximal HCs that developed in E6.5 BPs from the left ear that were cultured 4 days in vehicle-control medium, fixed, and immunolabeled with Espin. Left panel shows the gray scale from Alexa Fluor-488-phalloidin labeling and the right panel shows the gray scale image from Espin labeling. HCs formed hair bundles with circular outlines. (d) Proximal HCs that developed in E6.5 BPs from the right ear that were cultured 4 days in medium supplemented with RA. Hair bundles in these HCs formed semicircular outlines with more pronounced Espin immunofluorescence. (e,f) Images showing z-axis of Espin (red) and HCS-1 (blue) merged immunofluorescence in proximal HCs of E6.5 BPs cultured 4 days with vehicle-control (e), or with RA (f). The Espin-positive hair bundles were noticeably longer in the HCs that were exposed to exogenous RA. Scale bars are 5 μm.

Proximal	Gene Description	Gene	Proximal	Mid	Distal	Fold Change
1	NADPH Oxidase 3	NOX3	170.5	3.5	1.5	113.7
2	Transmembrane Protease, Serine 3	TMPRSS3	105.5	5.5	1	105.5
3	Transmembrane Channel-like 2	TMC2	227.5	12.5	2.5	91
4	Olfactory Receptor OR24	OR24	5.3	5.1	0.1	84.9
5	Otolin 1	OTOL1	1330.5	122.5	16	83.2
6	Gastrulation Brain Homeobox 2	GBX2	775.5	97	21.2	36.5
7	Oncomodulin 2	OCM2	873	64.5	27.5	31.7
8	Seven in Absentia Homolog 3	SIAH3	72.5	10.5	2.5	29
9	Cholinergic Receptor, Nicotinic, Alpha 9	CHRNA9	27	2.5	1	27
10	Carbonic Anhydrase XII	RAP2B	11	2.5	0.5	26.7
11	Doublecortin Domain Containing 2	DCDC2	163	16	9	24.9
12	Alkylglycerol Monooxygenase	AGMO	9	3	0.5	22
13	Rh Family, C Glycoprotein	RHCG	9	3.5	0.5	18.1
14	Coagulation Factor IX	F9	8.5	1	0.5	17
15	Potassium Channel, Subfamily K, Member 13	KCNK13	17	4.5	1	17
16	Myosin, Heavy Chain 4, Skeletal Muscle	MYH4	25	22.1	1.5	16.6
17	Zic Family Member 1	ZIC1	2059.2	592.6	126.4	16.3
18	**Aldehyde Dehydrogenase 1 Family, Member A3**	**ALDH1A3**	11619	741	725	16
19	Wingless-type MMTV Integration Site Family, Member 2B	WNT2B	236	34	15	15.7
20	Glycine Receptor, Alpha 3	GLRA3	62	21	4	15.5
21	Glutamate Receptor, Ionotropic, Kainate 3	KRIK3	69	18.5	4.5	15.3
22	Growth Differentiation Factor 9	GDF9	38	5.5	2.5	15.2
23	Solute Carrier Family 9	SLC9A3	7.5	3	0.5	15
24	Proopiomelanocortin	POMC	51	4	3.5	14.6
25	Ankyrin Repeat and SOCS Box Containing 2	ASB2	14.5	11.5	1	14.5
26	Protein Wnt	F1NVM5	20.5	2	1.5	13.7
27	Agouti Signaling Protein	ASIP	81.5	51	6	13.6
28	Potassium Channel, Subfamily K, Member 17	KCNK17	6.6	3.5	0.5	13
29	Nodal Homolog	NODAL	18.5	7	1.5	12.3
30	Pappalysin 2	PAPPA2	178	26	14.5	12.3

Table 2-1. Top 30 most proximally enriched genes in E6.5 chick cochlea from two biological replicates, as determined through next-generation sequencing. Shown are the expression levels measured from the three cochlear regions

(Normalized Reads) as well as the differential expression levels between the proximal and distal ends (Fold Change).

Distal	Gene Description	Gene	Proximal	Mid	Distal	Fold Change
1	Olfactomedin 4	OLFM4	4.5	59.5	217.5	48.3
2	Von Willebrand Factor D and EGF Domains	VWDE	8	25.5	216	27
3	Apolipoprotein A-I	APOA1	114.7	1645.8	2350.5	20.5
4	Goosecoid Homeobox 2	GSC2	3.5	11	55.5	15.9
5	ABI Family, Member 3 (NESH) Binding Protein	ABI13BP	36.5	254.5	678.7	15.4
6	Choline O-Acetyltransferase	CHAT	5.5	46	69.5	12.6
7	Calcium Channel, Voltage-Dependent, T Type	CACNA1I	56.5	123	678.7	12
8	Polycystic Kidney Disease 2-like 1	PKD2L1	0.5	1.5	6	12
9	**Cytochrome P450, family 26, subfamily C, polyeptide 1**	**CYP26C1**	159	562.9	1880.5	11.8
10	Tectorin Beta	TECTB	78.5	597	924	11.8
11	Leucine-rich Repeats and transmemebrane domains 1	LRTM1	0.5	3	5.5	11
12	Troponin T Type 2	TNNT2	6	24.5	64	10.7
13	Serpin Peptidase Inhibitor	SERPINA3	3	12	31.5	10.5
14	Immunoglobulin-like and Fibronecting Type III Domain	IGFN1	91	244	904.5	9.9
15	Hepatocyte G Protein Coupled Receptor	HGF	44	85.5	382.5	8.7
16	Retinal G Protein Coupled Receptor	RGR	619	286	79.5	7.8
17	Zing Finger Protein 488	ZNF488	5.5	29	38.5	7
18	SRY (Sex Determining Region)-Box 14	SOX14	6	36	41.5	6.9
19	Galanin Receptor Type 1-like	LOC415713	3	10	19.5	6.5
20	Fibrinonogen-like Protein 1-like	LOC428073	50.5	37	8	6.3
21	Noggin	NOG	44	120.5	265	6
22	Mannose Receptor, C type 2-like	LOC418836	1	1.5	6	6
23	WNT1 Inducible Signaling Pathway Protein 1	WISP1	21.5	79.5	120	5.6
24	G Protein-Coupled Receptor 133	GPR133	14.1	20.1	75.4	5.4
25	Potassium Voltage-Gated Channel, Subfamily F	KCNF1	35	97.5	185	6.28
26	Fibroblast Growth Factor Receptor 3	FGFR3	1104	5155	5832.9	5.3
27	Integrin, beta-like 1	ITGBL1	9	42	47.5	5.3
28	Calcyphyosine-like	CAPSL	3.5	9	18	5.2
29	ADAMTS-like 5	ADAMTSL5	39	107.5	200	5.1
30	Hydroxyacid Oxidase 2	HAO2	1.5	4	7.5	5

Table 2-2. Top 30 most distally enriched genes in E6.5 chick cochlea from two biological replicates, as determined through next-generation sequencing. Shown are the expression levels measured from the three cochlear regions (Normalized

Reads) as well as the differential expression levels between the distal and proximal ends (Fold Change).

	Normalized Reads in Proximal BP	Normalized Reads in Middle BP	Normalized Reads in Distal BP	Log_2 (Distal/Proximal)
Raldh2	1274	962	447	-1.51
Raldh3	11619	741	725	-4.00
Cyp26a1	130.5	24.5	50	-1.38
Cyp26b1	980.5	1041.5	286	-1.78
Cyp26c1	159.037	562.941	1880.53	3.56

Table 2-3. Expression levels in the E6.5 chicken BP for a subset of expressed genes that are involved in RA signaling. Expression levels (Normalized Reads) and differential expression level comparisons between the distal and proximal cochlea are depicted. Sequencing results from the distal end of the BP also include genes, which may be expressed in the developing lagena macula (LM), an otolithic organ. Genes with $Log_2 > 1$ expression level differences are more significantly expressed in the distal cochlea ($Log_2 < -1$ significant in proximal). *Raldh3* encodes an enzyme that synthesizes RA; *Cyp26c1* encodes for an enzyme that is involved in the breakdown of RA.

Upstream Regulator	Molecule Type	Predicted Activation	Absolute Activation z-score	p-value of overlap
tretinoin	chemical - endogenous mammalian	Activated	5.546	9.40E-08
trichostatin A	chemical drug	Activated	4.490	1.96E-05
hydrogen peroxide	chemical - endogenous mammalian	Activated	4.405	2.57E-02
TP53	transcription regulator	Activated	4.355	5.28E-02
decitabine	chemical drug	Activated	4.202	1.45E-04
LY294002	chemical - kinase inhibitor	Inhibited	4.149	3.19E-06
Vegf	group	Activated	4.107	4.64E-07
MITF	transcription regulator	Activated	4.022	7.30E-04
U0126	chemical - kinase inhibitor	Inhibited	3.971	4.31E-03
F2	peptidase	Activated	3.832	1.55E-04

Table 2-4. Top 10 upstream regulators derived from IPA analysis comparing the differentially expressed genes between the E6.5 proximal and distal ends of the BP, arranged by absolute activation z-score.

	Control		RA		Citral	
	Proximal	**Distal**	**Proximal**	**Distal**	**Proximal**	**Distal**
Stereocilia Number Mean ± S.E.M.	79.3 ± 5.6 n_{BPs} = 8 n_{HCS} = 96	48.6 ± 3.2 n_{BPs} = 8 n_{HCS} = 65	54.4 ± 3.1 n_{BPs} = 6 n_{HCS} = 54	26.0 ± 1.8 n_{BPs} = 6 n_{HCS} = 53	104.6 ± 10.1 n_{BPs} = 8 n_{HCS} = 68	56.9 ± 3.2 n_{BPs} = 8 n_{HCS} = 76
Stereocilia Length (μm)	2.14 ± 0.23 n_{BPs} = 8 n_{HCS} = 169	3.03 ± 0.13 n_{BPs} = 8 n_{HCS} = 282	3.48 ± 0.17 n_{BPs} = 9 n_{HCS} = 218	2.79 ± 0.23 n_{BPs} =9 n_{HCS} = 181	1.42 ± 0.12 n_{BPs} = 6 n_{HCS} = 156	1.80 ± 0.21 n_{BPs} = 6 n_{HCS} = 114
Luminal Surface Area (μm^2)	28.4 ± 2.44 n_{BPs} = 15 n_{HCS} = 242	11.17 ± 0.85 n_{BPs} = 15 n_{HCS} = 228	14.82 ± 1.48 n_{BPs} = 20 n_{HCS} = 359	9.15 ± 0.72 n_{BPs} = 20 n_{HCS} = 322	33.07 ± 3.37 n_{BPs} = 12 n_{HCS} = 189	13.74 ± 0.94 n_{BPs} = 12 n_{HCS} = 197

Table 2-5. Quantitative analyses of the hair cell phenotypes that formed in proximal and distal regions of E6.5 BPs treated with control media or media supplemented with RA or citral. Values shown are mean ± S.E.M.

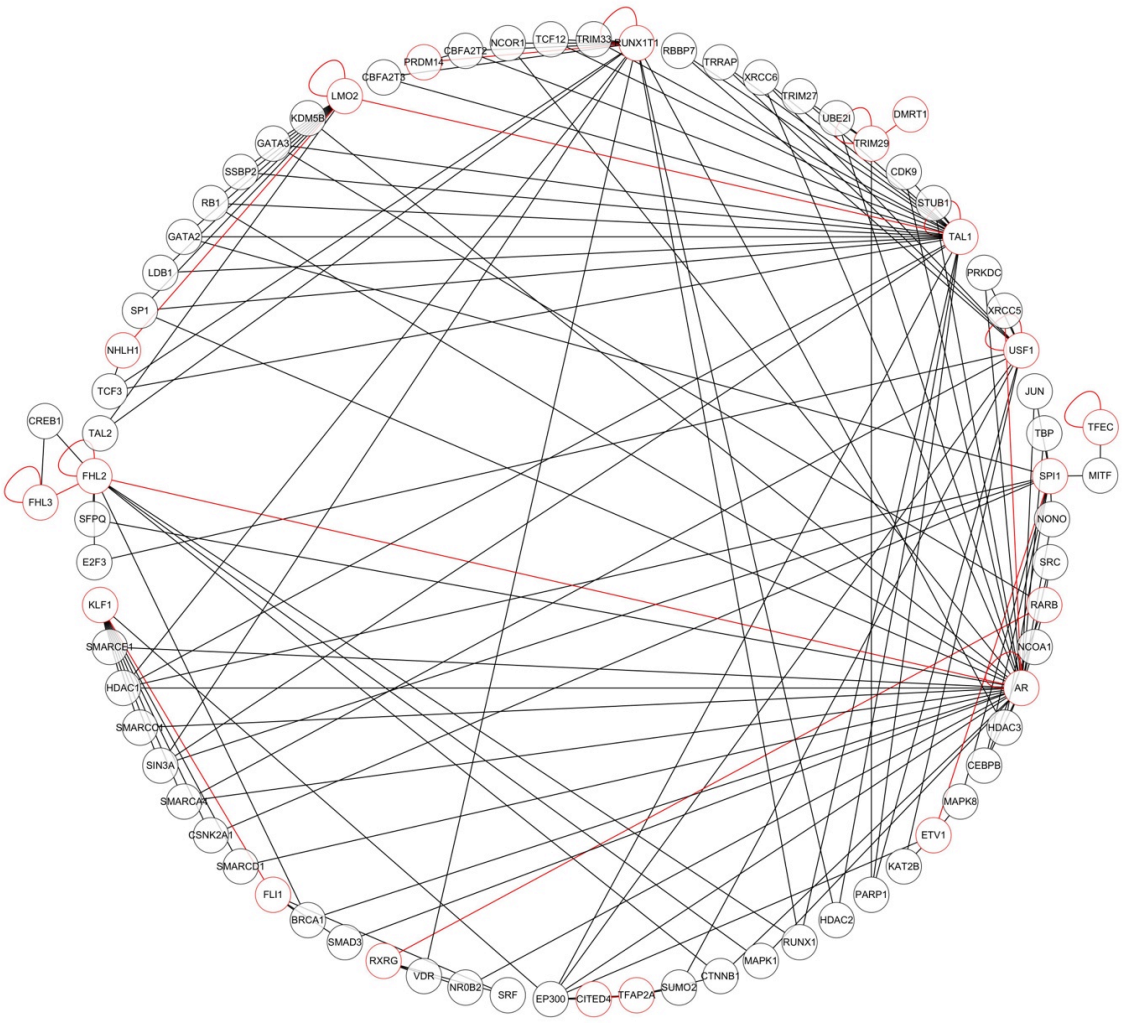

Supplemental Figure 2-1. Network interactions amongst 75 genes that are differentially expressed between the proximal and distal ends of the E6.5 chicken cochlea provide evidence of a complex set of regulatory interactions.

Red nodes depict 23 of the 112 differentially expressed transcription factors. Interactions were extracted from g:Profiler and were visualized in Cytoscape. Literature supported interactions are shown by lines with the red

lines linking pairs of differentially expressed TF genes, which are known to interact.

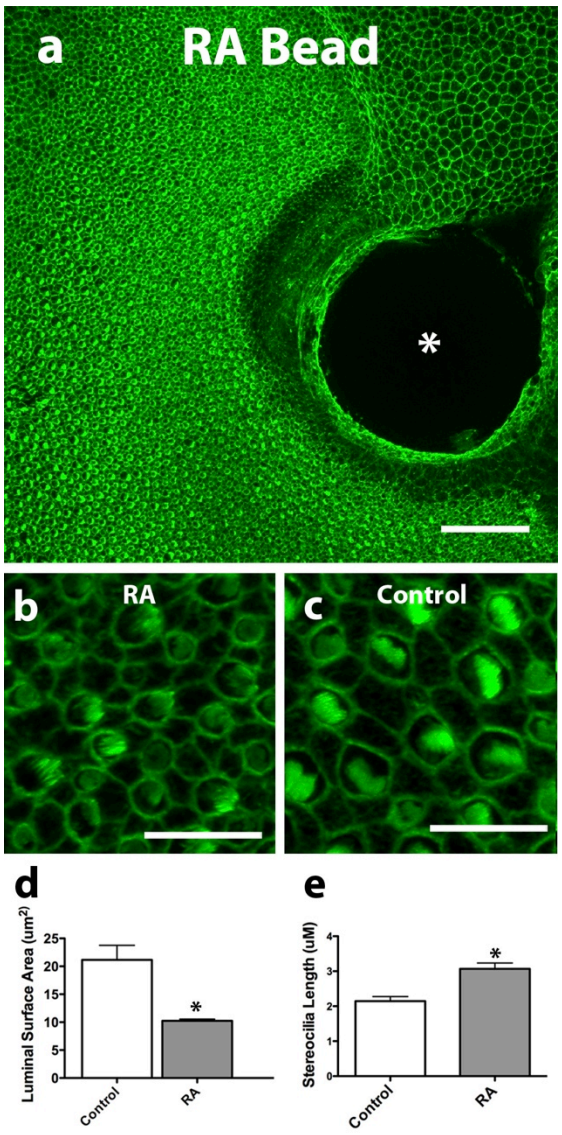

Supplemental Figure 2-2. Local application of RA is sufficient to induce HCs in the proximal region of developing cochleae to develop distal-like phenotypes.

(a) E6.5 BPs were implanted proximally with beads soaked in RA or vehicle-control then maintained in culture for 6 days. Shown is a low magnification micrograph of the proximal region of a cochlea implanted with an RA-soaked

bead. The bead is marked with an (*). BP is labeled with Alexa Fluor 488-phalloidin. (b,c) Representative high magnification micrographs of hair cells that formed in the proximal region of BPs implanted with RA-soaked (b) or vehicle-control beads (c). (d) Quantification of the HC luminal surface area that formed within 100 μm of the bead. Proximal HCs from BPs implanted with RA-soaked beads developed smaller luminal surface areas compared to BPs implanted with vehicle-control beads. (p = 0.0013; Student's t-test; n_{BPs} = 6). (e) Quantification of the stereocilia lengths that formed within 100 μm of the bead. Proximal HCs from BPs implanted with RA-soaked beads developed longer stereocilia compared to BPs implanted with vehicle-control beads. (p = 0.0015; Student's t-test; n_{BPs} = 6). Scale bars in a: 50 μm; b,c: 10 μm

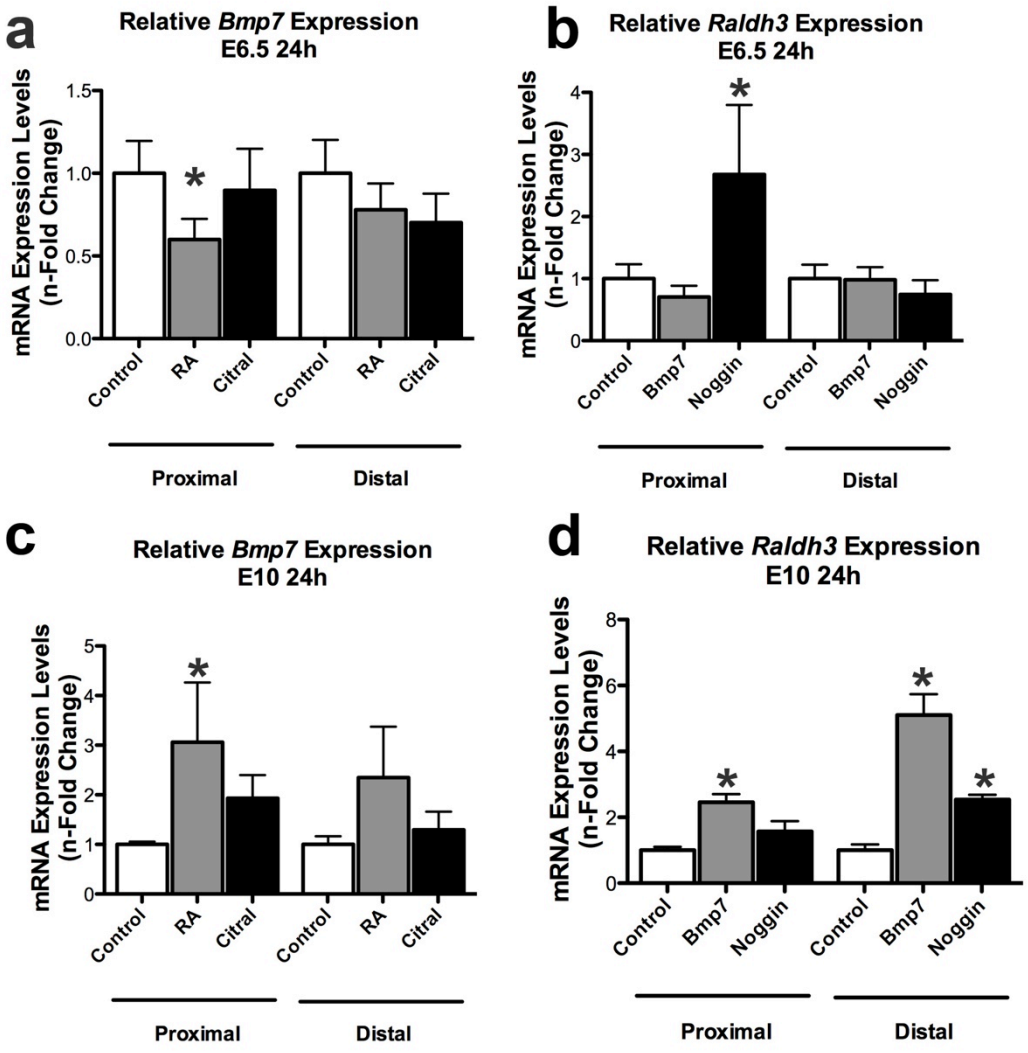

Supplemental Figure 2-3. Reciprocal inhibitory feedback loops between Bmp7 and Retinoic Acid signaling.

(a) Relative *Bmp7* expression levels in proximal and distal regions of E6.5 BPs treated with RA or citral for 24 h. Expression levels were normalized relative to the average mRNA expression levels in vehicle controls. *Bmp7* was significantly downregulated in the distal region of BPs after 24 h RA-treatments ($p < 05$;

ANOVA with Newman-Keuls Post-test, *n* = 10). (b) Relative *Raldh3* expression levels in proximal and distal regions of E6.5 BPs treated with Bmp7 or noggin for 24h. Expression levels were normalized relative to the average mRNA expression levels in controls. *Raldh3* expression was significantly elevated in the proximal region after 24 h noggin treatments ($p < 05$; ANOVA with Newman-Keuls Post-test, *n* = 4). (c) Relative *Bmp7* expression levels in E10 BPs treated with RA or citral for 24 h. Expression levels were normalized to controls. *Bmp7* expression was elevated in the proximal region of BPs treated with RA ($p < 05$; ANOVA with Newman-Keuls Post-test, *n* = 5). (d) Relative *Raldh3* expression levels in E10 BPs treated with Bmp7 or noggin for 24 h. Expression levels were normalized to controls. *Raldh3* expression was elevated in both the proximal and distal regions of BPs treated with Bmp7 ($p < 05$; ANOVA with Newman-Keuls Post-test, *n* = 7) and its expression was elevated in the distal region of BPs treated with noggin ($p < 05$; ANOVA with Newman-Keuls Post-test, *n* = 7)

CHAPTER 3

Permeation of Fluorophore-Conjugated Phalloidin into Live Hair Cells of the Inner Ear is Modulated by P2Y Receptors[2]

SUMMARY

Phalloidin, a toxin isolated from the death cap mushroom, Amanita phalloides, binds to filamentous actin with high affinity, and this has made fluorophore-conjugated phalloidin a useful tool in cellular imaging. Hepatocytes take up phalloidin via the liver-specific organic anion transporting polypeptide 1b2, but phalloidin does not permeate most living cells. Rapid entry of styryl dyes into live hair cells has been used to evaluate function, but the usefulness of those fluorescence dyes is limited by broad and fixed absorption spectra. Since phalloidin can be conjugated to fluorophores with various spectra, I investigated whether it would permeate living hair cells. When I incubated mouse utricles in 66 nM phalloidin-CF488A and followed that by washes in phalloidin-free medium, I observed that it entered a subset of hair cells and labeled entire hair bundles fluorescently after 20 min. Incubations of 90 min labeled nearly all the hair bundles. When phalloidin-treated utricles were cultured for 24 h after washout, the label disappeared from the hair cells and progressively but heterogeneously labeled filamentous actin in the supporting cells. I investigated how phalloidin may enter hair cells and found that P2 receptor antagonists, pyridoxalphosphate-6-azophenyl-2′, 4′-disulfonic acid and suramin, blocked phalloidin entry, while the

[2] This chapter is a reproduction of Thiede and Corwin, JARO. 2014 Feb; 15 (1): 13-30. It has been re-formatted to match the terminology and style within this thesis.

P2Y receptor ligands, uridine-5'-diphosphate and uridine-5'-triphosphaste, stimulated uptake. Consistent with that, the P2Y6 receptor antagonist, MRS 2578, decreased phalloidin uptake. The results show that phalloidin permeates live hair cells through a pathway that requires metabotropic P2Y receptor signaling and suggest that phalloidin can be transferred from hair cells to supporting cells in culture.

INTRODUCTION

Styryl dyes, such as DASPEI, FM 1–43, and FM 4–64, can be used to label live hair cells (HC) in vitro and in vivo (Jorgensen 1989; Balak et al. 1990). Those dyes appear to rapidly enter hair cells through mechanotransduction channels that are in the open state and through ligand-gated P2X receptors (Gale et al. 2001;Meyers et al. 2003; Crumling et al. 2009). Yet, the broad and fixed absorption spectra of styryl dyes can be a hindrance for research that uses additional fluorescent probes. For example, FM 1–43 labeling could pose difficulties while using GFP-fluorescent tissue, since both FM 1–43 and GFP have similar absorbance spectra. For that reason, it would be advantageous to have other fluorophore choices to label live HCs.

Phalloidin, a toxin isolated from the mushroom, Amanita phalloides, binds to filamentous actin (F-actin) at the interface between subunits. Phalloidin has a high affinity for F-actin, and it lowers the critical actin concentration while increasing filament polymerization and stabilization (Dancker et al. 1975; Wieland et al. 1975; Faulstich et al. 1977; Estes et al. 1981; Coluccio and Tilney 1984).

Fluorophore-conjugated phalloidin is widely used for visualizing F-actin in fixed, permeabilized tissue. Although phalloidin does not permeatemost intact cellmembranes, it permeates heptatocytes via liver-specific organic anion uptake transporting polypeptides (Frimmer et al. 1980; Walli et al. 1981; Faulstich et al. 1983; Munter et al. 1986; Petzinger and Frimmer 1988; Fehrenbach et al. 2003; Meier-Abt et al. 2004; Lu et al. 2008).

When low concentrations of fluorophore-conjugated phalloidin are microinjected into live cells it produces fiduciary marks that do not disrupt actin dynamics, allowing the microinjected phalloidin to be followed in vitro via fluorescent speckle microscopy. This provides dynamic measures of localized directions and rates of Factin flow (Lin and Forscher 1995; Waterman-Storer et al. 1998; Schaefer et al. 2002, 2008; Burnette et al. 2008).

Here I report that fluorophore-conjugated phalloidin permeates live HCs in mouse utricles and that the fluorescence persists after aldehyde fixation. When phalloidin-treated utricles are cultured for 24 h after washout, the fluorescent label gradually disappears from HCs and appears in the neighboring supporting cells. Tests with pharmacological activators and inhibitors indicated that P2Y receptor signaling is required for the permeation of phalloidin into HCs and that uridine-5’-diphosphate (UDP) and uridine-5’-triphosphaste (UTP), which are agonists for a subset of P2Y receptors, enhance the permeation. I suspect that fluorophore-conjugated phalloidin might provide a tool useful for measuring the dynamics of actin assembly and turnover in the inner ear.

MATERIALS AND METHODS

Dissection of utricles

All animal experiments were performed according to protocols approved by the Animal Care and Use Committee at the University of Virginia. Swiss Webster mice were obtained from Charles River Labs (Wilmington, MA). Pups were anesthetized on ice and then decapitated. Adult mice were killed by CO2 asphyxiation and then decapitated. Temporal bones were dissected in ice-cold Dulbecco's modified Eagle' s medium (DMEM)/F-12 (Invitrogen, Carlsbad, CA), where the utricles were isolated, the roof dissected away, and the otoconia were removed using protease XXIV for 5 min (50 μg/mL, Sigma, St. Louis, MO).

Fluorophore-conjugated phalloidin treatment

The 2 μL of Cell Tak (BD Bioscience, San Jose, CA) was air-dried on 14 mm microwell glass-bottom culture dishes (MatTek, Ashland, MA). Live neonatal mouse utricles (P0 to P7) were plated nerve-side-down in 60 μl of DMEM/F-12 onto the dried Cell Tak. Phalloidin-CF488A (Biotium, Hayward, CA) was dissolved in water. After testing phalloidin-CF488A concentrations of 13.2 to 500 nM, I did not observe differences in uptake, and I used 66 nM phalloidin-CF488A for the analytical experiments reported here.

The 140 μl of DMEM/F-12 containing 94.29 nM phalloidin-CF488A and 1 % fetal bovine serum (FBS, Gibco) were added to the 60 μl volumes of culture media in the MatTek dishes to produce a final volume of 200 μl of 66 nM phalloidin-CF488A in each dish. Utricles were then incubated at 37 °C for 1 to

120 min, depending on the experiment. To wash out the phalloidin-containing media, 1 mL of DMEM/F-12 was added to each dish, and after 30 s, 1 mL was removed. This was repeated three times. For live imaging, utricles were gently lifted off the dish with fine forceps and mounted nerve-side-up in a 60 µl drop of DMEM/F-12 on a coverglass chamber. Coverglass chambers were prepared by adhering two strips of double-sided Scotch tape to create a bridge with the tape acting as spacers so that, when utricles were mounted between the top and bottom coverglasses, the hair bundles were not bent or damaged. The utricle remained in place for imaging after the smaller top coverglass was placed over it. All images of live utricles were taken within 10 min.

To examine whether unconjugated CF488A fluorophore alone would permeate into cells of the inner ear, live neonatal utricles were plated on air-dried Cell Tak in Mat Tek dishes in 60 µl of DMEM/F-12 as described above. CF488A, amine (Biotium, Hayward, CA) was dissolved in water. The 140 µl of DMEM/F-12 containing 94.29 nM CF488A and 1 % fetal bovine serum (FBS, Gibco) were added to the 60 µl volumes of culture medium in the MatTek dishes to produce a final volume of 200 µl of 66 nM CF488A in each dish. Utricles were then incubated at 37 °C for 30 min. The CF488A-containing media was then washed out as described above, and the utricles were then imaged live.

In some experiments, mounted utricles were treated with 66 nM Alexa Fluor 647 phalloidin for 20 min. The phalloidin-containing medium was then washed out three times with DMEM/F-12, and the utricles were exposed to 5 µM FM 1–43 in DMEM/F-12 for 10 s as previously described (Meyers et al. 2003).

Then, that was washed out with three changes of DMEM/F-12, and the utricles were imaged live.

In other experiments, after the three washes in label-free medium, fresh DMEM/F-12 containing 1 % FBS, 0.25 µg/ml Fungizone, and 10 µg/ml ciprofloxacin (Bayer, Berlin, Germany) were added back to the dish, and the utricles were cultured in that phalloidin-free medium at 37 °C for either 3, 6, 12, 18, 24 h, or 7 days.

Aldehyde fixation and actin staining

For certain experiments, live phalloidin-treated utricles were washed three times with phalloidin-free DMEM/F-12 and fixed for 25 min in 4 % paraformaldehyde in phosphate-buffered saline (PBS) at room temperature (RT), then imaged directly or after staining in Alexa Fluor 647-phalloidin (132 nM) in PBS containing 0.2 % Triton X-100 (PBST). Samples were mounted in SlowFade (Invitrogen), and images were taken with Zeiss LSM 510 and Zeiss LSM 710 confocal microscopes. Images of control and drug-treated groups were acquired using identical exposure settings to allow for comparisons between the groups.

To compare fluorescence between utricles that were treated with phalloidin-CF488A before fixation and utricles treated with phalloidin-CF488A after fixation, freshly dissected neonatal utricles were separated into two groups. One group of utricles was treated live with 66 nM phalloidin-CF488A for 30 min as described above. These utricles were then fixed with 4 % paraformaldehyde for 25 min and imaged as described. The other group of freshly dissected utricles

was treated with protease XXIV for 5 min (50 µg/mL, Sigma, St. Louis, MO) and then fixed with 4 % paraformaldehyde in PBS for 25 min. After the fix was washed out with three washes of PBS, the utricles were then incubated in 200 µl of 66 nM phalloidin-CF488A (dissolved in water) for 30 min at room temperature. Utricles were then washed with PBS and imaged.

Immunocytochemistry

Mouse anti-myosin VIIA (1:100, Developmental Studies Hybridoma Bank) and rabbit anti-Sox2 (1:1000, Millipore, Temecula, CA) were used to label hair cell somata and supporting cell nuclei, respectively. Fixed utricles were washed in PBS and then incubated for 30 min at RT with PBST and 10 % normal goat serum (Vector Laboratories, Burlingame, CA). Samples were then incubated overnight in primary antibodies in PBST with 2 % normal goat serum. The next day, samples were washed three times with PBS and then incubated with Alexa-conjugated secondary antibodies (1:200, Invitrogen) in PBST for 1 hr at RT. Then, utricles were rinsed in PBS three times and mounted in SlowFade for imaging.

Examination of phalloidin uptake using pharmacological antagonists

To investigate whether phalloidin permeation requires P2 receptor signaling, utricles were incubated in the P2 receptor antagonists pyridoxalphosphate-6-azophenyl-2′, 4′-disulfonic acid (PPADS, 100 µM, Tocris Biosciences, Ellisville, MO, for 15 min at 37 °C) or suramin (Sigma, 100 µM, for

15 min at 37 °C). In some experiments, utricles were pre-treated with PPADS (100 μM, 15 min at 37 °C), then incubated with PPADS (100 μM) and phalloidin-CF488A (66 nM) for 90 min at 37 °C. After three washes in DMEM/F-12, the utricles were incubated an additional 90 min at 37 °C with 66 nM phalloidin-CF488A to test whether the PPADS treatment would lead to a persistent inhibition of phalloidin permeation. After three additional washes in phalloidin-free DMEM/F-12, those utricles were imaged live. In other experiments, mounted utricles that had been treated with PPADS were exposed to PPADS and 5 μM FM 1–43 in DMEM/F-12 for 10 s as previously described (Meyers et al. 2003), then that was washed out with three changes of DMEM/F-12, and the utricles were imaged live.

To investigate P2 receptor agonists that might enhance permeation of phalloidin-CF488A, I incubated utricles with either adenosine 5'-triphosphate (ATP, 1mM, Sigma), 2′(3′)-O-(4-Benzoylbenzoyl) adenosine-5′-triphosphate triethylammonium (BzATP, 100 μM, Tocris), adenosine 5'-diphosphate (ADP, 1 mM, Sigma), uridine 5'-triphosphate (UTP, 1 mM, Sigma), uridine 5'diphosphoglucose disodium (UDP-glucose, 1 mM, Sigma), or uridine 5'-diphosphate (UDP, 1 mM, Tocris) for 15 min at 37 °C. Then they were incubated an additional 20 min at 37 °C with both the respective nucleotide and phalloidin-CF488A (66 nM), and rinsed three times in DMEM/F-12 before they were imaged live or before fixation in 4 % paraformaldehyde.

To investigate whether phalloidin permeation requires P2Y6 receptors, I used MRS 2578, a potent antagonist for P2Y6 receptors. MRS 2578 was

dissolved in dimethyl sulfoxide (DMSO) (Sigma). Utricles were treated with MRS 2578 for 15min at 37 °C. Utricles were then cultured an additional 20 min at 37 °C with MRS 2578 and phalloidin-CF488A (66 nM). After three washes in DMEM/F-12, utricles were fixed with 4 % paraformaldehyde as above and imaged. MRS 2578-treated utricles were compared against vehicle controls.

To investigate whether phalloidin permeation requires PLC or PKC second messenger signaling, I used U-73122 hydrate (10 μM, Sigma), an inhibitor of phospholipase C, and bisindolylmaleimide II (BIM II; 50 μM, Sigma), an inhibitor of all protein kinase C subtypes. These drugs were dissolved in DMSO. Utricles were treated with individual drugs for 20 min at 37 °C. Utricles were then cultured an additional 20 min at 37 °C with the respective drug and phalloidin-CF488A (66 nM). After three washes in DMEM/F-12, utricles were fixed with 4 % paraformaldehyde as above and imaged. Fluorescence levels in U-73122- and BIMII-treated utricles were compared against vehicle controls. Additionally, to investigate whether these pharmacological inhibitors would be sufficient to prevent agonist-induced stimulation of phalloidin-CF488A uptake, utricles were treated with 1 mM UDP and either U-73122 or BIM II for 20 min at 37 °C. They were then cultured an additional 20 min at 37 °C with UDP and the respective drug and phalloidin-CF488A (66 nM). After three washes in DMEM/F-12, utricles were fixed with 4 % paraformaldehyde as above and imaged. Fluorescence was compared against vehicle controls.

To test for an involvement of OATs or OATPs in the permeation of phalloidin, utricles were treated with probenecid (2 mM, Sigma). Utricles were

treated with probenecid for 20 min at 37 °C. They were then cultured an additional 20 min at 37 °C with the probenecid and phalloidin-CF488A (66 nM). After three washes in DMEM/F-12, utricles were fixed with 4 % paraformaldehyde as above and imaged. Utricles were compared against vehicle controls.

To test for the involvement of pannexin channels in the permeation of phalloidin into hair cells, utricles were treated with 100 μM carbenoxolone (CBX, Sigma) for 15 min at 37 °C. Utricles were then cultured an additional 20 min at 37 °C with the drug and phalloidin-CF488A (66 nM). After three washes in DMEM/F-12, utricles were fixed with paraformaldehyde and imaged.

RNA extraction, RT-PCR, and quantitative PCR

To delaminate the sensory epithelium, utricles from P5 mice were incubated in thermolysin (0.5 mg/ml in DMEM/F-12; Sigma) at 37 °C for 60 minutes, and then transferred to DMEM/F-12 where the macula and its surrounding non-sensory epithelium were carefully separated from the underlying stromal tissue in each utricle by microdissection (Saffer et al. 1996). Delaminated epithelia and stromal tissue samples were collected and pooled separately. RNA was extracted from those samples as well as from P0 kidney and liver tissue using the RNAqueous kit (Ambion) according to the manufacturer's protocol. Poly-A RNA was reverse transcribed using a High Capacity RNA-to-cDNA kit (Applied Biosystems) and quantitative PCR was performed in triplicate (i.e., starting material was collected and pooled three times independently) using a

SensiMix SYBR Green and Fluorescein kit (Quantace) on a MyIQ/iCycler (Biorad). Cyclophilin was used as an endogenous reference. Gene expression was analyzed using the Real-time PCR miner algorithm (Zhao and Fernald 2005). The following primers were used: Cyclophilin (Forward: CAGTGCTCAGAGCTCGAAAGT; Reverse: GTGTTCTTCGACATCACGGC), Oat1 (Forward: TGCACAGTTGGCCTCCCTGC; Re v e r s e: GCTCACTATGCTGCCCACCCG), Oatp2b1 (Forward: AGCAGGGCTTCTACCACACCTGA; Reverse: TCCTGTCTGGCATCCGGGGC), Oatp3a1 (Forward: AAACCACGAGGGCGGGCTGA; Re v e r s e : GCAGCCCTCAGCTTCGCACAA), Oatp1b2 (Forward: TCGCCAGCCTAGGCCAAATGC; R e v e r s e : TGGGCAGCTTTGCTTGGATGCT), and Oatp2a1 (Forward: GGGACGGTGCCCATTCAGCC; Reverse: GGCTCCGATCCACCGAGGGT).

For RT-PCR analysis, cDNA was prepared as described above from 100 ng total RNA extracted from the delaminated P5 mouse utricle sensory epithelium and stroma samples. Control experiments testing for the presence of genomic DNA contamination in the RNA where no reverse transcriptase was added to the reactions were negative (data not shown). mRNA expression was evaluated on a MyIQ/iCycler (Biorad) using Taq DNA Polymerase (1 unit final, Invitrogen), 10X PCR Buffer (Invitrogen), 2mMMgCl2 (Invitrogen), and 0.2 mM dNTP mix (Invitrogen).

The following PCR primers were used: Cyclophilin (Forward: CAGTGCTCAGAGCTCGAAAGT; Reverse: GTGTTCTTCGACATCACGGC),

P2Y1 (Forward: AGGAAAGCTTCCAGGAGGAG; R e v er s e: CGTGTCTCCATTCTGCTTGA), P2Y2 (Forward: GTCAGCAGTGACGACTCAAGAC; Reverse: TCAGAGGATATCAGCCCCTTTA), P2Y4 (Forward: GCAGGCGTGAAGTGAGGCCA; Re v e r s e : TGGAGGGTAAGGAGCACCATCTTAG), P2Y6 (Forward: GGCGGCTCGTATGGCTGTGG; Reverse: GCAAGAGACACCGGGCGTGG), P2Y12 (Forward: CCGCACGGACACTTTCCCGTA; Re v e r s e : TGCCGGTGAAGGTGAGTTGCC), P2Y13 (Forward: GGCCACTAGATGTCACCTTTTC; Reverse: GATGGTGGGGTGGTAACTAGAA), P2Y14 (Forward: GGAATTCTCTCTTCCGAATCCT; Reverse : TGTTCATCTTCTCACCTCTGGA). Primers were first tested using cDNA synthesized from RNA extracted from P5 mouse brain.

Specimens were preheated at 94 °C for 3 min followed by 35 cycles at 94 °C for 30 sec, 60 °C for 30 sec, and 72 °C for 30 sec, then 72 °C for 2 min. PCR products were then separated on a 1 % agarose gel.

Data analysis

Each experiment was repeated at least three times and analyzed with Student's t-test or one-way ANOVA with Newman-Keuls Multiple Comparisons post-test (GraphPad Prism; α level=0.05 in all cases). All descriptive statistics are presented as the mean± S.E.M. All Student's t-test analyses were performed with

two-tails. Images were carefully selected to demonstrate the average effect.

RESULTS

Phalloidin permeates live hair cells and supporting cells in mouse utricles

To determine whether phalloidin could permeate and fluorescently label cells in living mouse utricles, I bathed utricles in phalloidin-CF488A for 20 min. I counted the number of hair cells and supporting cells phalloidin-CF488A permeated into. I identified HCs based upon the presence of fluorescent hair bundles or cuticular plates and I identified supporting cells based upon an absence of a hair bundle and cuticular plate and the presence of their characteristic circumferential F-actin belts, which are shown in the inset in Figure 3-1B. In each utricle, I detected 83.0 ± 11.8 fluorescent hair bundles and 37.8 ± 5.9 fluorescent supporting cells (Fig. 3-1A, B; n=24). I also detected punctate fluorescence throughout the sensory epithelium. These results indicate that phalloidin-CF488A can permeate both hair cells and supporting cells.

I tested whether phalloidin-CF488A could permeate into auditory HCs by incubating neonatal mouse cochleae in phalloidin-CF488A for 20 min as described (n=6). When I imaged these live cochleae I observed that many of the HCs had become highly fluorescent. Thus, the permeation of phalloidin-CF488A is not limited to vestibular HCs (Fig. 3-1C).

I incubated utricles for 90 min to determine whether longer incubations would allow more cells to take up the phalloidin. Phalloidin permeated more hair cells and supporting cells, as I observed 906 ± 74.6 fluorescent hair bundles

(Student's *t*test, $t(27)= 20.04$, $p<0.0001$, Fig. 3-1D, E; $n=5$) and 225 ± 72.1 fluorescent supporting cells (Student's *t*test, $t(27)=5.641$, $p<0.0001$, Fig. 3-1D, E; $n=5$). This indicates that phalloidin can permeate living hair cells and supporting cells, but the permeation is not rapid.

To ensure that this labeling phenomenon was not due to any unique properties of the CF488A fluorophore, I also incubated utricles with phalloidin conjugated to Texas Red, Alexa Fluor 488, Alexa Fluor 568, and Alexa Fluor 647. In each of these experiments I observed comparable labeling patterns (data not shown). I also incubated utricles with unconjugated CF488A fluorophore. After I bathed utricles for 30min with 66 nM CF488A, I did not detect any fluorescence (Fig. 3-1F). This suggests that the fluorophore-conjugated phalloidin entry into hair cells and supporting cells is due to the unique properties of phalloidin.

We investigated whether phalloidin-CF488A permeation impairs the capacity for hair cells to take up a brief exposure (10 sec) of FM 1–43. Rapid uptake of FM 1–43 is considered an indicator of functional mechanotransduction channels (Meyers et al. 2003). For this, I incubated utricles for 20 min with phalloidin conjugated to Alexa Fluor 647. After washing out the Alexa Fluor 647 phalloidin, I incubated the utricles for 10 sec with FM 1–43. The FM 1–43 dye was then washed out and the utricles were imaged live. I detected both Alexa Fluor 647 phalloidin and FM 1–43 fluorescence in these utricles (Fig. 3-1G). HCs throughout the maculae took up FM 1–43, and the FM 1–43 labeling pattern in the HCs that were Alexa Fluor 647 phalloidin-positive appeared to be

indistinguishable from that in the HCs that were Alexa Fluor 647-phalloidin-negative. The results suggest that the permeation of phalloidin-CF488A into HCs does not cause an overwhelming block of mechanotransduction channels.

Since phalloidin has a high affinity for F-actin, I tested whether it would remain bound in culture. I incubated utricles for 90 min with phalloidin-CF488A and then maintained them in phalloidin-free media for 24 hr. I found that the number of fluorescent hair bundles diminished, and supporting cells throughout the maculae became fluorescent (Fig. 3-1H, I; n=6).

We sought to determine more precisely when the label disappeared from hair cells and began to appear more robustly amongst supporting cells, so I fixed utricles at various time points after the phalloidin-CF488A incubation (Fig. 3-2). Hair bundles were fluorescent 3 hr after the phalloidin washout. However, by 12 hr there were noticeable gaps in fluorescence throughout the sensory epithelium. I detected only 298.3±64.7 fluorescent hair bundles at this time, significantly less than after the 0 hr timepoint (Student's *t*test, $t(9)=6.183$, $p<0.0001$, Fig. 3-2B, H; n=6)., By 18 hr, supporting cells throughout the sensory epithelium had taken up the label and were fluorescent. These results show that after incubating utricles with phalloidin-CF488A, less than half the hair cells retain the label 12 hr after a washout and that nearly all the supporting cells take up the label and become fluorescent by 18 hr.

The absence of fluorescent labeling of HCs in phalloidin-CF488A treated utricles that were maintained in culture over extended periods of time (> 18 hr) led us to investigate whether HCs died or experienced deleterious effects after

phalloidin-treated utricles were maintained in culture. To test for this, I treated P2 utricles with 66 nM phalloidin-CF488A as above, washed out the label, and then maintained the utricles in culture for 24 hr. At this time point, I fixed the utricles, immunolabeled them with a monoclonal antibody directed against myosin VIIA, which labels HCs, and then took high magnification confocal micrographs. I measured the density of myosin VIIA-positive HCs remaining in these cultures from 15 separate 50 μm x 50 μm regions from each cultured utricle. In utricles treated with phalloidin-CF488A, I detected an average HC density of 43.82 HCs/2500 μm^2 (*n*=3). This is comparable to the previously reported density of 46.75 HCs/2500 μm^2 in P2 mouse utricles that were fixed in vivo (Burns et al. 2012). Furthermore, P2 utricles maintained 24 hr in culture that were not treated with phalloidin-CF488A had 42.51 HCs/2500 μm^2 (Fig. 3-3). These results show that at least over the period of 24 hr, there is not a substantial amount of HC degeneration resulting from the phalloidin-CF488A treatments.

We next sought to determine whether HCs in phalloidin-treated utricles maintain their hair bundles over longer periods in culture. For this, I treated four utricles with phalloidin-CF488A as described, washed out the phalloidin-containing medium, and then incubated the utricles in phalloidin-free culture medium for 7 days. After that, I fixed and permeabilized the utricles and incubated them with Alexa Fluor 647-phalloidin to stain all the F-actin. The presence of substantial numbers of Alexa Fluor 647-phalloidin labeled hair bundles in these utricles showed that the loss of phalloidin-CF488A fluorescence had not resulted from a substantial HC or hair bundle loss caused by the prior

live treatment with phalloidin-CF488A and that the prior treatment did not cause substantial hair bundle losses even after long periods in culture (Fig. 3-3I–L).

The manner and the mechanism by which the label disappears from the hair bundles over time in culture remains unknown. However, I investigated whether HCs in cultured, phalloidin-treated utricles remained capable of taking up fluorophore-conjugated phalloidin. For this, I treated utricles with phalloidin-CF488A for 90 min, washed out the label, and then cultured them for 24 hr. After imaging two of these utricles, I confirmed that fluorescence was lost from the HCs at this time. The remaining utricles were then incubated with Alexa Fluor 647-phalloidin and imaged. I detected Alexa Fluor 647-phalloidin positive hair bundles throughout these utricles, suggesting that HCs in these cultured utricles remain capable of taking up fluorophore-conjugated phalloidin (data not shown, n=4).

We tested whether the fluorescent labeling pattern would change after fixation. I incubated utricles with phalloidin-CF488A for 20 min then fixed with paraformaldehyde. There were 84.33 ± 15.0 fluorescent hair bundles after fixation, which did not differ from what I observed in living utricles (Student's *t*test, $t(28)=0.055$, $p=0.957$, Fig. 3-4A; $n=6$). From this I determined that the phalloidin-labeling pattern in hair cells is not changed with aldehyde fixation.

For deeper antibody penetration, many immunofluorescence protocols require detergents, such as Triton X-100, to permeabilize the tissue. I sought to determine whether using this detergent could alter the distribution of phalloidin labeling. I incubated fixed phalloidin-treated utricles in PBS containing 0.2

%Triton X-100 and 132 nM Alexa Fluor 647 phalloidin for 30 min at RT. I found that the fluorescence from the CF488A fluorophore, which is conjugated to the phalloidin used to treat the live utricles, became diffuse throughout the tissue (Fig. 3-4B). All F-actin structures throughout the epithelium displayed fluorescence with noticeable intensity differences. So while treating live utricles with fluorophore-conjugated phalloidin may produce a labeling pattern that persists after aldehyde fixation, treatment with detergents such as Triton-X 100 can cause the fluorescence to become diffuse.

We investigated whether the permeation of phalloidin-CF488A into cells of the inner ear involves an active pathway (channel), or whether it would also be able to permeate into fixed tissues. For this, I compared fluorescence between utricles that were treated with phalloidin-CF488A before fixation to utricles that were treated with phalloidin-CF488A after fixation (Fig. 3-5). Utricles were incubated with 66 nM phalloidin-CF488A for 20 min, washed three times, fixed with 4 % paraformaldehyde and then imaged (Fig. 3-5C). Fluorescence in these were compared against utricles that were dissected, fixed with 4 % paraformaldehyde, then treated with 66 nM phalloidin-CF488A for 20 min (Fig. 3-5D). To compare uptake amongst samples, I measured average fluorescence intensities in five 100 µm x 100 µm regions of the sensory epithelium from maximum projection images using ImageJ (NIH) (Fig. 3-5A). I normalized fluorescent intensities to the mean intensities in controls. I detected significantly more fluorescence in the utricles treated with phalloidin-CF488A before fixation (Student's *t*test, $t(4)=4.173$, $p=0.014$, Fig. 3-5B). This suggests that the

permeation of phalloidin-CF488A into sensory cells of the utricle involves an active pathway.

P2 receptors contribute to the permeation of phalloidin into hair cells

P2 receptors are involved in the permeation of large molecular weight molecules and dyes including YOPRO-1, TO-PRO-1, ethidium, lucifer yellow, and calcein (Surprenant et al. 1996; North 2002; Cankurtaran-Sayar et al. 2009). P2 receptors are subdivided into two distinct families: P2X and P2Y receptors. P2Xreceptors have two plasma membrane-spanning domains and respond to extracellular ATP as gated, cation-selective channels. In contrast, P2Y receptors are metabotropic, G protein-coupled receptors (GPCR) with seven transmembrane domains, and various P2Y family members have shown coupling to G_q/11, G_i, or G_s proteins (Housley 1998; Housley et al. 2009; Housley and Gale 2010).

HCs express both P2X and P2Y receptors (Housley et al. 1992; Housley et al. 1998; Housley et al. 1999; Szücs et al. 2004; Huang et al. 2010). I investigated whether these receptors are required for phalloidin entry through hair cells using PPADs and suramin, non-selective P2 antagonists (Lambrecht et al. 1992; Li 2000; Surprenant et al. 2000; Lambrecht et al. 2002; North 2002; Trujillo et al. 2006). I pre-incubated utricles with the antagonist for 15 min, then applied phalloidin-CF488A in the presence of the antagonist for 90 min. I found that both PPADS and suramin effectively blocked phalloidin uptake. Phalloidin only permeated into 4.3 ± 1.2 hair cells in the presence of PPADS, a significant

decrease compared to controls (Student's *t*test, $t(30)=3.801$, $p=0.0007$, Fig. 3-6B; $n=8$). Suramin similarly decreased phalloidin uptake, where only 15.3 ± 11.6 hair cells were fluorescent (Student's *t*test, $t(26)=2.278$, $p=0.0312$, Fig. 3-6E; $n=4$). I fixed PPADS- and suramin-treated utricles and stained them with Alexa Fluor 647 phalloidin to confirm that hair cells were still present (Fig. 3-6C, D). These results indicate that P2 receptor signaling is required for phalloidin entry into live hair cells.

The styryl dye FM 1–43 enters mechanotransduction channels that are in the open state (Meyers et al. 2003). FM 1–43 is also widely used to investigate whether hair cells possess functional mechanotransduction currents (Kawashima et al. 2011). I applied FM 1–43 to PPADS-treated utricles to determine whether PPADS interferes with mechanotransduction, and found that these hair cells had normal FM 1–43 uptake (Fig. 3-6F; $n=4$). These results are consistent with the hypothesis that the decreased dye uptake is not due to an effect of PPADS on the mechanotransduction channel.

The inhibition of P2 receptor signaling by PPADS is reversible (Li 2000). Accordingly, I found that while uptake of phalloidin-CF488A was blocked in the presence of PPADS (Fig. 3-6G), hair cells were able to take up phalloidin-CF488A after PPADS was washed out (Fig. 3-6H). This indicates that the PPADS-mediated inhibition of phalloidin permeation is reversible.

P2Y nucleotide agonists enhance phalloidin-CF488A permeation

P2X and P2Y receptors are extracellularly gated by purine and pyrmidine

nucleotides. In pharmacological studies, ATP is a major agonist for all P2X receptors and BzATP can potently activate P2X7 receptors. ADP, UTP, UDP, and UDP-glucose are major agonists that activate specific P2Y receptor subtypes (North 2002). I individually pretreated utricles with these to determine which P2 receptor subtypes might be involved in the phalloidin permeation.

We found that ATP decreased phalloidin uptake by 32.3% (One-way analysis of variance [ANOVA] with Newman-Keuls Multiple Comparisons test, $p<0.05$, Fig. 3-7A, C; $n=12$). While extracellular ATP activates P2X channels, it can antagonize P2Y receptor subtypes (Kennedy et al. 2000). I observed no significant differences in fluorescence in utricles pretreated with BzATP, another P2X agonist (One-way ANOVA with Newman-Keuls Multiple Comparisons test, $p<0.05$, Fig. 3-7A, D; $n=9$). This indicates that P2X channels are not required for phalloidin uptake.

We further examined fluorescence from phalloidin-CF488A permeation upon pretreating with P2Y agonists. ADP, an agonist for P2Y1, P2Y12, and P2Y13 receptors, did not increase fluorescence from phalloidin-CF488A labeling (One-way ANOVA with Newman-Keuls Multiple Comparisons test, $p<0.05$, Fig. 3-7A, E; $n=6$). I also observed no significant differences in fluorescence after treating with UDP-glucose, a P2Y14 agonist (One-way ANOVA with Newman-Keuls Multiple Comparisons test, $p<0.05$, Fig. 7A, G; $n=4$). However, UTP (P2Y2, P2Y4, and P2Y6), increased fluorescence by 29 % (One-way ANOVA with Newman-Keuls Multiple Comparisons test, $p<0.05$, Fig. 3-7A, F; $n=11$). Another P2Y agonist, UDP (P2Y6), enhanced fluorescence by 56% (One-way ANOVA

with Newman-Keuls Multiple Comparisons test, $p<0.05$, Fig. 3-7A, G; $n=6$). These results implicate P2Y receptor signaling in the uptake of phalloidin.

P2Y-PLC-PKC signaling contributes to the permeation of fluorophore-conjugated phalloidin

We evaluated the presence of P2Y receptor subtype expression in the neonatal utricular maculae and underlying stroma using RT-PCR (Fig. 3-8A; $n=3$). I detected mRNA expression of P2Y1, P2Y2, P2Y6, P2Y13, and P2Y14 in the maculae. Since P2Y6 can be activated by both UTP and UDP, I evaluated the effects of MRS 2578, a P2Y6 antagonist, on the permeation of phalloidin-CF488A (Mamedova et al. 2004). Treating with 500 nM MRS 2578 decreased the resulting fluorescence by 27.0 % (Student's *t*-test, $t(16)=3.498$, $p=0.003$, Fig. 3-8B; $n=4$).This is consistent with the hypothesis that P2Y6 signaling is involved in the permeation of phalloidin. While PPADs and suramin almost completely prevented the permeation of phalloidin-CF488A into hair cells,MRS 2578 significantly decreased fluorescence by only 27.0%. I tested MRS 2578 at 500 nM, a concentration higher than the IC_{50} of 98 nM previously for this inhibitor in rats (Mamedova et al. 2004). I suspect that other P2Y receptors may be involved in the permeation, such as P2Y2, which also is responsive to uridine nucleotides and is expressed in the utricle sensory epithelium.

P2Y6, along with P2Y1, P2Y2, P2Y4, and P2Y11, can bind to Gq/11 to activate protein kinase C (PKC) via phospholipase C (PLC) (Burnstock 2004; Jacobson and Boeynaems 2010). To determine whether PLC-PKC signaling is

involved downstream of P2Y activation in the permeation of phalloidin-CF488A, I examined the effects of U-73122, a PLC inhibitor, and BIM II, a PKC inhibitor, on phalloidin-CF488A entry. I also tested whether these antagonists would decrease phalloidin-CF488A uptake in the presence of the agonist, UDP. Fluorescence was decreased 37.5 % in the presence of U-73122 (One-way ANOVA with Newman-Keuls Multiple Comparisons Test, $p<0.05$, Fig. 3-8C; $n=5$). Additionally, BIM II treatments decreased fluorescence by 41.5 % (One-way ANOVA with Newman-Keuls Multiple Comparisons Test, $p<0.05$, Fig. 3-8C; $n=6$). There also was decreased fluorescence in U-73122 and BIM II treated utricles that were additionally treated with UDP (One-way ANOVA with Newman-Keuls Multiple Comparisons Test, $p<0.05$, $n=4$).

The effectiveness of PPADS and suramin in blocking phalloidin uptake (Fig. 3-6B, E), together with the potency of UDP and UTP in stimulating phalloidin uptake (Fig. 3-7A, F, G), and the effectiveness of MRS 2578, U-73122, and BIM II in decreasing phalloidin-CF488A labeling (Fig. 3-8B, C), implicate P2Y-PLC-PKC signaling in the permeation of phalloidin into the neonatal mouse utricle.

Evaluation of OATPs in the permeation of phalloidin in the inner ear

The plasma membrane anionic transporters (OATs) and organic anion transporting polypeptides (OATPs) are transmembrane proteins capable of transporting diverse organic compounds (Obaidat et al. 2012; Roth et al. 2012). Phalloidin permeates hepatocytes through OATPs (Fehrenbach et al. 2003;

Meier-Abt et al. 2004). Eleven OATPs and ten OATs have been discovered in a diversity of human tissues. To evaluate the potential roles of OATPs or OATs in the permeation of phalloidin in the inner ear, I measured the levels of expression for a subset of these transporters in the neonatal maculae, and compared them to the expression levels in the underlying stroma, the kidney, and the liver. I quantified mRNA expression for Oat1, Oatp2b1, Oatp2a1, Oatp3a1, and Oatp1b2, which is the OATP that allows rodent hepatocytes to take up phalloidin (Cihlar et al. 1999; Fehrenbach et al. 2003; Meier-Abt et al. 2004). I detected Oat1, Oatp2a1, and Oatp3a1 expression in the maculae (Fig. 3-9A; n=3). There was 40.9-fold more Oatp3a1 expression in the maculae than in the liver, but the liver expressed 2.3-fold more Oatp2a1 transcripts. Oat1 plays a key role in transporting anions in the kidney, where I found its expression to be 2.1- and 28.9-fold more abundant compared to the maculae and liver, respectively. I did not detect abundant expression of the liver-specific Oatp1b2, in the utricle, kidney, or liver.

In a pharmacological test for the involvement of OATs or OATPs in the permeation of phalloidin in the utricle, I used probenecid, which inhibits many OATs and OATPs (Sugiyama et al. 2001; Yasui-Furukori et al. 2005; Jorgensen et al. 2007; Silverman et al. 2008). Consistent with a potential involvement for OATPs or OATs in the permeation of phalloidin, probenecid significantly inhibited phalloidin permeation and decreased fluorescence by 33.9% (Student's *t*test, $t(16)=3.472$, $p=0.0003$, Fig. 3-9B, n=15). Future investigations into whether a specific OATP or OAT is required for phalloidin permeation in hair cells may

clarify a role for these transporters.

Besides OATs and OATPs, probenecid also inhibits pannexin channels (Silverman et al. 2008; Sandilos and Bayliss 2012). Pannexins are transmembrane proteins closely related to the gap-junction forming connexins (Baranova et al. 2004). Also, P2 receptor coupling to pannexin channels can cause cellular permeability to large dye molecules (North 2002). I used the pannexin channel inhibitor, CBX, to evaluate a potential role for these channels in the uptake of phalloidin-CF488A (Locovei et al. 2006). I observed no significant differences in fluorescence after CBX treatments (Student's *t*test, $t(5)= 0.4321$, $p=0.6837$, $n=4$), suggesting that pannexins are not involved in the permeation of fluorophore-conjugated phalloidin.

DISCUSSION

Permeation of fluorophore-conjugated phalloidin requires P2 receptor signaling

Our main finding is that phalloidin-CF488A can permeate living cells of the mouse utricle. The number of fluorescently labeled supporting cells in phalloidin-CF488A-treated utricles increases over time as utricles are maintained in phalloidin-free medium. P2 receptor antagonists effectively block phalloidin's permeation into hair cells. I also found that permeation is stimulated with UTP and UDP pretreatments, which are nucleotide agonists for a subset of P2Y receptors. Additionally, specific P2Y6, phospholipase c (PLC), and protein kinase C (PKC) inhibitors decrease permeation, implicating P2Y-PLC–PKC signaling in

the uptake of phalloidin-CF488A.

Hair cells can take up a diversity of compounds through multiple different permeation routes. Styryl dyes enter hair cells via the mechanotransduction channel, endocytotic vesicles, and P2X channels (Balak et al. 1990; Nishikawa and Sasaki 1996; Griesinger et al. 2002; Meyers et al. 2003; Griesinger et al. 2004; Marcotti et al. 2005; Kaneko et al. 2006; Crumling et al. 2009). Ototoxic aminoglycosides also enter hair cells through multiple routes including the mechanotransduction channel, endocytosis, chloride/ bicarbonate exchangers, and TRPA1 channels (Alharazneh et al. 2011; Stepanyan et al. 2011; Hailey et al. 2012). This is the first reported evidence of living hair cells taking up phalloidin.

Unlike styryl dyes, I did not observe rapid uptake of phalloidin-CF488A into hair cells. Phalloidin-CF488A entered a subset of hair cells after 20 min, but robust phalloidin permeation and fluorescent labeling did not occur until I incubated utricles for longer durations. I found that permeation required metabotropic P2Y and PLC-PKC second messenger signaling, which might explain why the permeation is not rapid. As P2Y receptors are not pore-forming, the route of permeation route is unknown, although OATPs are a likely possibility.

Liver-specific OATPs mediate the permeation of phalloidin into hepatocytes (Fehrenbach et al. 2003; Meier-Abt et al. 2004). Organic anion transporter polypeptides mediate sodium independent transport of a wide diversity of organic compounds, and currently 11 human OATP proteins have

been described (Hagenbuch and Meier 2004; Roth et al. 2012). Rodent Oatp1b2 and human OATP1B1 and OATP1B3 enable phalloidin uptake into hepatocytes (Fehrenbach et al. 2003; Meier-Abt et al. 2004; Lu et al. 2008). OATs, similar to OATPs, mediate transport of organic compounds, although with smaller molecular weights (VanWert et al. 2010).

Several lines of evidence suggest an involvement of OATs or OATPs in the permeation of phalloidin into hair cells. First, I found that an OATP and OAT antagonist, probenecid, decreased phalloidin permeation. Second, I detected mRNA expression of Oat1 and some OATPs in the sensory epithelium. Our investigation is limited since I did not examine and compare the expression levels for all 15 rodent OATP genes. I only sought to discover whether the neonatal mouse maculae expressed OATPs. I did not discover Oatp1b2 expression in the utricle, which is the transporter that mediates hepatocellular phalloidin uptake. Thirdly, second messenger systems, including PKC, can regulate OATP transport activity (Kock et al. 2010; Roth et al. 2012). P2Y6 activates a phosphatidylinositol-calcium second messenger system leading to PKC activation (Kim et al. 2003). I discovered decreased phalloidin-CF488A labeling with PLC and PKC antagonists, which lends support to a potential requirement for second messenger signaling in the permeation of phalloidin in HCs. Future investigations into the expression pattern and localizations of specific OATPs may provide insight into a potential role for these transporters in the uptake of phalloidin into hair cells.

It appears that second messenger signaling pathways under the

regulation from P2Y receptors control the expression and activity of OATPs to mediate phalloidin uptake into hair cells. Many different organic compounds are transported through OATPs. Although I have seen no evidence, it remains possible that aminoglycosides, which are ototoxic and nephrotoxic, could enter hair cells through this mechanism.

Evidence for supporting cell coupling within sensory epithelium

When phalloidin-treated utricles were cultured 24 h in phalloidin-free media after washout, the fluorescent label disappeared from HCs and appeared in the supporting cells. Supporting cells in the vestibular epithelia and the organ of Corti are coupled through gap junctions formed by connexins (Santos-Sacchi and Dallos 1983; Sato and Santos-Sacchi 1994; Zhao and Santos-Sacchi 2000; Forge et al. 2003; Zhang et al. 2005; Jagger and Forge 2006; Zhu and Zhao 2010). Connexins are expressed in the supporting cells of all mouse vestibular epithelia (Forge et al. 2003; Qu et al. 2007). Gap junctions form channels in the membrane of a cell in register with the membrane of a neighboring cell and allow for direct communication between the cells. This coupling is required for normal HC physiology and K+ recycling (Wangemann 2002). Phalloidin became localized throughout the supporting cells 24 h after the label was washed out, and it is possible that it diffuses through the gap junction-coupled supporting cell network.

We did not investigate how phalloidin permeated into the supporting cells, whether phalloidin was directly transferred from neighboring hair cells or whether

supporting cells took it up through the extracellular media. Supporting cells possess unpaired plasma membrane connexin hemichannels that can take in anionic molecules (Zhao 2005). It remains possible that hair cells transfer the phalloidin to the neighboring supporting cells, and then the phalloidin freely transfers throughout the coupled supporting cells.

Potential applications of fluorophore-conjugated phalloidin labeling inner ear hair cells

The permeation of fluorophore-conjugated phalloidin into cells of the inner ear provides a novel mechanism to vitally label sensory hair cells. Phalloidin has high affinity for filamentous actin ($Kd=3.6x10^{-8}$) (Wieland et al. 1975; Faulstich et al. 1977). Upon permeating hair cells, it specifically labels F-actin-rich cellular structures, including stereocilia, and cuticular plates. Due to phalloidin's affinity for F-actin, it is useful for investigating retrograde F-actin flow and the coordination between the actin and microtubules cytoskeletal networks advancing growth cones and neurites (Schaefer et al. 2002; Burnette et al. 2007, 2008; Schaefer et al. 2008). If a low enough concentration of fluorophore-conjugated phalloidin is introduced into HCs, this could provide a new method for analyzing retrograde actin flow in HCs and treadmilling rates within stereocilia (Schneider et al. 2002; Zhang et al. 2012).

In summary, I have found that fluorophore-conjugated phalloidin permeates living hair cells of the mouse utricle and that this requires activation of P2Y receptors and appears to work through PLC–PKC second messenger

signaling. In the 24 h after washout of the label in culture, the fluorescence gradually disappears from HCs and increases in the neighboring SCs. The implications of our results may be useful for live cell imaging and the study of actin dynamics in hair cell epithelia.

REFERENCES

Alharazneh A, Luk L, Huth M, Monfared A, Steyger PS, Cheng AG, Ricci AJ (2011) Functional hair cell mechanotransducer channels are required for aminoglycoside ototoxicity. Plos One 6:e22347

Balak KJ, Corwin JT, Jones JE (1990) Regenerated hair cells can originate from supporting cell progeny: evidence from phototoxicity and laser ablation experiments in the lateral line system. J Neurosci 10:2502–2512

Baranova A, Ivanov D, Petrash N, Pestova A, Skoblov M, Kelmanson I, Shagin D, Nazarenko S, Geraymovych E, Litvin O, Tiunova A, Born TL, Usman N, Staroverov D, Lukyanov S, Panchin Y (2004) The mammalian pannexin family is homologous to the invertebrate Innexin gap junction proteins. Genomics 83:706–716

Burnette DT, Schaefer AW, Ji L, Danuser G, Forscher P (2007) Filopodial actin bundles are not necessary for microtubule advance into the peripheral domain of aplysia neuronal growth cones. Nat Cell Biol 9:1360–1369

Burnette DT, Ji L, Schaefer AW, Medeiros NA, Danuser G, Forscher P (2008) Myosin II activity facilitates microtubule bundling in the neuronal growth cone neck. Dev Cell 15:163–169

Burns JC, On D, Baker W, Collado MS, Corwin JT (2012) Over half the hair cells in the mouse utricle first appear after birth, with significant numbers originating from early postnatal mitotic production in peripheral and striolar growth zones. J Assoc Res Otolaryngol 13:609–627

Burnstock G (2004) Introduction: P2 receptors. Curr Top Med Chem 4:793–803

Cankurtaran-Sayar S, Sayar K, Ugur M (2009) P2x7 receptor activates multiple selective dye-permeation pathways in RAW 264.7 and human embryonic kidney 293 cells. Mol Pharmacol 76:1323–1332

Cihlar T, Lin DC, Pritchard JB, Fuller MD, Mendel DB, Sweet DH (1999) The antiviral nucleotide analogs cidofovir and adefovir Are novel substrates for human and rat renal organic anion transporter 1. Mol Pharmacol 56:570–580

Coluccio LM, Tilney LG (1984) Phalloidin enhances actin assembly by preventing monomer dissociation. J Cell Biol 99:529–535

Crumling MA, Tong M, Aschenbach KL, Liu LQ, Pipitone CM,

Duncan RK (2009) P2X antagonists inhibit styryl dye entry into hair cells. Neuroscience 161:1144–1153

Dancker P, Löw I, Hasselbach W, Wieland T (1975) Interaction of actin with phalloidin: polymerization and stabilization of F-actin. Biochim Biophys Acta 400:407–414

Estes JE, Selden LA, Gershman LC (1981) Mechanism of action of phalloidin on the polymerization of muscle actin. Biochemistry 20:708–712

Faulstich H, Schafer AJ, Weckauf M (1977) The dissociation of the phalloidin-

actin complex. Hoppe Seylers Z Physiol Chem 358:181–184

Faulstich H, Trischmann H, Mayer D (1983) Preparation of tetramethylrhodaminyl-phalloidin and uptake of the toxin into short-term cultured hepatocytes by endocytosis. Exp Cell Res 144:73–82

Fehrenbach T, Cui Y, Faulstich H, Keppler D (2003) Characterization of the transport of the bicyclic peptide phalloidin by human hepatic transport proteins. Naunyn Schmiedeberg's Arch Pharmacol 368:415–420

Forge A, Becker D, Casalotti S, Edwards J, Marziano N, Nevill G (2003) Gap junctions in the inner ear: comparison of distribution patterns in different vertebrates and assessement of connexin composition in mammals. J Comp Neurol 467:207–231

Frimmer M, Petzinger E, Ziegler K, Veil LB (1980) Uptake of 3H-demethylphalloin by isolated hepatocytes in the presence of various concentrations of phalloin or phalloidin. Naunyn Schmiedebergs Arch Pharmacol 311:91–94

Gale JE, Marcotti W, Kennedy HJ, Kros CJ, Richardson GP (2001) FM1-43 dye behaves as a permeant blocker of the hair-cell mechanotransducer channel. J Neurosci 21:7013–7025

Griesinger CB, Richards CD, Ashmore JF (2002) FM1-43 reveals membrane recycling in adult inner hair cells of the mammalian cochlea. J Neurosci 22:3939 3952

Griesinger CB, Richards CD, Ashmore JF (2004) Apical endocytosis in outer hair cells of the mammalian cochlea. Eur J Neurosci 20:41–50

Hagenbuch B, Meier PJ (2004) Organic anion transporting polypeptides of the

OATP/ SLC21 family: phylogenetic classification as OATP/SLCO superfamily, new nomenclature and molecular/ Functional properties. Pflugers Arch 447:653–665

Hailey DW, Roberts B, Owens KN, Stewart AK, Linbo T, Pujol R, Alper SL, Rubel EW, Raible DW (2012) Loss of Slc4a1b chloride/bicarbonate exchanger function protects Mechanosensory hair cells from aminoglycoside damage in the zebrafish mutant persephone. Plos Genetics 8:e1002971

Housley GD (1998) Extracellular nucleotide signaling in the inner ear. Mol Neurobiol 16:21–48

Housley G, Gale J (2010) Purinergic signalling in the inner ear-perspectives and progress. Purinergic Signal 6:151–153

Housley GD, Greenwood D, Ashmore JF (1992) Localization of cholinergic and purinergic receptors on outer hair cells isolated from the guinea-pig cochlea. Proc Biol Sci 249:265–273

Housley GD, Luo L, Ryan AF (1998) Localization of mRNA encoding the P2X2 receptor subunit of the adenosine 5′-triphosphate-gated ion channel in the adult and developing rat Inner ear by in situ hybridization. J Comp Neurol 393:403–414

Housley GD, Kanjhan R, Raybould NP, Greenwood D, Salih SG, Järlebark L, Burton LD, Setz VC, Cannell MB, Soeller C, Christie DL, Usami S, Matsubara A, Yoshie H, Ryan AF, Thorne PR (1999) Expression of the P2X(2) receptor subunit of the ATP-gated ion channel in the cochlea: implications for sound transduction and auditory neurotransmission. J

Neurosci 19:8377–8388

Housley GD, Bringmann A, Reichenbach A (2009) Purinergic signaling in special senses. Trends Neurosci 32:128–141

Huang LC, Thorne PR, Vlajkovic SM, Housley GD (2010) Differential expression of P2Y receptors in the rat cochlea during development. Purinergic Signal 6:231–248

Jacobson KA, Boeynaems JM (2010) P2Y nucleotide receptors: promise of therapeutic applications. Drug Discov Today 15:570–578

Jagger DJ, Forge A (2006) Compartmentalized and signal-selective gap junctional coupling in the hearing cochlea. J Neurosci Off J Soc Neurosci 26:1260–1268

Jorgensen JM (1989) Evolution of octavolarteralis sensory cells. In:Coombs S, Gorner P, Munz H (eds) The mechanosensory lateral line: neurobiology and evolution. Springer-Verlag, New York, p 115–145

Jorgensen L, Van Beek J, Lund S, Schousboe A, Badolo L (2007) Evidence of Oatp and Mdr1 in cryopreserved rat hepatocytes. European Journal of Pharmaceutical Sciences: Official Journal Of the European Federation for Pharmaceutical Sciences 30:181–189

Kaneko T, Harasztosi C, Mack AF, Gummer AW (2006) Membrane traffic in outer hair cells of the adult mammalian cochlea. Eur J Neurosci 23:2712–2722

Kawashima Y, Géléoc GS, Kurima K, Labay V, Lelli A, Asai Y, Makishima T, Wu DK, Della Santina CC, Holt JR, Griffith AJ (2011) Mechanotransduction in mouse inner ear hair cells requires transmembrane channel-like genes. J

Clin Invest 121:4796–4809

Kennedy C, Qi AD, Herold CL, Harden TK, Nicholas RA (2000) ATP, an agonist at the rat P2Y(4) receptor, is an antagonist at the human P2Y(4) receptor. Mol Pharmacol 57:926–931

Kim SG, Gao ZG, Soltysiak KA, Chang TS, Brodie C, Jacobson KA (2003) P2Y6 nucleotide receptor activates PKC to protect 1321N1 astrocytoma cells against tumor necrosis factor-induced apoptosis. Cell Mol Neurobiol 23:401–418

Kock K, Koenen A, Giese B, Fraunholz M, May K, Siegmund W, Hammer E, Volker U, Jedlitschky G, Kroemer HK, Grube M (2010) Rapid modulation of the organic anion transporting polypeptide 2B1 (OATP2B1, SLCO2B1) function by protein kinase C-mediated internalization. J Biol Chem 285:11336–11347

Lambrecht G, Friebe T, Grimm U, Windscheif U, Bungardt E, Hildebrandt C, Baumert HG, Spatz-Kumbel G, Mutschler E (1992) PPADS, a novel functionally selective antagonist of P2 purinoceptor-mediated responses. Eur J Pharmacol 217:217–219

Lambrecht G, Braun K, Damer M, Ganso M, Hildebrandt C, Ullmann H, Kassack MU, Nickel P (2002) Structure-activity relationships of suramin and pyridoxal-5’-phosphate derivatives as P2 receptor antagonists. Curr Pharm Des 8:2371–2399

Li C (2000) Novel mechanism of inhibition by the P2 receptor antagonist PPADS of ATP-activated current in dorsal root ganglion neurons. J Neurophysiol

83:2533–2541

Lin CH, Forscher P (1995) Growth cone advance is inversely proportional to retrograde F-actin flow. Neuron 14:763–771

Locovei S, Bao L, Dahl G (2006) Pannexin 1 in erythrocytes: function without a gap. Proc Natl Acad Sci USA 103:7655–7659

Lu H, Choudhuri S, Ogura K, Csanaky IL, Lei X, Cheng X, Song PZ, Klaassen CD (2008) Characterization of organic anion transporting polypeptide 1B2-null mice: essential role in hepatic uptake/toxicity of phalloidin and microcystin-lr. Toxicol Sci 103:35–45

Mamedova LK, Joshi BV, Gao ZG, Von Kügelgen I, Jacobson KA (2004) Diisothiocyanate derivatives as potent, insurmountable antagonists of P2Y6 nucleotide receptors. Biochem Pharmacol 67:1763–1770

Marcotti W, Van Netten SM, Kros CJ (2005) The aminoglycoside antibiotic dihydrostreptomycin rapidly enters mouse outer hair cells through the mechano-electrical transducer channels. J Physiol 567:505–521

Meier-Abt F, Faulstich H, Hagenbuch B (2004) Identification of phalloidin uptake systems of rat and human liver. Biochim Biophys Acta 1664:64–69

Meyers JR, Macdonald RB, Duggan A, Lenzi D, Standaert DG, Corwin JT, Corey DP (2003) Lighting up the senses: FM1-43 loading of sensory cells through nonselective ion channels. J Neurosci 23:4054–4065

Munter K, Mayer D, Faulstich H (1986) Characterization of a transporting system in rat hepatocytes. Studies with competitive and non-competitive inhibitors of phalloidin transport. Biochimica Et Biophysica Acta 860:91–98

Nishikawa S, Sasaki F (1996) Internalization of styryl dye FM1-43 in the hair cells of lateral line organs in xenopus larvae. The Journal of Histochemistry and Cytochemistry : Official Journal of the Histochemistry Society 44:733–741

North RA (2002) Molecular physiology of P2X receptors. Physiol Rev 82:1013–1067

Obaidat A, Roth M, Hagenbuch B (2012) The expression and function of organic anion transporting polypeptides in normal tissues and in cancer. Annu Rev Pharmacol Toxicol 52:135–151

Petzinger, E, Frimmer, M. (1988) Comparative investigations on the uptake of phaliotoxins, bile acids, bovine lactoperoxidase and horseradish peroxidase into rat hepatocytes in suspension and in cell cultures. Biochimica Et Biophysica Acta 135–144.

Qu Y, Tang W, Dahlke I, Ding D, Salvi R, Sohl G, Willecke K, Chen P, Lin X (2007) Analysis of connexin subunits required for the survival of vestibular hair cells. J Comp Neurol 504:499–507

Roth M, Obaidat A, Hagenbuch B (2012) OATPs, OATs and OCTs: the organic anion and cation transporters of the SLCO and sLC22A gene superfamilies. Br J Pharmacol 165:1260–1287

Saffer LD, Gu R, Corwin JT (1996) An RT-PCR analysis of mRNA for growth factor receptors in damaged and control sensory epithelia of rat utricles. Hear Res 94:14–23

Sandilos JK, Bayliss DA (2012) Physiological mechanisms for the modulation of pannexin 1 channel activity. J Physiol 590:6257–6266

Santos-Sacchi J, Dallos P (1983) Intercellular communication in the supporting cells of the organ of corti. Hear Res 9:317–326

Sato Y, Santos-Sacchi J (1994) Cell coupling in the supporting cells of corti's organ: sensitivity to intracellular H^{+} and Ca^{+2}. Hear Res 80:21–24

Schaefer AW, Kabir N, Forscher P (2002) Filopodia and actin arcs guide the assembly and transport of two populations of microtubules with unique dynamic parameters in neuronal growth cones. J Cell Biol 158:139–152

Schaefer AW, Schoonderwoert VT, Ji L, Mederios N, Danuser G,

Forscher P (2008) Coordination of actin filament and microtubule dynamics during neurite outgrowth. Dev Cell 15:146–162

Schneider ME, Belyantseva IA, Azevedo RB, Kachar B (2002) Rapid renewal of auditory hair bundles. Nature 418:837–838

Silverman W, Locovei S, Dahl G (2008) Probenecid, a gout remedy, inhibits pannexin 1 channels. Am J Physiol Cell Physiol 295:c761–c767

Stepanyan RS, Indzhykulian AA, Vélez-Ortega AC, Boger ET, Steyger PS, Friedman TB, Frolenkov GI (2011) TRPA1-mediated accumulation of aminoglycosides in mouse cochlear outer hair cells. J Assoc Res Otolaryngol 12:729–740

Sugiyama D, Kusuhara H, Shitara Y, Abe T, Meier PJ, Sekine T, Endou H, Suzuki H, Sugiyama Y (2001) Characterization of the efflux transport of 17beta-estradiol-d-17beta-glucuronide from the brain across the blood–brain barrier. J Pharmacol Exp Ther 298:316–322

Surprenant A, Rassendren F, Kawashima E, North RA, Buell G (1996) The

cytolytic P2Z receptor for extracellular ATP identified as a P2X receptor (P2X7). Science 272:735–738

Surprenant A, Schneider DA, Wilson HL, Galligan JJ, North RA (2000) Functional properties of heteromeric P2X(1/5) receptors expressed in hek cells and excitatory junction potentials in guinea-pig submucosal arterioles. J Auton Nerv Syst 81:249–263

Szücs A, Szappanos H, Tóth A, Farkas Z, Panyi G, Csernoch L, Sziklai I (2004) Differential expression of purinergic receptor subtypes in the outer hair cells of the guinea pig. Hear Res 196:2–7

Trujillo CA, Nery AA, Martins AH, Majumder P, Gonzalez FA, Ulrich H (2006) Inhibition mechanism of the recombinant rat P2X(2) receptor in glial cells by suramin and TNP-ATP. Biochem 45:224–233

Vanwert AL, Gionfriddo MR, Sweet DH (2010) Organic anion transporters: discovery, pharmacology, regulation and roles in pathophysiology. Biopharm Drug Dispos 31:1–71

Walli AK, Wieland E, Wieland T (1981) Phalloidin uptake by the liver of cholestatic rats in vivo, in isolated perfused liver and isolated hepatocytes. Naunyn Schmiedebergs Arch Pharmacol 316:257–261

Wangemann P (2002) K^+ cycling and the endocochlear potential. Hear Res 165:1–9

Waterman-Storer CM, Desai A, Bulinski JC, Salmon ED (1998) Fluorescent speckle microscopy, a method to visualize the dynamics of protein assemblies in living cells. Curr Biol 8:1227–1230

Wieland T, De Vries JX, Schäfer A, Faulstich H (1975) Spectroscopic evidence for the interaction of phalloidin with actin. Febs Lett 54:73–75

Yasui-Furukori N, Uno T, Sugawara K, Tateishi T (2005) Different effects of three transporting inhibitors, verapamil, cimetidine, and probenecid, on fexofenadine pharmacokinetics. Clin Pharmacol Ther 77:17–23

Zhang Y, Tang W, Ahmad S, Sipp JA, Chen P, Lin X (2005) Gap junction-mediated intercellular biochemical coupling in cochlear supporting cells is required for normal cochlear functions. Proc Natl Acad Sci USA 102:15201–15206

Zhang DS, Piazza V, Perrin BJ, Rzadzinska AK, Poczatek JC, Wang M, Prosser HM, Ervasti JM, Corey DP, Lechene CP (2012) Multi-isotope imaging mass spectrometry reveals slow protein turnover in hair-cell stereocilia. Nature 481:520–524

Zhao HB (2005) Connexin26 is responsible for anionic molecule permeability in the cochlea for intercellular signalling and metabolic communications. Eur J Neurosci 21:1859–1868

Zhao S, Fernald RD (2005) Comprehensive algorithm for quantitative real-time polymerase chain reaction. J Comput Biol 12:1047–1064

Zhao HB, Santos-Sacchi J (2000) Voltage gating of gap junctions in cochlear supporting cells: evidence for nonhomotypic channels. J Membr Biol 175:17–24

Zhu Y, Zhao HB (2010) ATP-mediated potassium recycling in the cochlear supporting cells. Purinergic Signaling 6:221–229

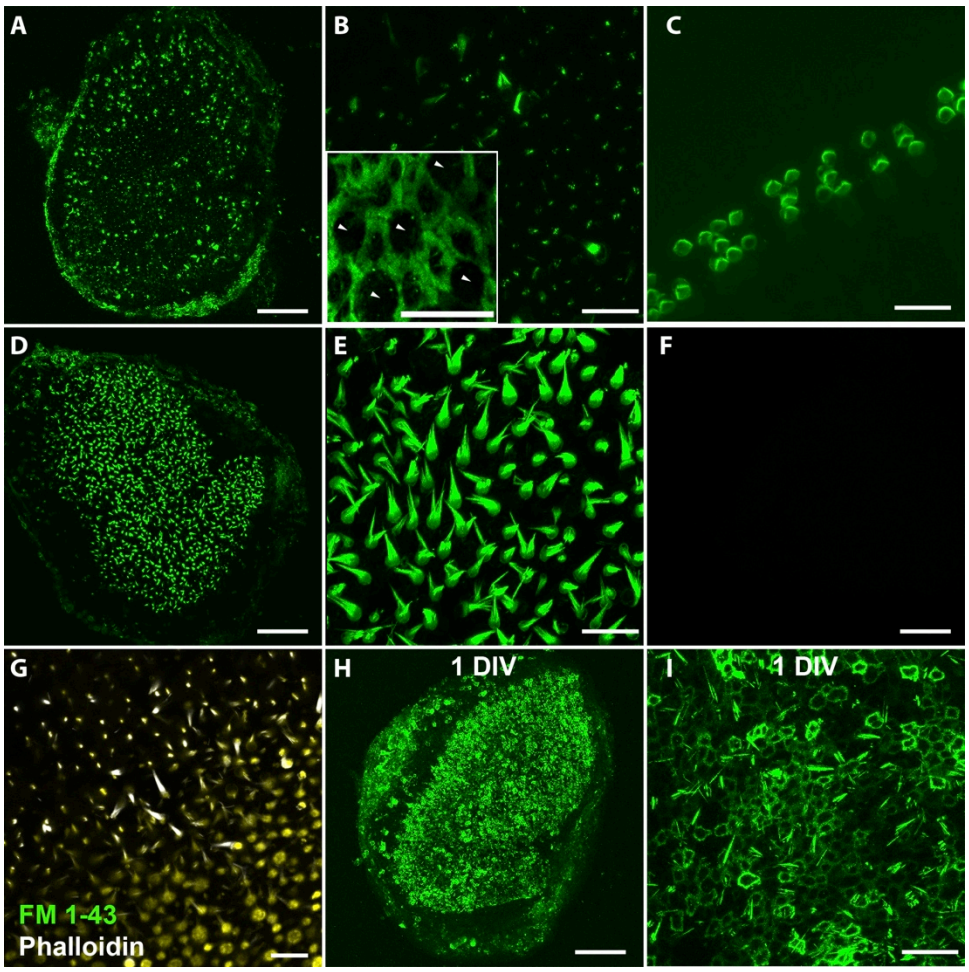

Figure 3-1. Phalloidin permeates into live cells of the inner ear. **A** Maximum intensity Z-projection image of fluorescence observed after freshly dissected whole mount mouse utricles treated with phalloidin-CF488A for 20 min (37 °C) were imaged live. **B** Higher magnification from **(A).** Fluorescence can be observed throughout the entire hair bundle in only a few hair cells and in a discrete, punctate location within the stereocilia in the majority of hair cells. Inset depicts characteristic circumferential F-actin belts found among supporting cells

(P86 utricle). Five presumptive HCs, which characteristically have circular apical surfaces, have been labeled with arrowheads while the remaining cells display the thick circumferential F-actin belts characteristic of mouse utricle supporting cells. **C** Maximum intensity Z-projection image of fluorescence observed after whole mount mouse cochlea treated with phalloidin-CF488A for 20 min and imaged live. **D** Example image from a live utricle treated with phalloidin-CF488A for 90 min. E Higher magnification from **(D)** depicts phalloidin uptake throughout the entire hair bundle in nearly all hair cells with this longer treatment of phalloidin. **F** No fluorescence observed in mouse utricles treated with the CF488A fluorophore alone. **G** Hair cells are able to take up FM 1–43 after Alexa Fluor 647 phalloidin treatment. Mouse utricles were incubated with Alexa Fluor 647 phalloidin for 20 min. The Alexa Fluor 647 phalloidin was then washed out with DMEM/F-12. Utricles were then treated with FM 1–43 for 10 s. FM 1–43 was washed out, and the utricles were imaged live. **H, I** Fluorescence observed in the circumferential F-actin belts of supporting cells and a few stereocilia after utricles were maintained 1 DIV (24 h) after a phalloidin treatment. **I** High magnification region from **(H).** Scale bars in A, D, F, and H are 100 μm; B, C, E, G, I are 20 μm; inset in B is 10 μm.

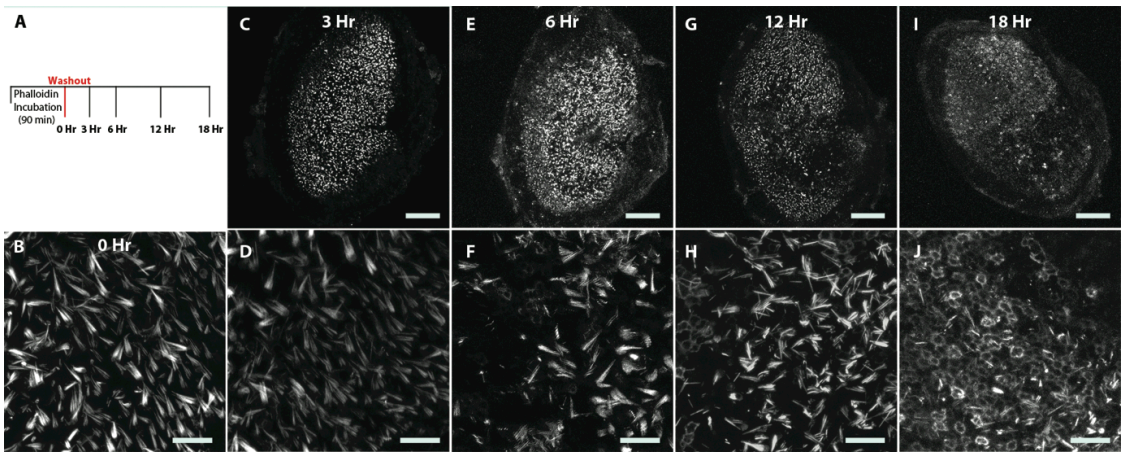

Figure 3-2. Time series of fluorescence observed after culturing utricles that had been treated with phalloidin-CF488A. Fluorescence disappears from hair cells and appears within circumferential F-actin belts of supporting cells in culture. **A** Experimental outline. Utricles were treated with phalloidin-CF488A for 90 min, then the label was washed out three times with DMEM/F-12, and then the media was replaced with DMEM/F-12 containing 1 % FBS. Utricles were then maintained in culture at 37 °C. Utricles were mounted and imaged live immediately (0 h; **B**), or after 3 h **(C, D)**, 6 h **(E, F)**, 12 h **(G, H)**, or 18 h in culture **(I, J)**. Around 6 h, the label begins to disappear from hair cells and supporting cells become fluorescent **(F)**, and by 18 h, nearly all supporting cells are fluorescent **(J)**. Scale bars in B, C, E, G, and I are 100 μm; scale bars in D, F, H, and J are 20 μm.

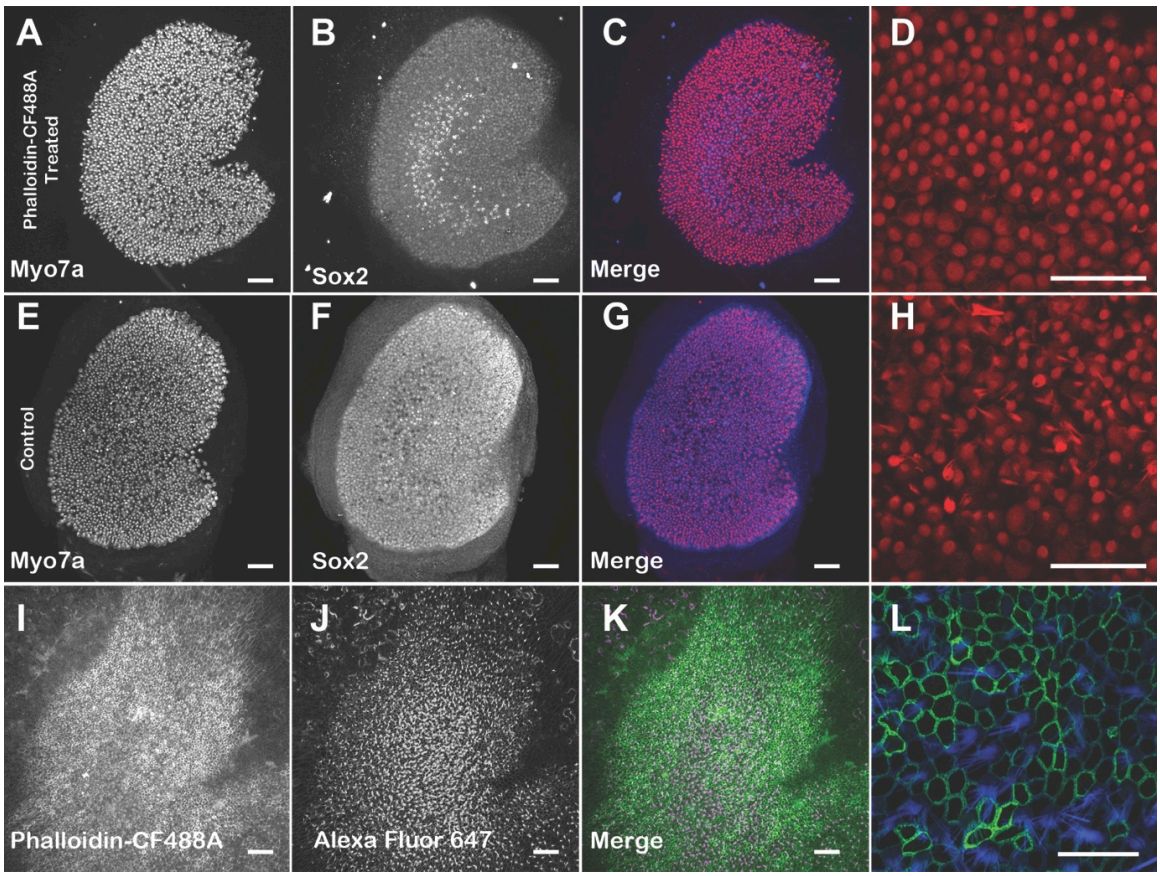

Figure 3-3. Hair cell density was not affected in phalloidin-treated utricles maintained in culture 24 h. **(A–D)** P2 mouse utricles were treated 90 min with 66 nM phalloidin-CF488A and then maintained in culture for 24 h. The resulting hair cell density was compared against control P2 utricles that were maintained in culture for 24 h but were not treated with phalloidin-CF488A **(E–H)**. After culturing, utricles were immunolabeled with myosin VIIa **(A, E)** and Sox2 **(B, F)**. The merged images are also displayed in **C, G**. Higher magnification images of myosin VIIA immunofluorescence from utricles that were treated with phalloidin-CF488A **(D)** and utricles that were not phalloidin-treated **(H)**. There were no differences in HC density per 2,500 μm2 in these utricles. **I–L** Maximum intensity

Z-projection images of utricles that were treated live with phalloidin-CF488A, then maintained in culture for 7 days, fixed, and additionally stained with Alexa Fluor 647 phalloidin. **I** Utricles that were treated with phalloidin-CF488A maintained the fluorescence after 7 days in culture. **J** Staining with Alexa Fluor 647 phalloidin reveals that these utricles still have HCs. K Merge. **L** Higher magnification of region showing fluorescence from phalloidin-CF488A (green) and Alexa Fluor 647 phalloidin. Scale bars in A–C, E–G, and I–K are 100 μm; scale bars in D, H are 50 μm; scale bar in L is 20 μm.

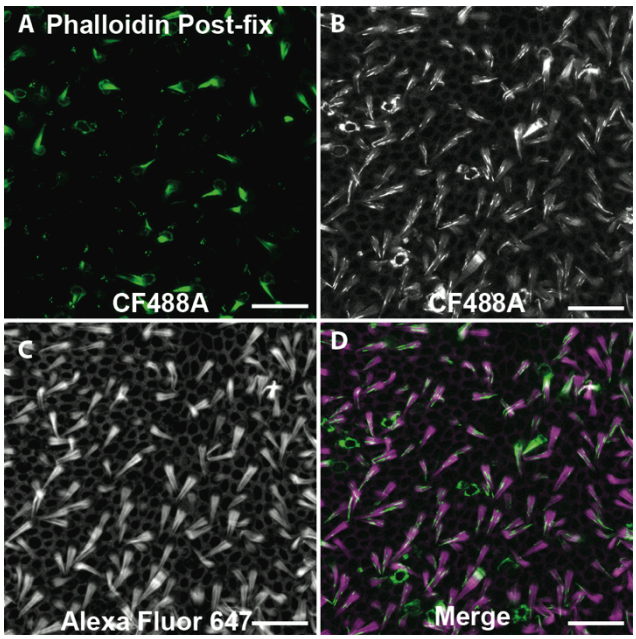

Figure 3-4. Phalloidin permeation in live cells of inner ear is fixable. Example image of a utricle treated live with phalloidin-CF488A for 30 min then fixed with 4 % paraformaldehyde **(A)**. **B–D** CF488A fluorescence maintained after phalloidin-CF488A-treated utricles were fixed as in **(A)**, and then counterstained with Alexa Fluor 647 phalloidin. Permeabilizing the post-fixed tissue to stain with Alexa Fluor 647 phalloidin causes the CF488A fluorescence to become more diffuse. Scale bars in A–D are 20 μm.

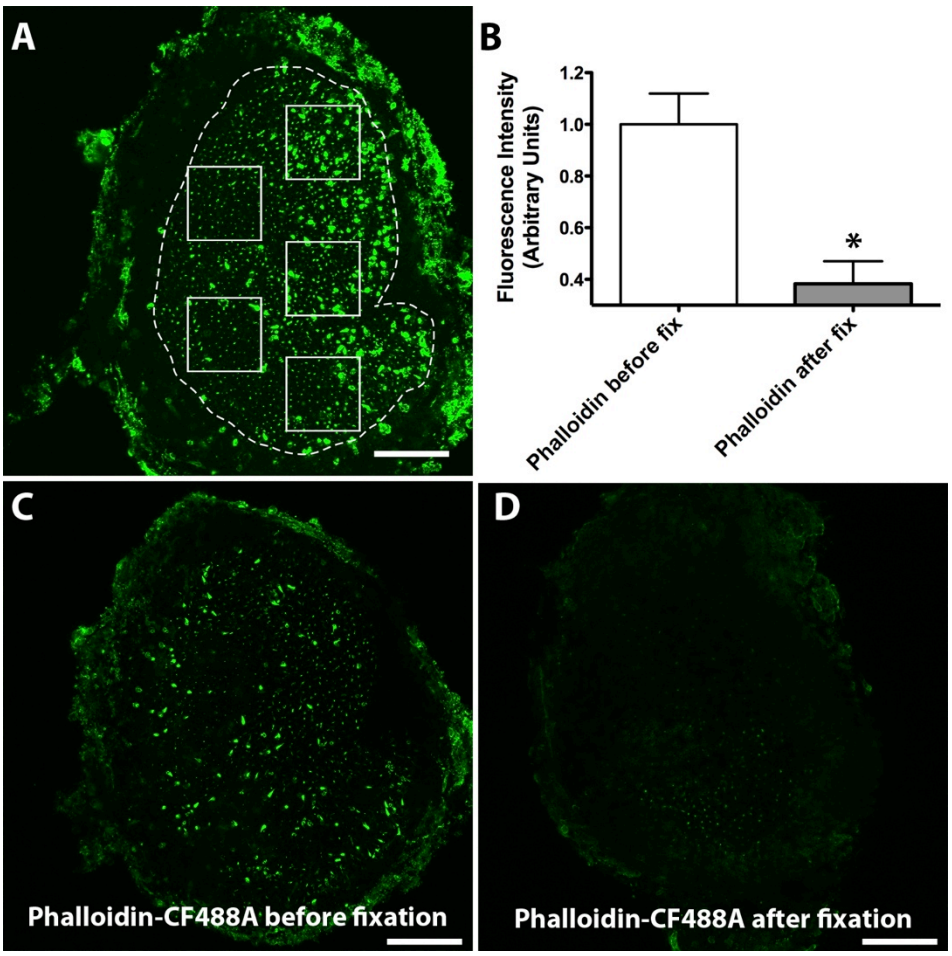

Figure 3-5. Phalloidin permeation into live cells of inner ear involves an active pathway. **A** Mean fluorescence intensity was measured in five separate 100 µm x 100 µm regions as depicted in the example image. **B** I observed more fluorescence in utricles that were treated with phalloidin-CF488A before fixation compared with utricles treated with phalloidin-CF488A after fixation (Student's *t*test, p=0.014). **C** Example micrograph of utricle treated with 66 nM phalloidin-CF488A and then fixed. **D** Example confocal micrograph of utricle fixed with paraformaldehyde for 20 min then treated with 66 nM phalloidin-CF488A. Scale bars are 100 µm.

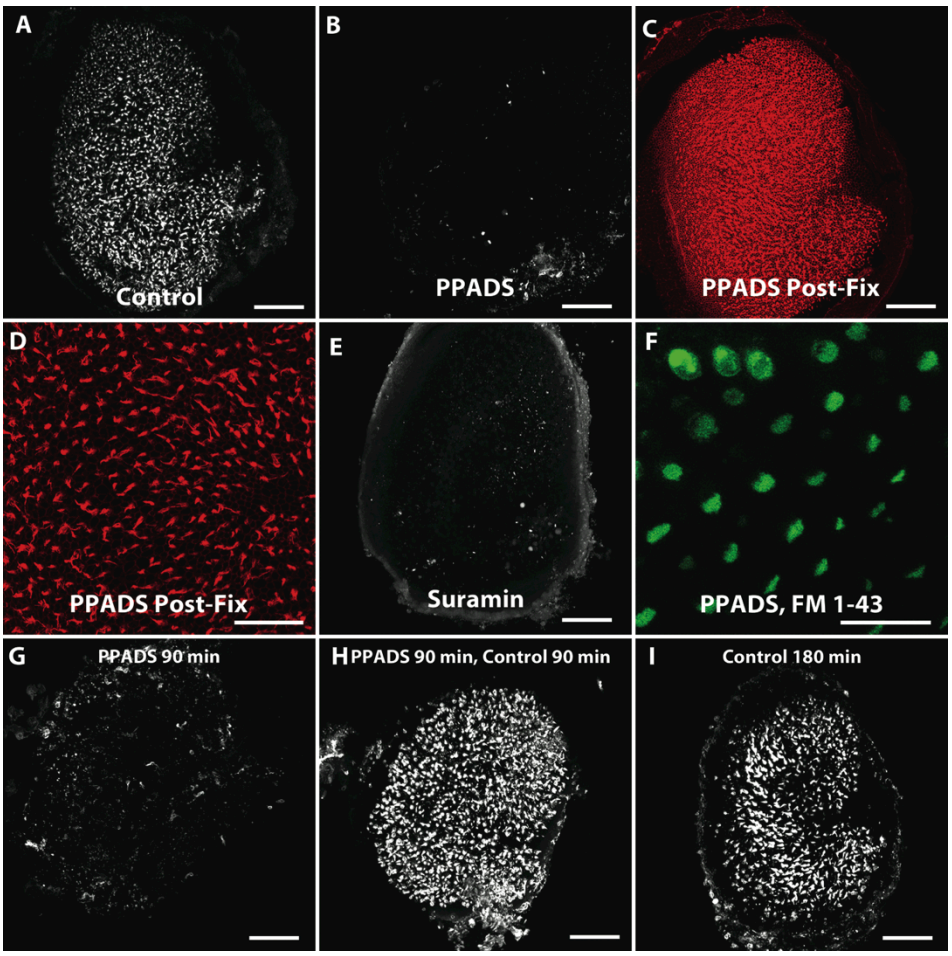

Figure 3-6. Effects of P2 receptor blockers on fluorophore-conjugated phalloidin permeation. Blockers of P2 receptors inhibit phalloidin uptake. **A** Example image of a control living utricle treated with phalloidin-CF488a as described. **B** Example image of a living utricle treated with P2 antagonist PPADS (100 µm, *n*=8) and then incubated with PPADS and phalloidin-CF488A. Living PPADS-treated utricle from **(B)** was fixed and counterstained with phalloidin-Alexa Fluor 568 to visualize the entire F-Actin network and ensure that hair cells were still present **(C, D). E** Example image of a living utricle treated with P2 antagonist suramin (100 µm, *n*=4). **F** PPADS-treated living utricle was co-incubated for 10 s with PPADS and 5 µM FM 1-43 and then imaged showing that PPADS does not

inhibit mechanotransduction. G–I Washing out PPADS restores the ability of hair cells to take up phalloidin-CF488A. **G** Example image of a utricle treated with 100 μm PPADS for 90 min at 37 °C. **H** After PPADS treatment and several washes in DMEM/F-12, some utricles were maintained in 66 nM phalloidin-CF488A for 90 min at 37 °C and imaged live. Phalloidin was able to enter the hair cells in these utricles at levels comparable to control utricles treated 180 min in 66 nM phalloidin-CF488A at 37 °C **(I).** Scale bars in A–C, E, and G–I are 100 μm; scale bar in D, and F are 50 μm.

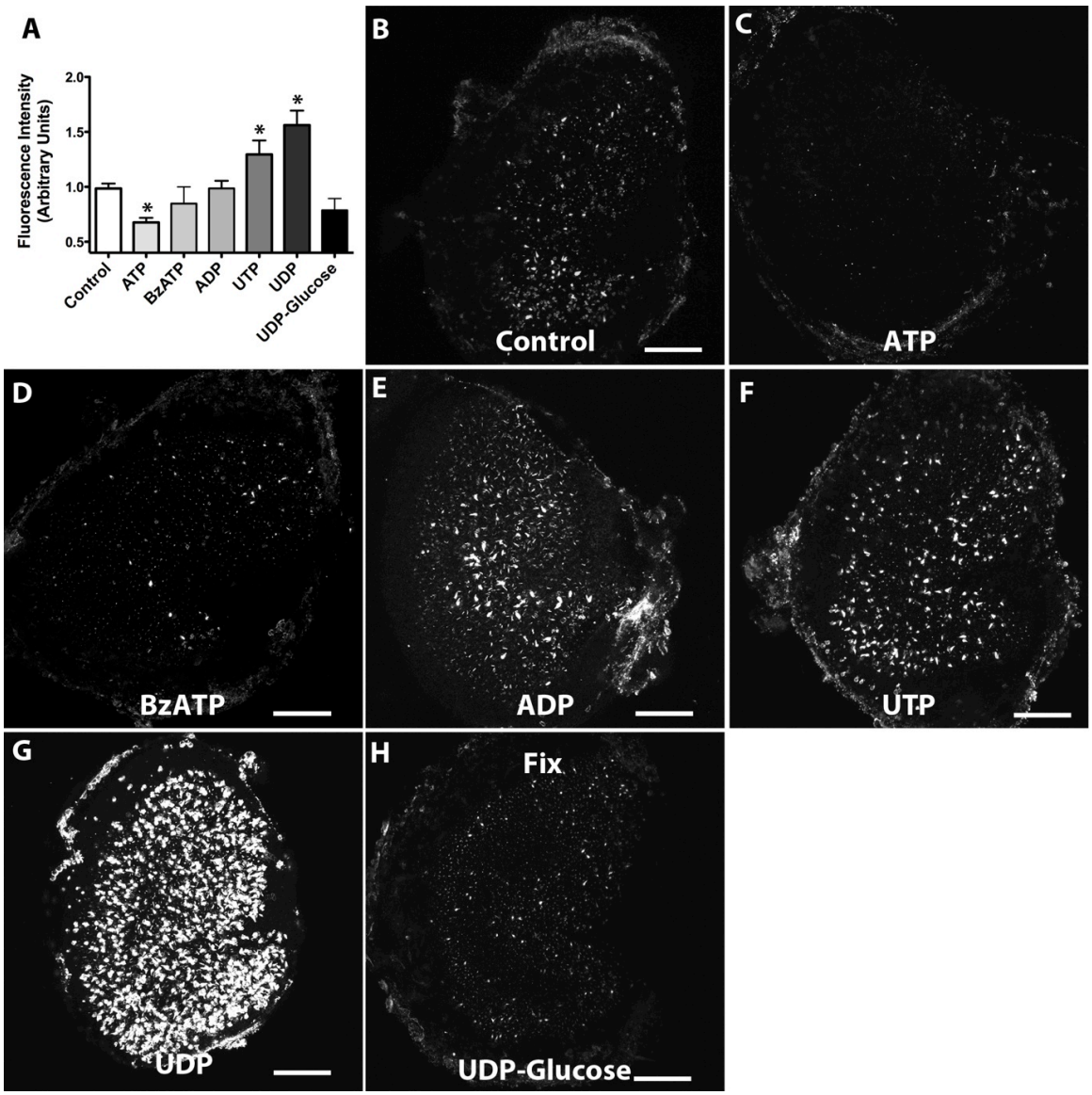

Figure 3-7. Effects of P2 receptor agonists on fluorophore-conjugated phalloidin permeation **A** Mean fluorescent intensity of phalloidin-CF488A detected after pretreating with the various P2 receptor agonists. Shown are example maximum intensity Z-projection images of control (*n*=21) **(B)**, ATP (*n*=12) **(C)**, BzATP (*n*=9) **(D)**, ADP (*n*=11) **(E),** UTP (*n*=11) **(F),** UDP (*n*=6) **(G)**, and UDP-glucose (*n*=4) **(H)** treated utricles. Both UTP and UDP significantly enhanced uptake of phalloidin-

CF488A (one-way ANOVA with Newman-Keuls multiple comparisons post-test, pG0.05) and ATP significantly blocked phalloidin-CF488A entry (one-way ANOVA with Newman-Keuls multiple comparisons post-test, $p<0.05$). Scale bars are 100 μm.

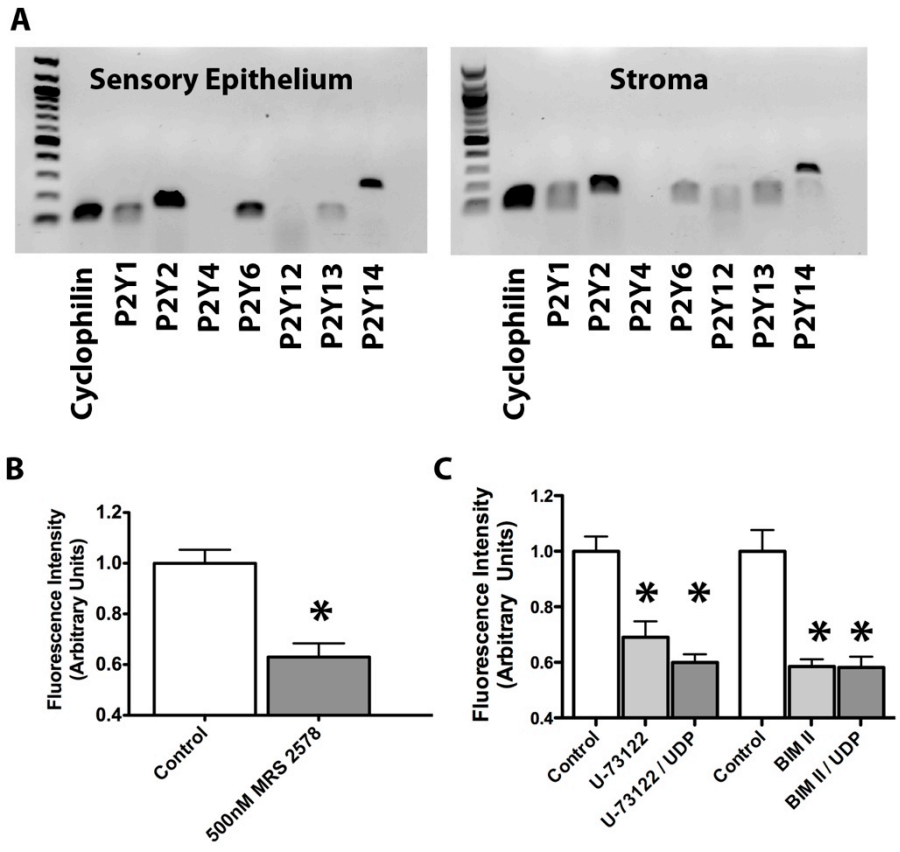

Figure 3-8. P2Y receptor subunit expression and effects of P2Y6, PLC, and PKC inhibitors on fluorophore-conjugated phalloidin uptake **(A)** RT-PCR amplification of P2Y receptors in the sensory epithelium and stroma of P5 mouse utricles. The 100 bp ladder shown. **B** 500 nM MRS 2578, a P2Y6 receptor antagonist, decreased fluorophore-conjugated phalloidin uptake (n=4). **C** Summary of effect of U-73122 (PLC antagonist) and BIM I I (PKC antagonist) on phalloidin-CF488A permeation. I observed decreased fluorescence from phalloidin-CF488A treatment in utricles treated with 10 μM U-73122 (*n*=5) or 50 μM BIM II (*n*=6). Utricles treated with UDP and either U-73122 (*n*=4) or BIM II (*n*=4) also had significantly decreased fluorescence compared with controls.

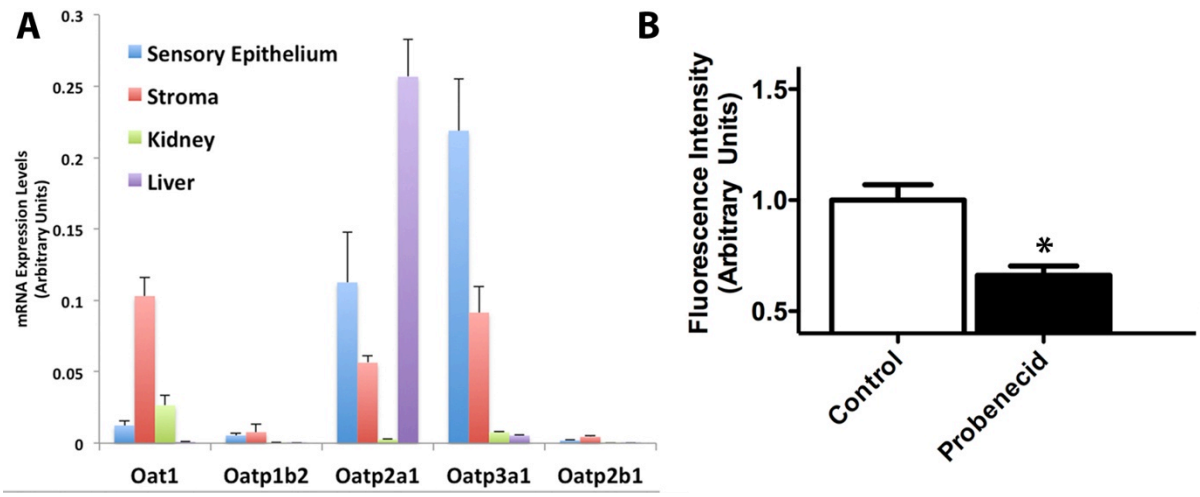

Figure 3-9. Mouse utricle expresses Oat1 and Oatps. **A** mRNA expression levels of four Oatps, including Oatp1b2, which mediates phalloidin uptake in rodent hepatocytes, and Oat1 in the neonatal mouse sensory epithelium, stroma, liver, and kidneys (*n*=3). **B** Probenecid treatments decreased fluorescence by 33.9 %.

CHAPTER 4

Conclusions

Loudness, timbre, and pitch are the primary auditory sensations. Loudness is the amplitude or intensity of sound, and is measured in a decibel (dB) scale. Timbre is the component known as the 'quality' or 'color' of sound, and is a feature that can distinguish between sounds with identical frequencies and amplitudes. Pitch is defined as the periodicity, or frequency, of an acoustic waveform, and is measured in hertz (Hz). The cochlea is spatially organized such that different sound frequencies stimulate different regions of the cochlea along the pitch axis, called frequency-to-place mapping, or tonotopy. This tonotopic organization is maintained at numerous levels of the auditory pathway from the cochlea up to the auditory cortex (Oxenham, 2012).

The cochlea, where tonotopy first manifests, is specialized to respond to different sound frequencies due to the passive properties of the underlying basilar membrane and due to cellular patterning along the pitch axis that yields frequency-tuned receptor cells. This specialization is required for frequency discrimination, which is an essential component of verbal communication. The overall goal of my dissertation research was to improve the understanding of how the pitch, or tonotopic, axis of the cochlea is patterned during development. I specifically sought to accomplish these aims: 1) identify factors that may be involved in setting up and establishing the location-specific HC phenotypes, 2) determine whether these candidate factors influence the development of the HC

phenotypes, and 3) investigate mechanisms how these factors may be involved in patterned the development of the phenotypes across the pitch axis.

The work in this dissertation addresses those aims and advances the field of developmental patterning in the inner ear in several different ways. In chapter two, I described how RNA sequencing was used to identify retinoic acid (RA) as a candidate morphogen that plays a role in patterning the gradient of HC phenotypes along the pitch axis of the cochlea. Morphogens have been predicted to be involved in generating the tonotopic arrangement of sensory cells, but definitive candidates had not been identified prior to this (Groves and Fekete, 2012; Kowalik and Hudspeth, 2011). I then showed that modulating RA levels influenced the graded morphological and mechanoelectrical features of HCs that developed along the pitch axis of the cochlea. I also found that increased RA levels enhanced expression of proteins involved in stereocilia elongation. This significantly improves our understanding of how this key aspect of sensory organ morphogenesis may be regulated by morphogen gradients during development. In chapter three, I demonstrated that fluorophore-conjugated phalloidin permeates living cells to brightly label F-actin rich structures in the inner ear.

This chapter discusses the findings in the context of the knowledge on inner ear development and highlights remaining questions and areas to be addressed with future investigations.

Morphogens and pattern formation

Morphogens are extracellulary secreted molecules that have ‘organizer’ properties, as originally discovered and described in the classical transplantation experiments performed by Hans Spemann and Hilde Mangold in gastrulating amphibian embryos in the 1920s (De Robertis, 2006). These experiments led to the discovery of the Spemann’s organizer (or Spemann-Mangold organizer), which is a small region of the embryo that specifies central nervous system formation, and is capable of inducing, or ‘organizing’ the development of a complete second nervous system when grafted onto another developing embryo (Spemann and Mangold, 2001). Modern investigations have discovered that the Spemann organizer contains a number of Bmp and Wnt antagonists that function as morphogens (De Robertis and Kuroda, 2004; De Robertis et al., 2000). Diffusion of morphogens from their source yields a morphogenetic gradient. The cells within this field then respond to the particular morphogen concentration levels, as conceptually described by the “French Flag Model” where the highest concentrations induce the activation of a “blue” gene, intermediate levels a “white” gene, and lower levels a “red” gene (Figure 4-1; Wolpert, 1969). While the cellular phenotypes patterned by morphogens are almost universally not this discrete, one particular exception exists in the inner ear. HCs that form along the pitch axis of the cochlea develop an integer number of stereocilia, a phenotype that grades from cell-to-cell across the BP. One cell may form 86 stereocilia, while its nearest neighbor along the tonotopic axis may form 87. Due to this uniquely quantifiable phenotype, the tonotopic axis of the cochlea is an attractive model for studying morphogentic gradients.

Inner ear morphogenesis has been described to rely upon the actions of a number of different morphogens at several key stages of development. At the otocyst stage, the D-V axis is specified by gradients of Sonic Hedgehog (Shh) and Wnt signaling (Bok et al., 2007; Riccomagno et al., 2002; Riccomagno et al., 2005), while the A-P axis is specified by graded RA signaling (Bok et al., 2011). Furthermore, gradients of both signals that activate and signals that antagonize Bmp signaling have been described to be capable of acting over distances as morphogens during inner ear development (Gerlach-Bank et al., 2004; Ohyama et al., 2010).

Based upon expression patterns, a morphogenetic gradient of Shh signaling has been proposed to play a role in patterning tonotopic identities in the cochlea (Groves and Fekete, 2012). Vertebrate embryos employ Shh gradients to establish positional identity in other organs, such as the limb and neural tube (Zeller et al., 2009). In neural tube patterning, Shh diffuses from the floor plate and notochord to form a morphogenetic gradient that organizes the pattern of cellular differentiation in the ventral neural tube (Dessaud et al., 2008; Ribes et al., 2010). The developing BP grows out and extends along the lateral-to-medial axis towards these Shh-expressing midline structures, suggesting that distal end of the BP becomes exposed to higher levels of Shh than the proximal end (Bok et al., 2005). Within the inner ear sensory epithelium itself, Shh signaling effectors and response genes are expressed in a D-V gradient at the otocyst stage, suggesting the presence of a gradient of Shh activity prior to cochlea morphogenesis (Bok et al., 2007).

The combined evidence highlights a possible role for a gradient of Shh signaling in specifying positional identity along the tonotopic axis of the BP. Based upon the timing of expression for the components of the Shh signaling pathway, were Shh to have a role in tonotopic patterning, it would occur several days before HCs differentiate and any morphological manifestations of positional identity are apparent (Groves and Fekete, 2012). In my unbiased RNA-seq screen in the developing chicken BP, I did not detect any robust gradients of expression for components of Shh signaling. This may be due to the fact that I compared transcriptomes from E6.5 embryos, which are several days older than when the theorized window that Shh is predicted to pattern the cochlea. Furthermore, I was able to influence the developing HC phenotypes in E6.5 BPs in culture, suggesting that tonotopic identity does not become fixed or determined until HCs start to differentiate and form their location-specific phenotypes. While this does not support the hypothesis that Shh is required for patterning the gradient of HC phenotypes, my results do not preclude the possibility that the Shh pathway could be involved in patterning earlier development stages than the ones I investigated.

Similar to the developing hindbrain, I discovered genes involved in the regulation of RA signaling to be expressed in gradients at opposite ends of the developing BP (Figure 2-1). The mRNA expression patterns for these genes suggest that a morphogenetic gradient of high RA activity is established at the proximal end of the BP at E6.5, when HCs are beginning to exit the cell cycle. At later stages, when HCs begin to differentiate and acquire location-specific

phenotypes, the expression patterns suggested that there is a gradient of high RA activity at the distal end. In support of that, I observed higher levels of soluble RA produced distally than proximally in E10 BPs (Figure 2-3). This distal gradient of RA activity also appeared to be critically involved in patterning the gradient of HC phenotypes during development.

Model for Tonotopic Patterning

In collaboration with members of the Matthew Kelley laboratory, we discovered that the Bmp signaling ligand *Bmp7* is expressed in a distally high gradient across the developing BP at all ages examined from E6.5 to P14. This differs from the mRNA expression pattern of the RA synthesizing enzyme, *Raldh3,* which is expressed in a pronounced proximally high gradient early in cochlear morphogenesis (E6.5), but at later developmental stages becomes and remains expressed in a distally high gradient, similar to *Bmp7*. I formulated a model for how the HCs along the tonotopic axis are patterned during development after synthesizing results from this dissertation and from results obtained through this collaboration.

The early opposing gradients of RA and Bmp signaling may be involved in establishing the pattern of HC density across the longitudinal axis. At stages of development when HCs are exiting the cell cycle and are beginning to differentiate, graded differences in HC density arises across the BP, such that HC density is lowest proximally and increases towards the distal end of the BP (Jacques et al., 2012). These graded differences may result from the combined

actions of a distal high Bmp7 gradient that promotes higher HC density levels and a proximal high RA gradient that promotes lower HC density levels.

Once HC density becomes established and HCs then begin to differentiate, there is weakening of the Bmp7 gradient throughout the BP. At this time the gradient of the RA synthesis enzyme *Raldh3* reverses, becoming a distally high gradient that increases and persists. I hypothesize that local differences in the numbers and spatial densities of HCs, which differ progressively along the sickle-shaped sensory epithelium of the chicken cochlea, may underlie that reversal since HCs are the cell-type that expresses Raldh3 during these later developmental stages (Figure 2-2). The formation of a distally high RA gradient then contributes to the specification of HC phenotypes by promoting bundle elongation and the expression of the β subunit for the BK channel.

Future *in vivo* investigations, while presumably technically challenging, may offer insights whether the HC phenotypes that result from altering RA activity levels correspondingly alter functional hearing abilities.

Lighting up the senses, part II

In chapter three I described results showing that fluorophore-conjugated phalloidin permeates living cells in the inner ear (Figure 3-1). This study provides a novel method for vitally labeling HCs with a fluorescent marker, which enables fluorophore-conjugated phalloidin to be a potentially useful tool for studying inner ear development.

Styryl dyes are currently the most widely used molecules for labeling live HCs, and their use for such purpose is well characterized in "*Lighting up the Senses: FM 1-43 Loading of Sensory Cells through Nonselective Ion Channels*" (Meyers et al., 2003). The styryl dye FM 1-43 was shown to rapidly permeate through ion channels in HCs; Merkel cells in whisker vibrissae, touch domes, and hair follicles; and in heterologous cell lines expressing TRP or P2X channels. Styryl dyes have been hypothesized to enter HCs via a number of different routes, including the mechanotransduction channel and P2X channels (Crumling et al., 2009; Gale et al., 2001; Meyers et al., 2003). These dyes are also useful to test for functional mechanotransduction channels, as HCs with inoperable mechanotransduction channels have additional impairments in styryl dye uptake (Kawashima et al, 2011). The main limitation for these dyes, however, is that they have fixed, broad absorption spectra.

Phalloidin on the other hand can beneficially be conjugated to a number of different fluorophores. In Chapter two I describe results where different fluorophore conjugations all appear to permeate and fluorescently label live HCs. I did not investigate whether fluorophore-conjugated phalloidin was capable of permeating and fluorescently labeling other sensory cells, which styryl dyes can. The results from my initial investigations were surprising, as phalloidin has been described to permeate only one living cell type previously—the hepatocytes of the liver (Wieland and Faulstich, 1977). Another surprising result was that phalloidin permeation required metabotropic P2Y receptor signaling, rather than P2X channels, which I hypothesized to be a likely route due to the involvement of

these channels in styryl dye permeation in HCs and their involvement in the permeation of larger dye molecules (North, 2002; Crumling et al., 2009). While future investigations into the route of phalloidin permeation may offer key insights into HC physiology, the results have implications for developmental studies that require live cell imaging.

Future Studies

Does RA regulate stereocilia lengths throughout the ear?

I discovered that increased RA levels led to enhanced *Espin* expression and increased stereocilia lengths in the proximal end of the developing BP. This suggests that RA may regulate the lengths of cochlear HC stereocilia by controlling Espin levels, although this has not yet been definitively proven. Future experiments should aim at investigating this potential causal mechanism.

Since I discovered that *Espin* is sensitive to RA levels, an interesting speculation is whether RA signaling regulates *Espin* expression and stereocilia elongation in other inner ear organs besides the cochlea. There is much research on the molecular machinery involved in the development and formation of stereocilia, including proteins such as Espin, but almost no information on how these proteins are regulated or how HCs form hair bundles of precisely specified lengths throughout the inner ear. This appears to be an important, unanswered question in the field, as there are dramatic differences in stereocilia lengths throughout the inner ear where hair bundles in the cochlear are as short as a 1-2 μm and hair bundles in the cristae can extend up to 120 μm (Lin et al., 2005).

This biophysical property is additionally important for hair cell function (Frishkopf and DeRosier, 1983; Holton and Hudspeth, 1983).

Previous work that investigated retinaldehyde dehydrogenase expression patterns in the developing chicken inner ear identified *Raldh3* as the primary RA synthesizing enzyme of the inner ear (Sanchez-Guardado et al., 2009). *Raldh3* expression was found in proximity to all of the inner ear sensory epithelia, and its localization in vestibular epithelia (E4) and the BP (E8) precedes both the onset of Espin expression and stereociliogenesis in those organs (Li et al., 2004; Sanchez-Guardado et al., 2009). This suggests that RA signaling may turn on and perhaps regulate the expression of genes involved in controlling stereocilia lengths. Future investigations on whether RA regulates Espin expression in vestibular epithelia, where HCs develop with longer stereocilia in comparison to cochlear HCs, may identify a fundamental stereociliogenesis mechanism necessary for length specification. Additional experiments that locally inhibit RA signaling during stages of stereocilia development and formation may also offer key insights into this possibility.

Does RA regulate tonotopic patterning in mammals?

Similar to the tonotopic organization in birds, there are HC phenotypic gradients along the pitch axis of the mammalian cochlea (Lim, 1980; Lim and Anniko, 1985). This raises the possibility that the mammalian cochlea is patterned by a gradient of RA activity similar to the results presented in this dissertation. There is evidence that RA signaling is important for normal cochlear

development in mammals, as components of RA signaling are expressed in the developing mouse cochlea (Raz and Kelley, 1999; Romand et al., 2006) and the cochlea releases soluble RA (Kelley et al., 1993). RA signaling also is necessary for cochlear HC differentiation and mammalian cochlear development (Raz and Kelley, 1999).

Investigations with mutant mice have the potential to offer insights into potential roles for RA signaling in patterning mammalian HCs along the pitch axis. Mice with targeted knockout of *Raldh2* unfortunately due not survive to cochlear formation (Niederreither et al., 1999; Niederreither et al., 2000). *Raldh3* knockout mice also are embryonic lethal (Dupé et al., 2003), but RA supplements given to mothers during pregnancy is sufficient to yield viable mutants. These *Raldh3* mutant mice interestingly have vestibular function deficiencies (Romand et al., 2013). Cochlear HCs in these mice unfortunately were not analyzed for patterning defects.

Interestingly, no mutants have been found that have defects in the tonotopic patterning of HCs along the cochlea (Kowalik and Hudspeth, 2011). One possible explanation for this is that the signals involved in patterning the cochlea may also be required during earlier stages of embryogenesis or may be involved in early stages of inner ear development. Disrupting these hypothetical signals throughout embryogenesis may have consequences, such as embryonic lethality, that precede and preclude cochlear formation and tonotopic patterning. RA is one such possible signal, as it is required during embryogenesis and in the development of the otocyst at stages that precede cochlear formation (Bok et al.,

2011; Choo et al., 1998; Frenz et al., 2010; Kil et al., 2005; Niederreither et al., 1999). Many studies that have manipulated RA levels have resulted with embryos that do not survive to stages when the cochlea forms, or have yielded embryos with severe inner ear patterning defects arising prior to the formation of the cochlea. This would prevent any clear observations on whether RA signaling has a role in patterning the HCs along the tonotopic axis of the cochlea. It would be more informative to generate and analyze mice that have the RA synthesizing enzymes conditionally knocked out selectively in the inner ear during stages of cochlear morphogenesis (i.e. E12.5 to E17).

Does RA regulate tonotopic patterning in the regenerating cochlea?

Unlike in mammals, where HC regeneration is limited or non-existent, many non-mammalian vertebrates are capable of replacing lost HCs through a regenerative response throughout their lifetime (Burns and Corwin, 2013; Meyers and Corwin, 2008; Warchol, 2010). In the face of HC loss, neighboring supporting cells either re-enter the cell cycle to produce progenitors to replace the lost HCs or these supporting cells directly undergo phenotypic conversion into a HC phenotype without any mitotic proliferation. These regenerated HCs become innervated and hearing and balance sensitivity becomes restored within a few weeks (Meyers and Corwin, 2008).

In the avian cochlea, damaged BPs regenerate HCs with expected location-specific phenotypes (Corwin and Cotanche, 1988; Cotanche, 1987; Woolley and Rubel, 2002). This suggests that tonotopic patterning signals may

still be present within mature cochlea. As the HC regenerative response recapitulates several steps that occur during development (Cotanche and Kaiser, 2010), it may be possible that RA signaling is involved in specifying positional identity in regenerating cochlea. I detected a gradient of *Raldh3* mRNA expression in P14 BPs, the oldest age analyzed (Figure 2-1). RA signaling is critically involved in the regenerative response of some postnatal tissues (Maden, 2007), and a post-hatch distal-to-proximal gradient of RA signaling may have a role in patterning the HC phenotypes during regeneration. Investigations into modulating RA levels during HC regeneration may offer key insights into this possibility.

Morphogens are long-ranging, diffusible molecules, but not without limits. Experiments modeling the retinoid concentration gradient in embryonic tissue with RA-soaked beads found that RA is capable of diffusing approximately 1 mm away from a local source (Eichele and Thaller, 1987). A RA source in post-hatch chicken BPs exclusively located at the extreme distal end would appear to be insufficient to provide patterning cues across the ~3 mm long sensory epithelium. The RA source in the BP, however, appears to be intrinsically located within the HCs across the longitudinal axis of the BP. Damage to a particular band of cells along the proximal-to-distal axis may involve a regenerative mechanism whereby new cells are capable of “sensing” relative concentrations of RA emanating from pre-existing HCs located at the proximal and distal boundaries of the damaged region. Another outstanding question is whether SCs begin re-expressing Raldh3 after HC damage, similar to their ability to do so during development.

Preliminary experiments aimed at monitoring Raldh3 expression patterns during regenerative responses through immunohistochemistry may offer initial insights into this possibility.

It remains possible that HCs could receive location-specific patterning cues during development and regeneration from epigenetic factors. Epigenetics is broadly defined as a heritable change in gene expression or cellular phenotype caused by mechanisms other than changes in DNA sequence (Berger et al., 2009). Epigenetic mechanisms generate diverse phenotypes by controlling gene transcription through enzyme-mediated modifications of chromatin and DNA promoter sites (Copeland et al., 2010). Although information on epigenetics in the inner ear is limited, there is evidence that components of epigenetic regulatory machinery are expressed with the sensory epithelium (Slattery et al., 2009). Additionally, broad epigenetic pharmacological inhibitors have drastic effects on both HC differentiation and regeneration (Lu and Corwin, 2008; Slattery et al., 2009), highlighting a potentially important role for epigenetics in the developing and regenerating inner ear.

During chicken cochlear development, sensory cells that first exit the cell cycle reside in a line down the middle of the sensory epithelium and there are progressive additions of postmitotic cells at the superior and inferior edges of that line over the subsequent three days (Katayama and Corwin, 1989). It is possible that centrally located stem/progenitor cells in the embryonic BP undergo epigenetic changes, which are then inherited by the progeny. Additionally the SCs, which are the progenitors of HCs during regenerative responses, may

retain and harbor unique, location-specific epigenetic marks that provide location-specific patterning instructions (Figure 4-2). Future experiments should aim at identifying these potential epigenetic marks, or altering the epigenetic state of cells along the BP during development or regeneration.

In summary, I have demonstrated the presence of a gradient of RA along the tonotopic axis of the chick BP that correlates with the timing of the development of frequency-specific stereocilia bundles. Further, modulation of RA signaling induces specific changes in stereocilia morphologies that are consistent with a role for the RA gradient in specification of tonotopic identity. RA signaling regulates expression of stereocilia elongation factors, such as Espin and Fscn2, suggesting a direct role for RA in the development of key aspects of tonotopy along the BP.

References

Berger, S.L., T. Kouzarides, R. Shiekhattar, and A. Shilatifard. 2009. An operational definition of epigenetics. *Genes Dev*. 23:781-783.

Bok, J., M. Bronner-Fraser, and D.K. Wu. 2005. Role of the hindbrain in dorsoventral but not anteroposterior axial specification of the inner ear. *Development*. 132:2115-2124.

Bok, J., D.K. Dolson, P. Hill, U. Ruther, D.J. Epstein, and D.K. Wu. 2007. Opposing gradients of Gli repressor and activators mediate Shh signaling along the dorsoventral axis of the inner ear. *Development*. 134:1713-1722.

Bok, J., S. Raft, K.A. Kong, S.K. Koo, U.C. Drager, and D.K. Wu. 2011. Transient retinoic acid signaling confers anterior-posterior polarity to the inner ear. *Proc Natl Acad Sci U S A*. 108:161-166.

Burns, J.C., and J.T. Corwin. 2013. A historical to present-day account of efforts to answer the question: "what puts the brakes on mammalian hair cell regeneration?". *Hearing research*. 297:52-67.

Choo, D., J.L. Sanne, and D.K. Wu. 1998. The differential sensitivities of inner ear structures to retinoic acid during development. *Developmental Biology*. 204:136-150.

Copeland, R.A., E.J. Olhava, and M.P. Scott. 2010. Targeting epigenetic enzymes for drug discovery. *Curr Opin Chem Biol*. 14:505-510.

Corwin, J.T., and D.A. Cotanche. 1988. Regeneration of sensory hair cells after acoustic trauma. *Science*. 240:1772-1774.

Cotanche, D.A. 1987. Regeneration of hair cell stereociliary bundles in the chick cochlea following severe acoustic trauma. *Hearing research*. 30:181-195.

Cotanche, D.A., and C.L. Kaiser. 2010. Hair cell fate decisions in cochlear development and regeneration. *Hear Res*. 266:18-25.

Crumling, M.A., M. Tong, K.L. Aschenbach, L.Q. Liu, C.M. Pipitone, and R.K. Duncan. 2009. P2X antagonists inhibit styryl dye entry into hair cells. *Neuroscience*. 161:1144-1153.

Dabdoub, A., and M.W. Kelley. 2005. Planar cell polarity and a potential role for a Wnt morphogen gradient in stereociliary bundle orientation in the mammalian inner ear. *J Neurobiol*. 64:446-457.

De Robertis, E.M. 2006. Spemann's organizer and self-regulation in amphibian embryos. *Nat Rev Mol Cell Biol*. 7:296-302.

De Robertis, E.M., and H. Kuroda. 2004. Dorsal-ventral patterning and neural induction in Xenopus embryos. *Annu Rev Cell Dev Biol*. 20:285-308.

De Robertis, E.M., J. Larraín, M. Oelgeschläger, and O. Wessely. 2000. The establishment of Spemann's organizer and patterning of the vertebrate embryo. *Nat Rev Genet*. 1:171-181.

Dessaud, E., A.P. McMahon, and J. Briscoe. 2008. Pattern formation in the vertebrate neural tube: a sonic hedgehog morphogen-regulated transcriptional network. *Development*. 135:2489-2503.

Dupé, V., N. Matt, J.M. Garnier, P. Chambon, M. Mark, and N.B. Ghyselinck. 2003. A newborn lethal defect due to inactivation of retinaldehyde dehydrogenase type 3 is prevented by maternal retinoic acid treatment. *Proc Natl Acad Sci U S A*. 100:14036-14041.

Eichele, G., and C. Thaller. 1987. Characterization of concentration gradients of a morphogenetically active retinoid in the chick limb bud. *J Cell Biol*. 105:1917-1923.

Frenz, D.A., W. Liu, A. Cvekl, Q. Xie, L. Wassef, L. Quadro, K. Niederreither, M. Maconochie, and A. Shanske. 2010. Retinoid signaling in inner ear

development: A "Goldilocks" phenomenon. *Am J Med Genet A*. 152A:2947-2961.

Frishkopf, L.S., and D.J. DeRosier. 1983. Mechanical tuning of free-standing stereociliary bundles and frequency analysis in the alligator lizard cochlea. *Hear Res*. 12:393-404.

Gale, J.E., W. Marcotti, H.J. Kennedy, C.J. Kros, and G.P. Richardson. 2001. FM1-43 dye behaves as a permeant blocker of the hair-cell mechanotransducer channel. *J Neurosci*. 21:7013-7025.

Gerlach-Bank, L.M., A.R. Cleveland, and K.F. Barald. 2004. DAN directs endolymphatic sac and duct outgrowth in the avian inner ear. *Dev Dyn*. 229:219-230.

Groves, A.K., and D.M. Fekete. 2012. Shaping sound in space: the regulation of inner ear patterning. *Development*. 139:245-257.

Holton, T., and A.J. Hudspeth. 1983. A micromechanical contribution to cochlear tuning and tonotopic organization. *Science*. 222:508-510.

Jacques, B.E., A. Dabdoub, and M.W. Kelley. 2012. Fgf signaling regulates development and transdifferentiation of hair cells and supporting cells in the basilar papilla. *Hear Res*. 289:27-39.

Katayama, A., and J.T. Corwin. 1989. Cell production in the chicken cochlea. *J Comp Neurol*. 281:129-135.

Kawashima, Y., G.S. Geleoc, K. Kurima, V. Labay, A. Lelli, Y. Asai, T. Makishima, D.K. Wu, C.C. Della Santina, J.R. Holt, and A.J. Griffith. 2011.

Mechanotransduction in mouse inner ear hair cells requires transmembrane channel-like genes. *J Clin Invest*. 121:4796-4809.

Kelley, M.W., X.M. Xu, M.A. Wagner, M.E. Warchol, and J.T. Corwin. 1993. The developing organ of Corti contains retinoic acid and forms supernumerary hair cells in response to exogenous retinoic acid in culture. *Development*. 119:1041-1053.

Kil, S.H., A. Streit, S.T. Brown, N. Agrawal, A. Collazo, M.H. Zile, and A.K. Groves. 2005. Distinct roles for hindbrain and paraxial mesoderm in the induction and patterning of the inner ear revealed by a study of vitamin-A-deficient quail. *Dev Biol*. 285:252-271.

Kowalik, L., and A.J. Hudspeth. 2011. A search for factors specifying tonotopy implicates DNER in hair-cell development in the chick's cochlea. *Dev Biol*. 354:221-231.

Li, H., H. Liu, S. Balt, S. Mann, C.E. Corrales, and S. Heller. 2004. Correlation of expression of the actin filament-bundling protein espin with stereociliary bundle formation in the developing inner ear. *J Comp Neurol*. 468:125-134.

Lim, D.J. 1980. Cochlear anatomy related to cochlear micromechanics. A review. *J Acoust Soc Am*. 67:1686-1695.

Lim, D.J., and M. Anniko. 1985. Developmental morphology of the mouse inner ear. A scanning electron microscopic observation. *Acta Otolaryngol Suppl*. 422:1-69.

Lin, H.W., M.E. Schneider, and B. Kachar. 2005. When size matters: the dynamic regulation of stereocilia lengths. *Curr Opin Cell Biol*. 17:55-61.

Lu, Z., and J.T. Corwin. 2008. The influence of glycogen synthase kinase 3 in limiting cell addition in the mammalian ear. *Dev Neurobiol*. 68:1059-1075.

Maden, M. 2007. Retinoic acid in the development, regeneration and maintenance of the nervous system. *Nature reviews. Neuroscience*. 8:755-765.

Meyers, J.R., and J.T. Corwin. 2008. Morphological Correlates of Regeneration and Repair. *In* Hair Cell Regeneration, Repair, and Protection. Vol. 33. R.J. Salvi, R.R. Fay, and A.N. Popper, editors. Springer, New York City. 39-75.

Meyers, J.R., R.B. MacDonald, A. Duggan, D. Lenzi, D.G. Standaert, J.T. Corwin, and D.P. Corey. 2003. Lighting up the senses: FM1-43 loading of sensory cells through nonselective ion channels. *J Neurosci*. 23:4054-4065.

Morelli, L.G., K. Uriu, S. Ares, and A.C. Oates. 2012. Computational approaches to developmental patterning. *Science*. 336:187-191.

Niederreither, K., V. Subbarayan, P. Dollé, and P. Chambon. 1999. Embryonic retinoic acid synthesis is essential for early mouse post-implantation development. *Nat Genet*. 21:444-448.

Niederreither, K., J. Vermot, B. Schuhbaur, P. Chambon, and P. Dollé. 2000. Retinoic acid synthesis and hindbrain patterning in the mouse embryo. *Development*. 127:75-85.

North, R.A. 2002. Molecular physiology of P2X receptors. *Physiol Rev*. 82:1013-1067.

Ohyama, T., M.L. Basch, Y. Mishina, K.M. Lyons, N. Segil, and A.K. Groves. 2010. BMP signaling is necessary for patterning the sensory and nonsensory regions of the developing mammalian cochlea. *J Neurosci*. 30:15044-15051.

Oxenham, A.J. 2012. Pitch perception. *J Neurosci*. 32:13335-13338.

Raz, Y., and M.W. Kelley. 1999. Retinoic acid signaling is necessary for the development of the organ of Corti. *Dev Biol*. 213:180-193.

Ribes, V., N. Balaskas, N. Sasai, C. Cruz, E. Dessaud, J. Cayuso, S. Tozer, L.L. Yang, B. Novitch, E. Marti, and J. Briscoe. 2010. Distinct Sonic Hedgehog signaling dynamics specify floor plate and ventral neuronal progenitors in the vertebrate neural tube. *Genes Dev*. 24:1186-1200.

Riccomagno, M.M., L. Martinu, M. Mulheisen, D.K. Wu, and D.J. Epstein. 2002. Specification of the mammalian cochlea is dependent on Sonic hedgehog. *Genes Dev*. 16:2365-2378.

Riccomagno, M.M., S. Takada, and D.J. Epstein. 2005. Wnt-dependent regulation of inner ear morphogenesis is balanced by the opposing and supporting roles of Shh. *Genes Dev*. 19:1612-1623.

Romand, R., T. Kondo, V. Fraulob, M. Petkovich, P. Dollé, and E. Hashino. 2006. Dynamic expression of retinoic acid-synthesizing and -metabolizing enzymes in the developing mouse inner ear. *J Comp Neurol*. 496:643-654.

Romand, R., W. Krezel, M. Beraneck, L. Cammas, V. Fraulob, N. Messaddeq, P. Kessler, E. Hashino, and P. Dollé. 2013. Retinoic acid deficiency impairs the vestibular function. *J Neurosci*. 33:5856-5866.

Sanchez-Guardado, L.O., J.L. Ferran, J. Mijares, L. Puelles, L. Rodriguez-Gallardo, and M. Hidalgo-Sanchez. 2009. Raldh3 gene expression pattern in the developing chicken inner ear. *The Journal of comparative neurology*. 514:49-65.

Slattery, E.L., J.D. Speck, and M.E. Warchol. 2009. Epigenetic influences on sensory regeneration: histone deacetylases regulate supporting cell proliferation in the avian utricle. *Journal of the Association for Research in Otolaryngology : JARO*. 10:341-353.

Spemann, H., and H. Mangold. 2001. Induction of embryonic primordia by implantation of organizers from a different species. 1923. *Int J Dev Biol*. 45:13-38.

Tanaka, K., and C.A. Smith. 1978. Structure of the chicken's inner ear: SEM and TEM study. *Am J Anat*. 153:251-271.

Warchol, M.E. 2010. Sensory regeneration in the vertebrate inner ear: Differences at the levels of cells and species. *Hear Res*.

Wieland, T., and H. Faulstich. 1977. The action of phalloidin. *Curr Probl Clin Biochem*. 7:11-14.

Wolpert, L. 1969. Positional information and the spatial pattern of cellular differentiation. *J Theor Biol*. 25:1-47.

Woolley, S.M., and E.W. Rubel. 2002. Vocal memory and learning in adult Bengalese Finches with regenerated hair cells. *The Journal of neuroscience : the official journal of the Society for Neuroscience*. 22:7774-7787.

Zeller, R., J. López-Ríos, and A. Zuniga. 2009. Vertebrate limb bud development: moving towards integrative analysis of organogenesis. *Nat Rev Genet*. 10:845-858.

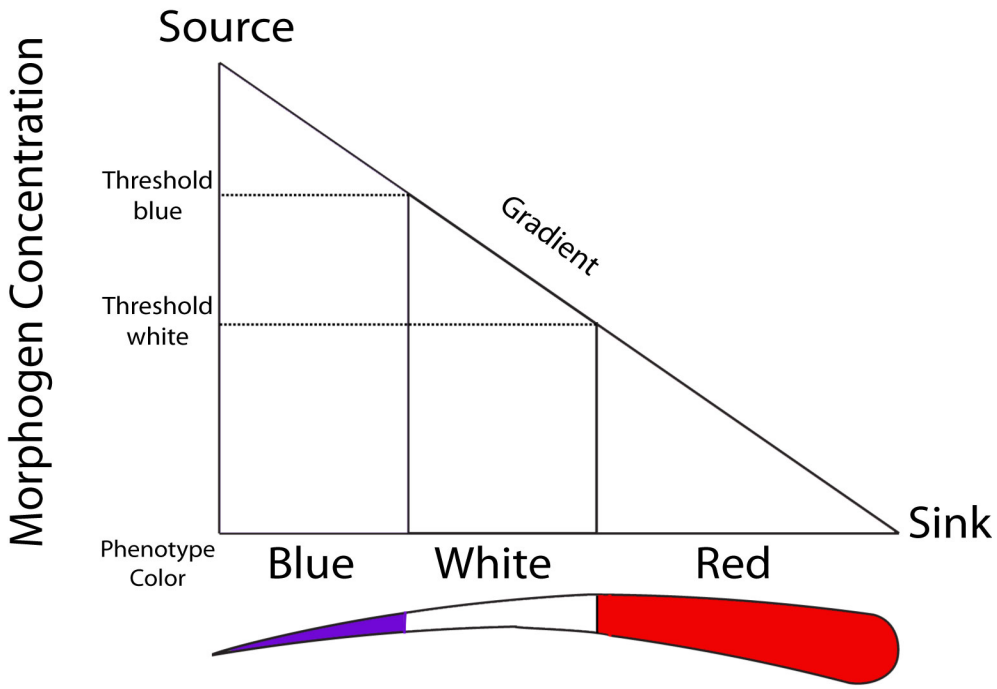

Figure 4-1. Lewis Wolpert's "French Flag" conceptual model for morphogen patterning. A morphogen is a signaling molecule that diffuses away from a source and orchestrates specific concentration-dependent cellular responses. The French Flag represents the morphogen concentration effects on cellular differentiation. Highest morphogen levels activate a "blue" gene within cells, intermediate levels a "white" gene, and the lowest levels a "red" gene. With the BP as an example, a proximal morphogen source instructs cells within the proximal end of the BP to acquire a "blue" phenotype, cells within the middle regions of the BP a "white" phenotype, and cells located in distal regions a "red" phenotype. Figure adapted from Morrelli LG et al., 2012.

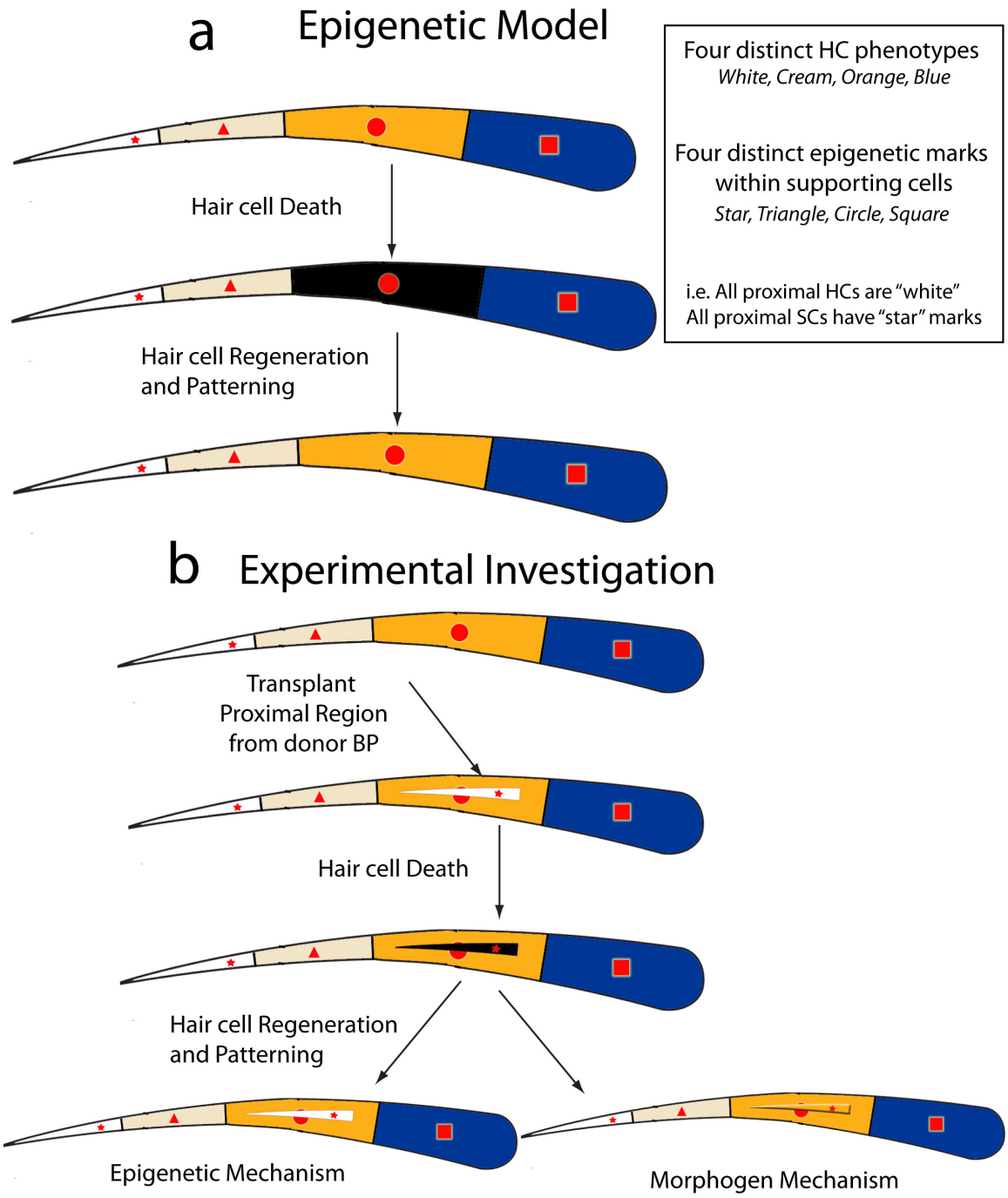

Figure 4-2. **a**) Hypothetical model depicting how epigenetics may play a role in specifying positional identity during regeneration in the BP. In this example there are four distinct hair cell phenotypes across the longitudinal axis of the BP: white, cream, orange, and blue. Hair cells that form in the proximal end are white, hair

cells in the mid-proximal region are cream, hair cells in the mid-distal region are orange, and hair cells at the distal end acquire a blue phenotype. Parallel to those phenotypes there also are unique and specific epigenetic marks within the supporting cells along there length of the BP, such that all the supporting cells located proximally have star epigenetic marks, mid-proximal have triangle marks, mid-distal have circle marks, and all the distal supporting cells have square marks. These epigenetic marks are then responsible for determining positional identity along the length of the BP, such that all supporting cells that harbor square marks give rise to hair cells that differentiate with a blue phenotype, all supporting cells that harbor star marks give rise to hair cells that differentiate with a white phenotype, etc. In an instance where sound stimulation kills a band of hair cells in the mid-distal regions, the supporting cells in that region respond and replace the lost hair cells. The epigenetic circle mark harbored within these supporting cells instruct the regenerating hair cell progeny to differentiate and acquire an orange phenotype. **b**) One example experiment to test this possibility involves transplanting the sensory epithelium from the proximal end of a donor BP onto the mid-distal region of an acceptor BP, and then kill the hair cells in that region of the acceptor BP. There are two possible outcomes dependent upon whether the newly regenerated hair cells are patterned through an epigenetics mechanism or through a morphogen mechanism. Under the epigenetics model, regenerated hair cells in the transplanted proximal region would acquire a white phenotype, since the supporting cells that give rise to these new hair cells possess a star epigenetics mark. Under a morphogen mechanism, regenerated

hair cells in the transplanted proximal region would acquire an orange phenotype based upon their relative location along the longitudinal axis.